SPIRE-AST-REP-002668

Title: **Evaluation of Instrument Thermal Interface Test Results**

CI-No: 120 000

Prepared by:	A. Hauser	Date:	10.03.06
Checked by:	J. Kroeker		13.3.2006
Product Assurance:	R. Stritter		13.03.06
Configuration Control:	W. Wietbrock		13.03.06
Project Management:	Dr. W. Fricke		14/03/2006

Distribution: See Distribution List (last page)

Issue	Date	Sheet	Description of Change	Release
1	10.03.06	all	First Issue	

Table of Content

Table of Figures

List of Tables

1 Scope

This technical report describes the evaluation of the measurement results obtained from the H-EPLM STM TB/TV qualification test performed in the LSS chamber at ESTEC. It contains the test evaluations related to the Instrument Interfaces L0, L1, L2 and L3. The performance evaluation described in this report is based on the measured data reported in RD 01. Furthermore, an extra test outside the LSS with a 90° tilted CVV was conducted in order to immerse the L0 open pods with liquid helium and thus to achieve quasi in-orbit conditions for those interfaces. The results of that test are reported, too.

2 Reference Documents and Abbreviations

2.1 Applicable Documents

AD 01 HERSCHEL/PLANCK Instrument Interface Document IID Part B for PACS, Doc.No.: SCI-PT-IIDB/PACS-02126, Issue 3.3, 21.05.2005

AD 02 HERSCHEL/PLANCK Instrument Interface Document IID Part B for SPIRE, Doc.No.: SCI-PT-IIDB/SPIRE-02124, Issue 3.3, 21.06.2004

AD 03 HERSCHEL/PLANCK Instrument Interface Document IID Part B for HIFI, Doc.No.: SCI-PT-IIDB/HIFI-02125, Issue 3.3, 21.10.2005

AD 04 Instrument Interface Temperatures, Doc.No.: HP-2-ASED-RD-0020, dated 26.04.2004, which is related to the three IIDBs AD 01 to AD 03

2.2 Reference Documents

RD 01 H-EPLM STM TB/TV Test Report, Doc.No.: HP-2-ASED-TR-0110, Issue 1, 17.01.2006

RD 02 MTD/OBA Flex Link Integration As-Built Status, HP-2-ASED-SD-0004, dated 10.02.2005

RD 03 H-EPLM TB/TV Test Specification – STM Phase, HP-2-ASED-SP-0020, Issue 1, dated 08.03.2005

RD 04 Integrated Test Procedure for H-EPLM STM TB/TV Test, Doc.No.: HP-2-ASED-TP-0056, Issue 1

RD 05 H-EPLM Thermal Model and Analysis, Doc.No.: HP-2-ASED-RP-0011, Issue 4, dated 15.04.04

RD 06 List of Acronyms, HP-1-ASPI-LI-0077, Issue 2, dated 12.07.2004

2.3 Abbreviations

IAD InterADapter
TTAP Thermal Test Adapter Payload
TTAS Thermal Test Adapter Spacecraft

Further Abbreviations are listed in RD 06.

2.4 Relevant Temperature Sensor Nomenclature

Sensor acronym	*Sensor Location*	*Type*
MT101	TH-HIFI-1, on L0 IF	C100
MT102	TH-HIFI-2, on L0 IF	C100
MT103	TH-HIFI-3, on L1 IF	C100
MT104	TH-HIFI-4, on L1 IF	C100
MT105	TH-HIFI-5, on FPU	C100
MT106	TH-HIFI-6, on FPU	C100
MT107	TH-HIFI-7, on FPU	Pt1000
MT108	TH-LOU-1, on LOU baseplate	Pt1000
MT109	TH-LOU-2, on LOU baseplate	Pt1000
MT110	TH-LOU-3, on LOU baseplate	Pt1000
MT201	TH-SPIRE-1, on detector L0 rigid pod	C100
MT202	TH-SPIRE-2, on detector L0 rigid pod	C100
MT203	TH-SPIRE-3, on cooler evaporator L0 rigid/open tank pod	C100
MT204	TH-SPIRE-4, on cooler evaporator L0 rigid/open tank pod	C100
MT205	TH-SPIRE-5, on cooler pump L0 rigid pod	C100
MT206	TH-SPIRE-6, on cooler pump L0 rigid pod	C100
MT207	TH-SPIRE-7, on SPIRE optical bench	C100
MT208	TH-SPIRE-8, on SPIRE optical bench	C100
MT213	TH-SPIRE-9, on SPIRE optical bench	Pt1000
MT250	TH-S-JFET-1, on S-J-FET baseplate	C100
MT251	TH-S-JFET-2, on S-J-FET baseplate	C100
MT252	TH-S-JFET-3, on S-J-FET baseplate	Pt1000
MT253	TH-P-JFET-1, on P-J-FET baseplate	C100
MT254	TH-P-JFET-2, on P-J-FET baseplate	C100
MT255	TH-P-JFET-3, on P-J-FET baseplate	Pt1000
MT301	TH-PACS-1, on Red Detector Assy (FPFPU.DET)	C100
MT302	TH-PACS-2, on Red Detector Assy (FPFPU.DET)	C100
MT303	TH-PACS-3, on Blue Detector Assy (FPFPU.BOL)	C100
MT304	TH-PACS-4, on Blue Detector Assy (FPFPU.BOL)	C100
MT305	TH-PACS-5, on cooler pump (FPFPU.COOL)	C100
MT306	TH-PACS-6, on cooler pump (FPFPU.COOL)	C100
MT307	TH-PACS-7, on cooler evaporator (FPFPU.COOL)	C100
MT308	TH-PACS-8, on cooler evaporator (FPFPU.COOL)	C100
MT309	TH-PACS-9, on L1-interface of Photometer optics	C100
MT310	TH-PACS-10, on L1-interface of Photometer optics	C100
MT311	TH-PACS-11, on L1-interface of collimator	C100
MT312	TH-PACS-12, on L1-interface of collimator	C100
MT313	TH-PACS-13, on L1-interface of Spectrometer housing	C100
MT314	TH-PACS-14, on L1-interface of Spectrometer housing	C100
MT315	TH-PACS-15, on FPU	Pt1000

Sensor acronym	*Sensor Location*	*Type*
T101	DLCM-1, tank lower side; -x-y; integrated in DLCM housing	C100
T102	DLCM-2, tank lower side; -x+y; integrated in DLCM housing	C100
T103	HTT lower side; -x+z-y; nearby outside	Pt1000
T104	DLCM-2, tank lower side; -x+y; integrated in DLCM housing	C100
T105	DLCM-1, tank lower side; -x-y; integrated in DLCM housing	C100
T106	HTT lower side; -x-z+y; nearby outside	C100
T107	HTT upper side; +x-z+y; nearby outside	C100
T111	HTT upper side; +x-y-z; integrated into PPS housing	C100
T112	HTT upper side; +x-y-z; integrated into PPS housing	C100
T113	Filling port end piece	C100
T114	Filling port end piece	C100
T202	OB Plate near PACS mounting foot (+z)	C100
T207	OB Plate near HIFI mounting foot (+z/-y)	Pt1000
T208	OB Plate near HIFI mounting foot (+z/-y)	C100
T211	Instrument Shield, close to HIFI	Pt1000
T212	Instrument Shield, close to PACS	C100
T213	Instrument Shield, close to SPIRE	C100
T221	L0 Cooling Strap 1; to PACS RED Detector	C100
T222	L0 Cooling Strap 2; to PACS Sorption Cooler Evaporator	C100
T223	L0 Cooling Strap 3; to PACS Sorption Cooler Pump	C100
T224	L0 Cooling Strap 4; to PACS BLUE Detector	C100
T225	L0 Cooling Strap 5; to SPIRE SM Detector enclosure	C100
T226	L0 Cooling Strap 6; to SPIRE Cooler Pump	C100
T227	L0 Cooling Strap 7; to SPIRE Cooler Evaporator	C100
T228	L0 Cooling Strap 8; to HIFI L0	C100
T231	L1 Ventline upstream strap 1 to PACS Phot.Optics (L1 Inlet)	C100
T232	L1 Ventline downstream strap 1 to PACS Phot.Optics	C100
T233	L1 Ventline downstream strap 2 to PACS Collimator	C100
T234	L1 Ventline downstream strap 3 to PACS Spect.Housing	C100
T235	L1 Ventline upstream strap 4 to SPIRE Optical Bench	C100
T236	L1 Ventline downstream strap 4 to SPIRE Optical Bench	C100
T237	L1 Ventline downstream strap 5 to HIFI interface (L1 outlet)	C100
T242	L1; on Strap 1 on PACS FPU Side	C100
T244	L1, on Strap 5 on HIFI FPU side	C100
T246	L3 Ventline to 6-JFET (JFET-Phot)	C100
T247	L3 Ventline to 2-JFET (JFET-Spec)	C100
T248	L1; on Strap 4 on SPIRE FPU side	C100
T249	On Spire 2-JFET (JFET-Spec)	Pt1000
T250	On Spire 2-JFET (JFET-Spec)	C100
T251	On Spire 6-JFET (JFET-Phot)	Pt1000
T252	On Spire 6-JFET (JFET-Phot)	C100
T253	OB Plate near SPIRE foot (center)	Pt1000

Sensor acronym	*Sensor Location*	*Type*
T254	OB Plate near SPIRE foot (center)	C100
T255	OB Plate near SPIRE foot (-z+y)	Pt1000
T256	OB Plate near SPIRE foot (-z+y)	C100
T258	OB Plate near SPIRE foot (-y-z)	C100

3 Thermal Performance of L0 Interfaces

3.1 Conditions during L0 Performance Measurement in LSS

The L0 measurement has been performed during the test phase TP4 on 23.October 2005 applying different electrical heating power on the L0 MTD's. The spacecraft was tilted by 14° and the helium filling level was about 90%. Inside the helium tank the interfaces of the L0 internal pods with the liquid are shown in **Figure 3.1-1**. Only the HIFI I/F is completely wetted with liquid helium, all others are partly wetted.

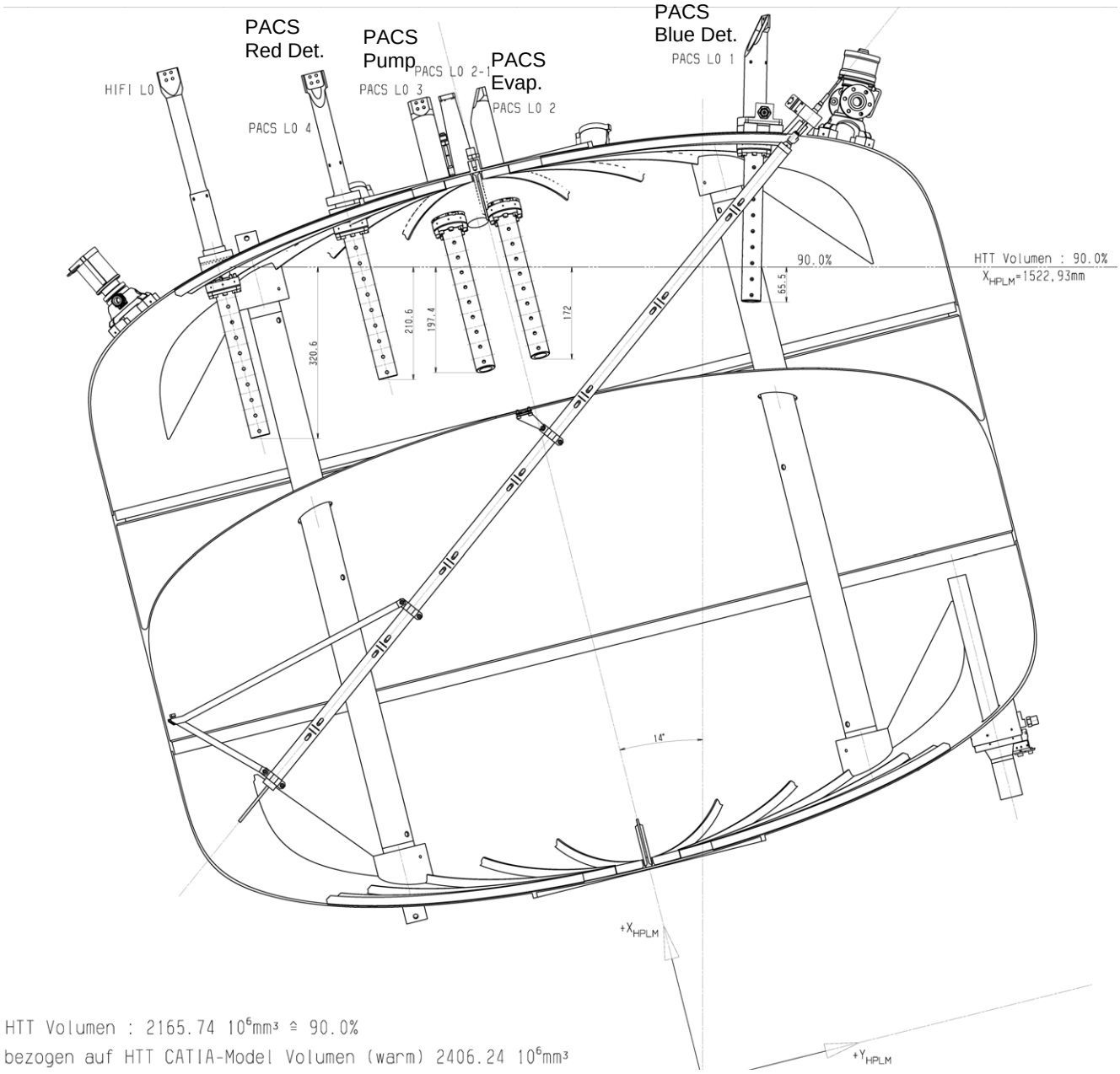

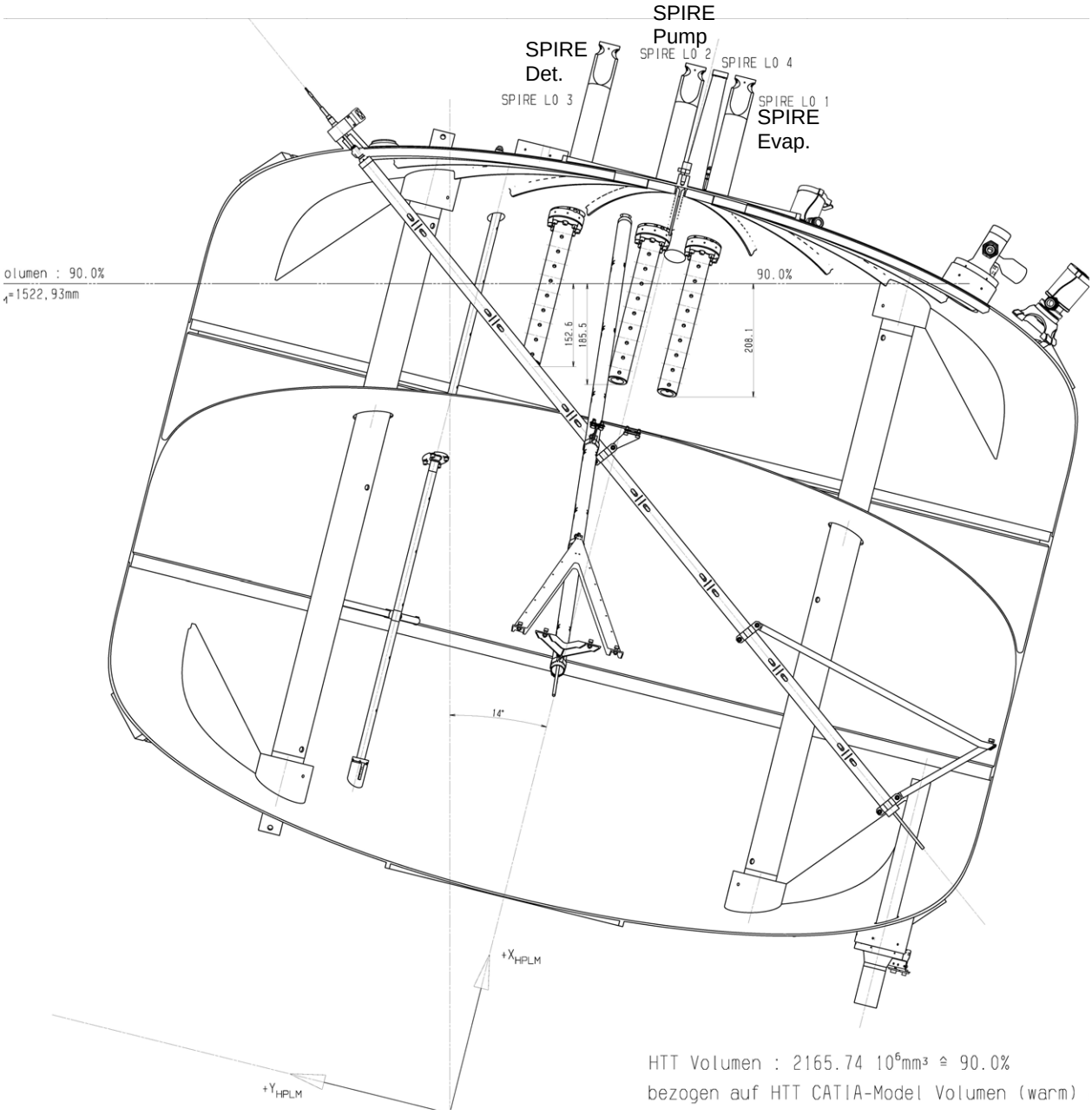

Figure 3.1-1: Helium Liquid Level Line at 14° Tilt and 90% Filling Charge

The temperature evolution of the HTT with its liquid helium content is shown in **Figure 3.1-2**. For the L0 performance evaluation the average of all DLCM sensors (T101, T102, T104 and T105) is taken as temperature for the liquid helium (red line).

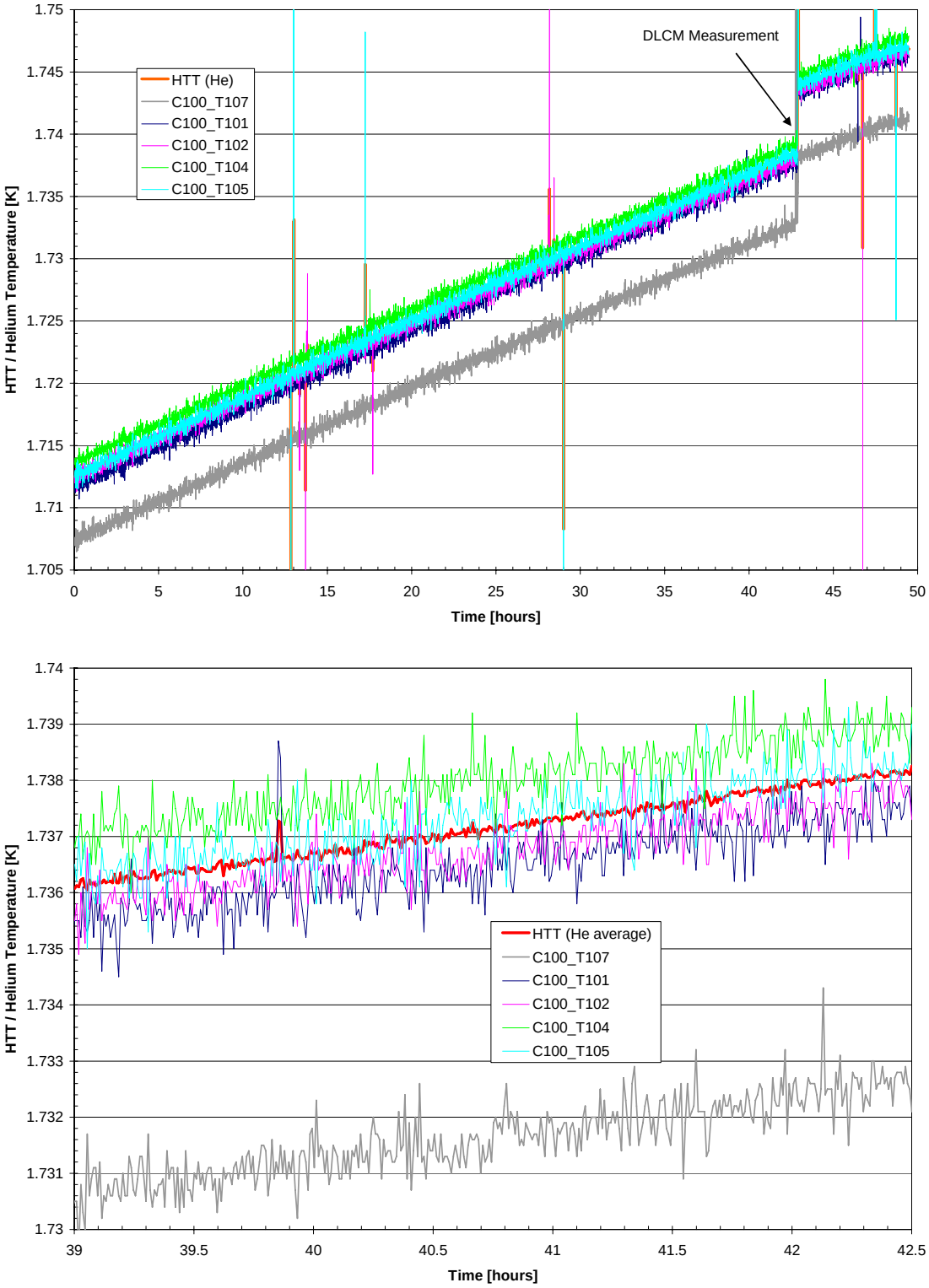

Figure 3.1-2: T107 and all DLCM Temperatures during TP4

A view from +X onto the HTT upper bulkhead with all L0 interfaces and temperature sensors is given in following **Figure 3.1-3**.

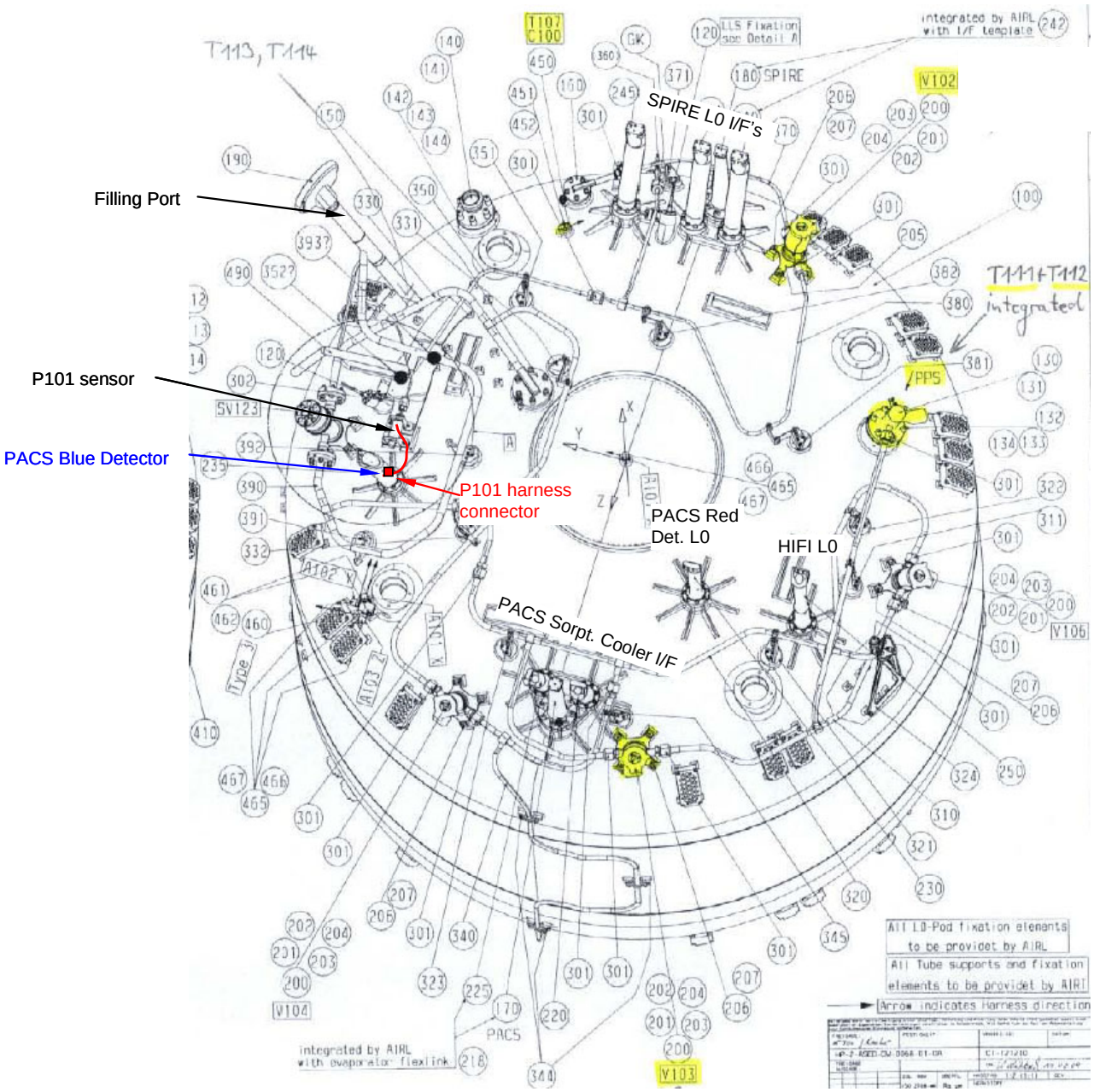

Figure 3.1-3: HTT Upper Bulkhead with L0 Rigid Pods HTT Temperature Sensors

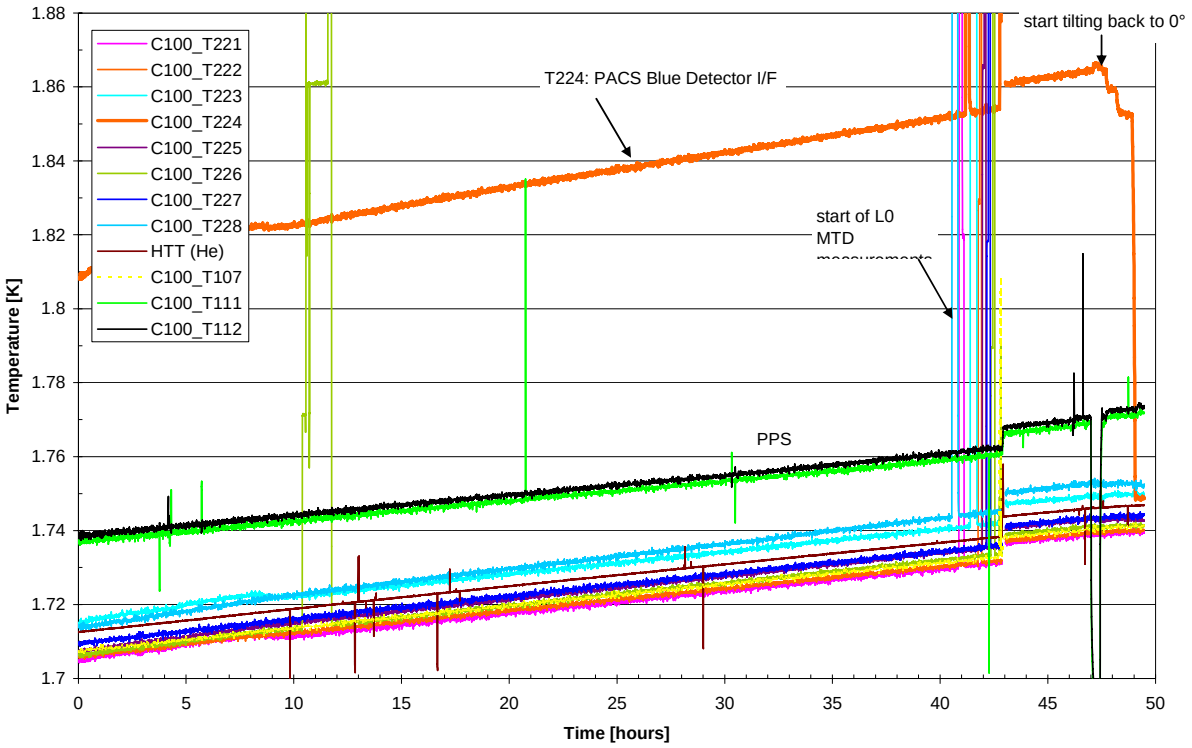

Figure 3.1-4: HTT Average, PPS and all L0 I/F Temperatures during TP4

3.2 PACS

The temperature sensors for PACS L0 are located on the flexible copper strap near the FPU side (see **Figure 3.2-1** to **Figure 3.2-4**).

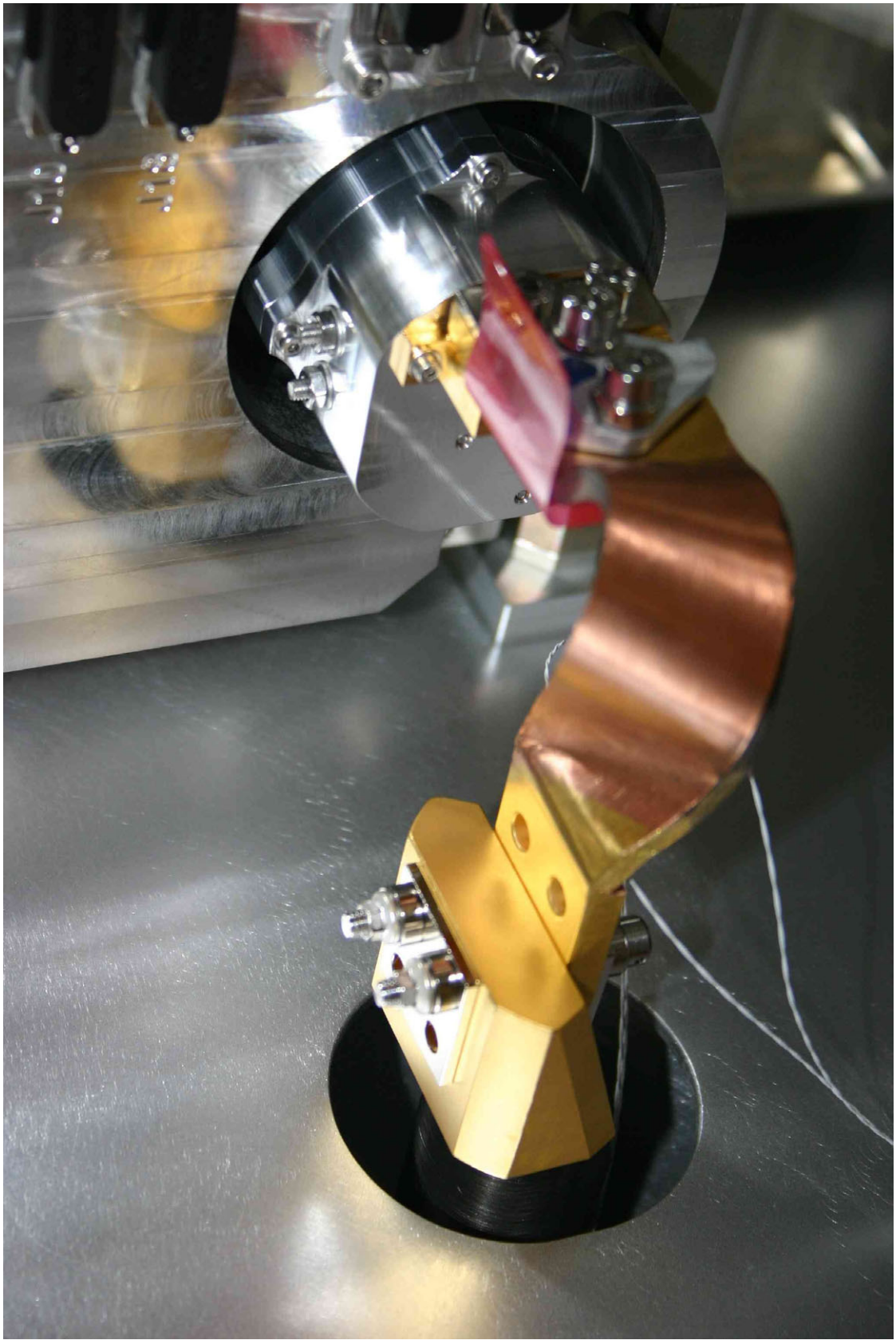

Figure 3.2-1: Temperature Sensor T221 – PACS Red Detector FPU I/F

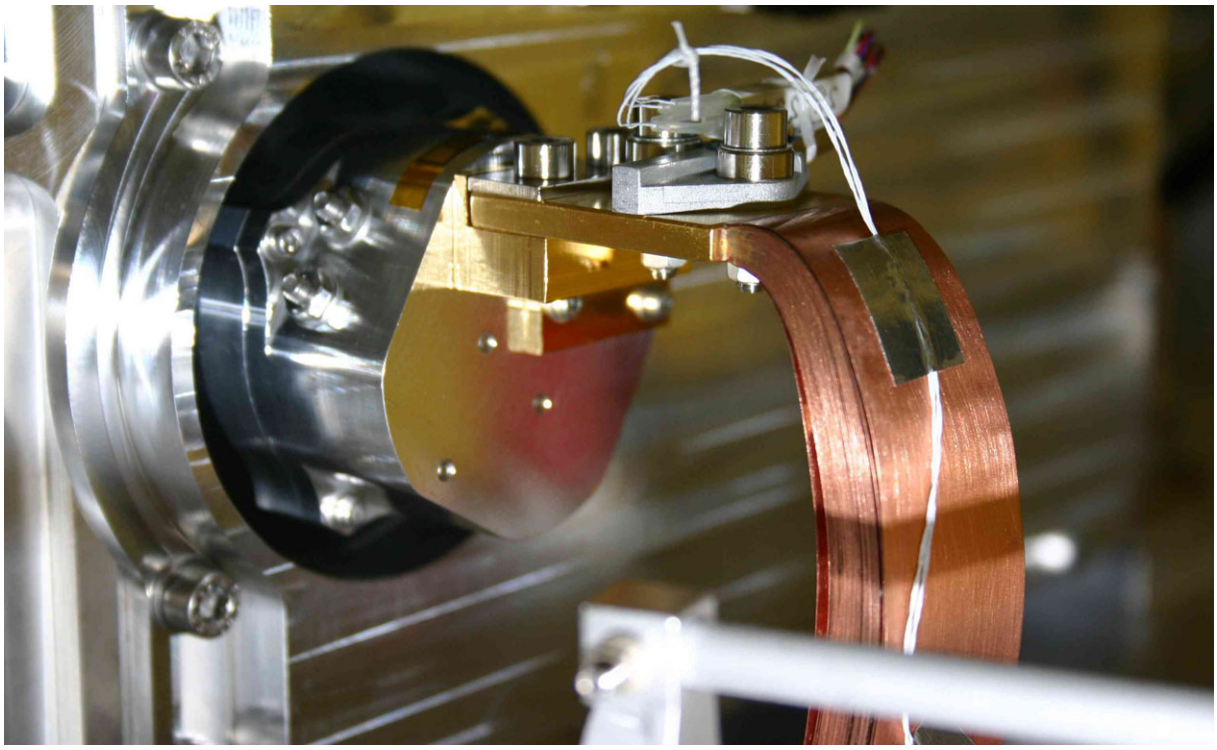

Figure 3.2-2: Temperature Sensor T224 – PACS Blue Detector FPU I/F

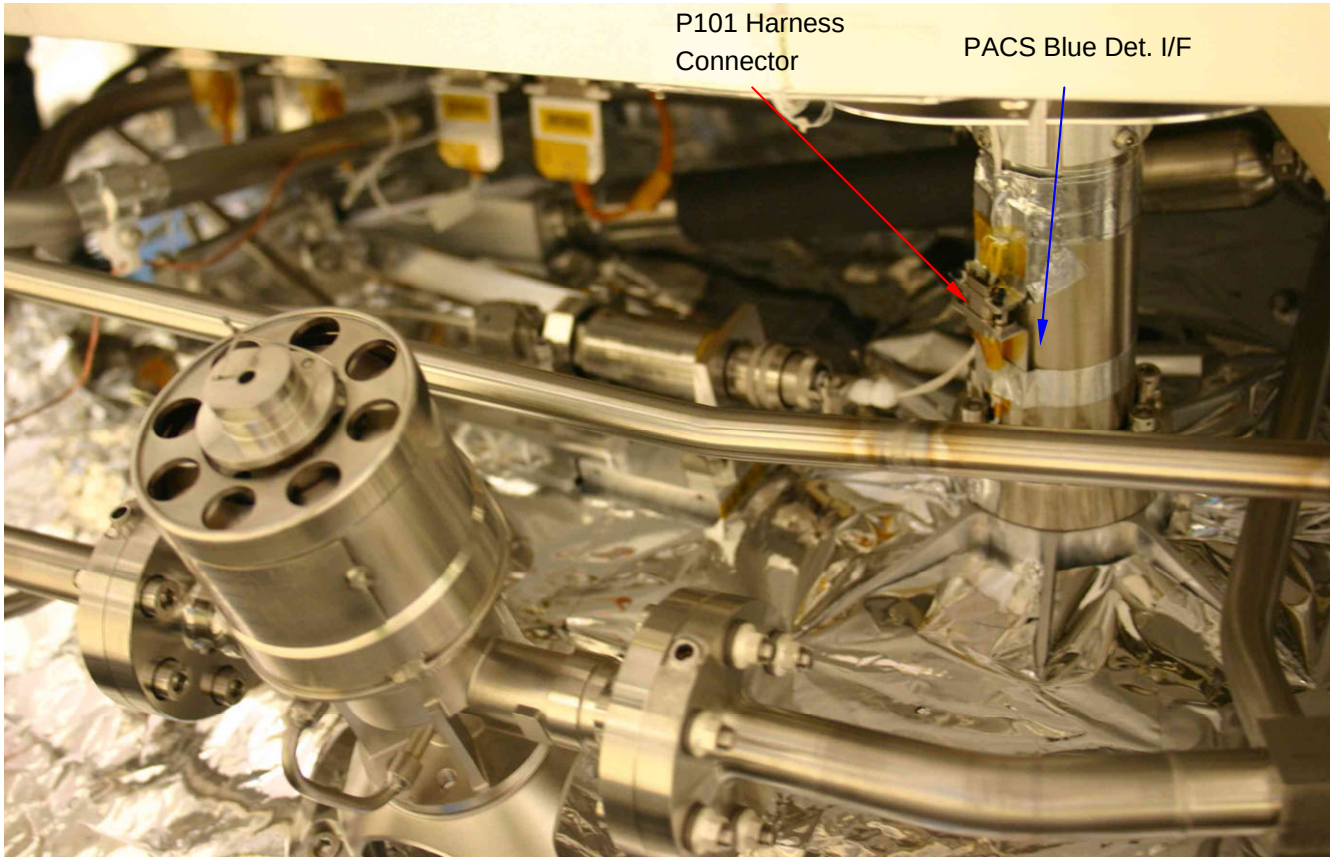

Figure 3.2-3: P101 Harness Connector on PACS Blue Detector L0 Rigid Pod

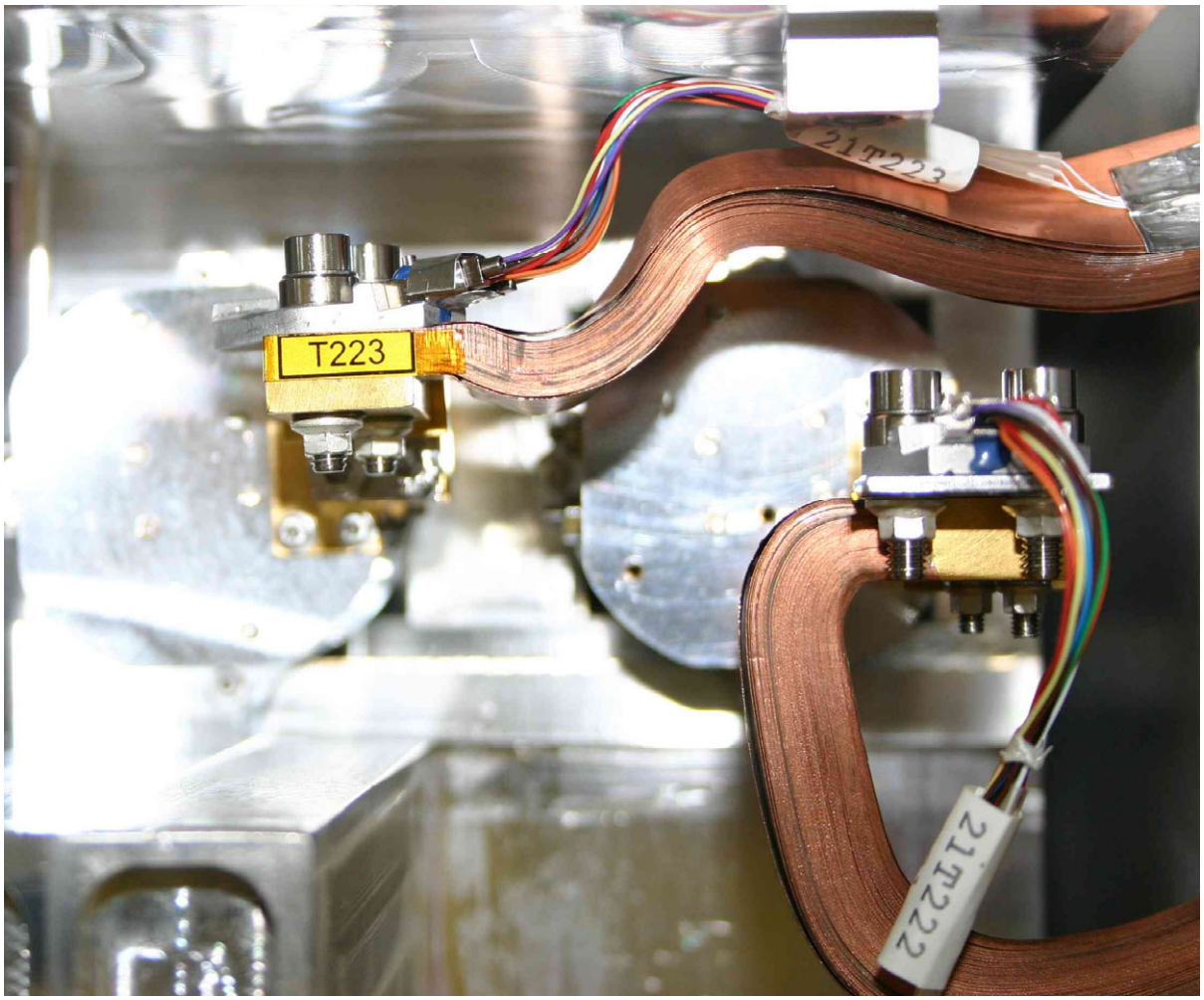

Figure 3.2-4: Temperature Sensors T222 and T223 – PACS Evaporator and Pump FPU I/F

The PACS L0 I/F temperature evolution is shown in **Figure 3.2-5** (thicker lines) together with the MTD temperatures (thinner lines). The MTD sensors for the Red Detector (MT301, MT302) are already out of range for temperatures above 2.1 K. The two MTD sensors for the Blue Detector MTD (MT303, MT304) show nearly the same temperature, whereas the Pump MTD sensor MT307 shows up to 0.1 K higher temperatures compared to the other Pump sensor MT308.

For the instrument interfaces the FM sensors T221, T222, T223 and T224 are the relevant ones. The Helium temperature as an average of the four DLCM sensors (T101, T102, T103, T104) is also shown in **Figure 3.2-5**. The corresponding electrical power applied at the L0 MTD's is given in **Figure 3.2-6** as thick lines together with the "transient" thermal conductance between the instrument I/F's and liquid helium (thin lines).

Figure 3.2-7 shows the temperature gradients across the L0 thermal links versus electrical heating power. The curves are almost linear and except for the Blue Detector all curves end in the origin. For the Blue Detector I/F it seems there is a parasitic heat load of about 2 mW. As evident in **Figure 3.1-4** the corresponding offset of about 0.1 K at the Blue Det. I/F is present until the S/C is tilted back to vertical position (from 14° to 0°). At vertical position obviously no parasitic heat load is present. Thus, one can conclude that heat is conducted from any warmer part of the HTT upper bulkhead part (i.e. not immersed

with liquid helium) probably near the filing port to the PACS Blue Det. L0 rigid pod and further via the internal pod to the liquid helium, see **Figure 3.1-3**. This effect may be enhanced by the copper harness between the pressure sensor P101 and the connector attached to the Blue Det. rigid pod, see also **Figure 3.2-3**.

The derived thermal conductance values of all PACS L0 interfaces are shown in **Figure 3.5-8**. A summary of all L0 I/F conductance values is also given in **Table 3.6-1**.

The decrease in thermal conductance for higher heater power of the evaporator indicates that superfluid film on the internal pod is burnt away at higher temperature (applicable only on ground).

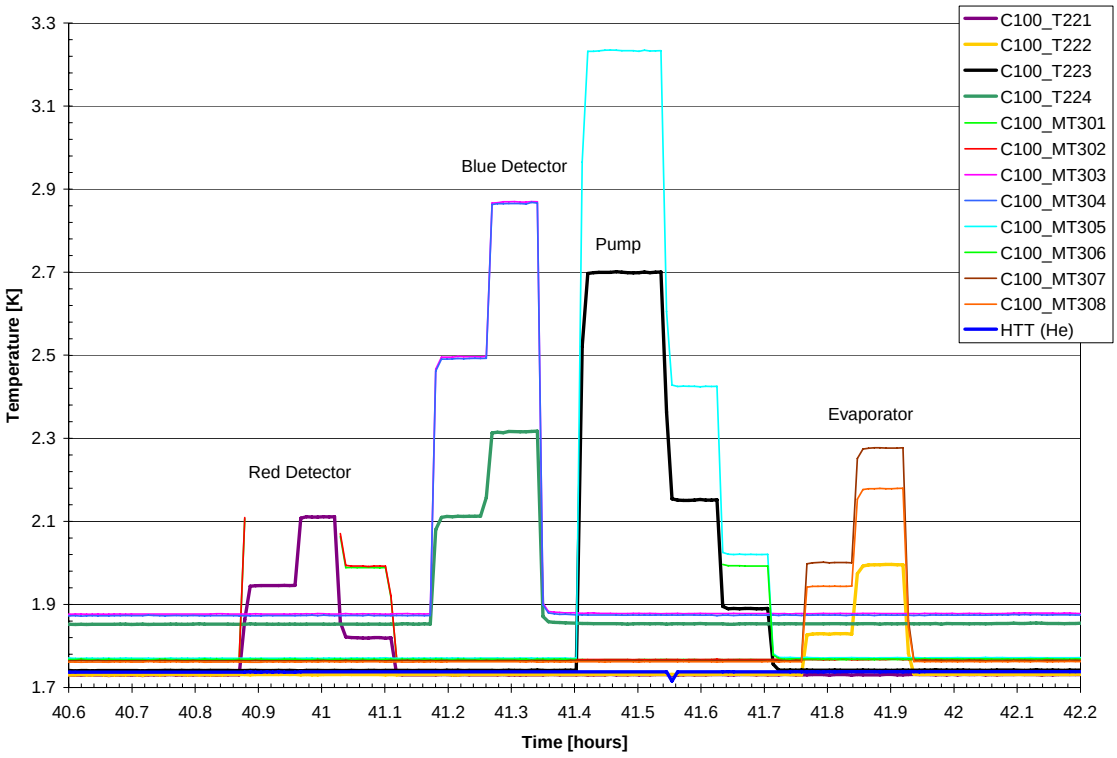

Figure 3.2-5: Temperature Evolution of PACS L0 Interfaces

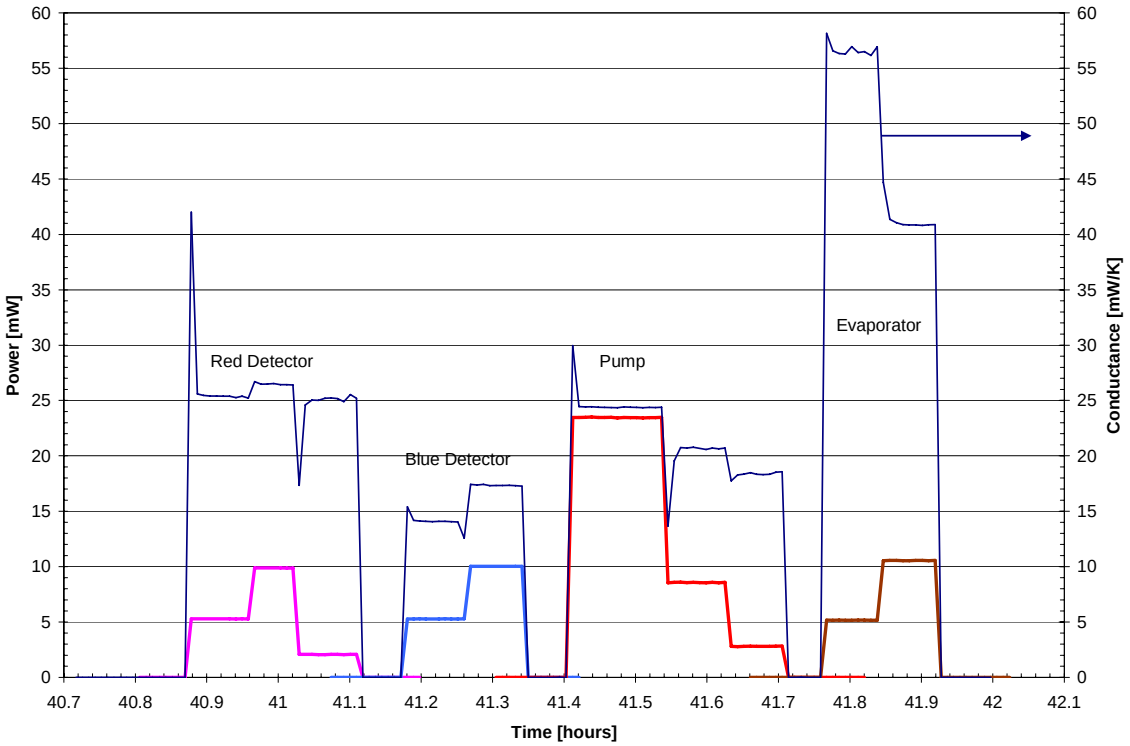

Figure 3.2-6: Electrical Heating Power and Thermal Conductance at PACS L0 Interfaces

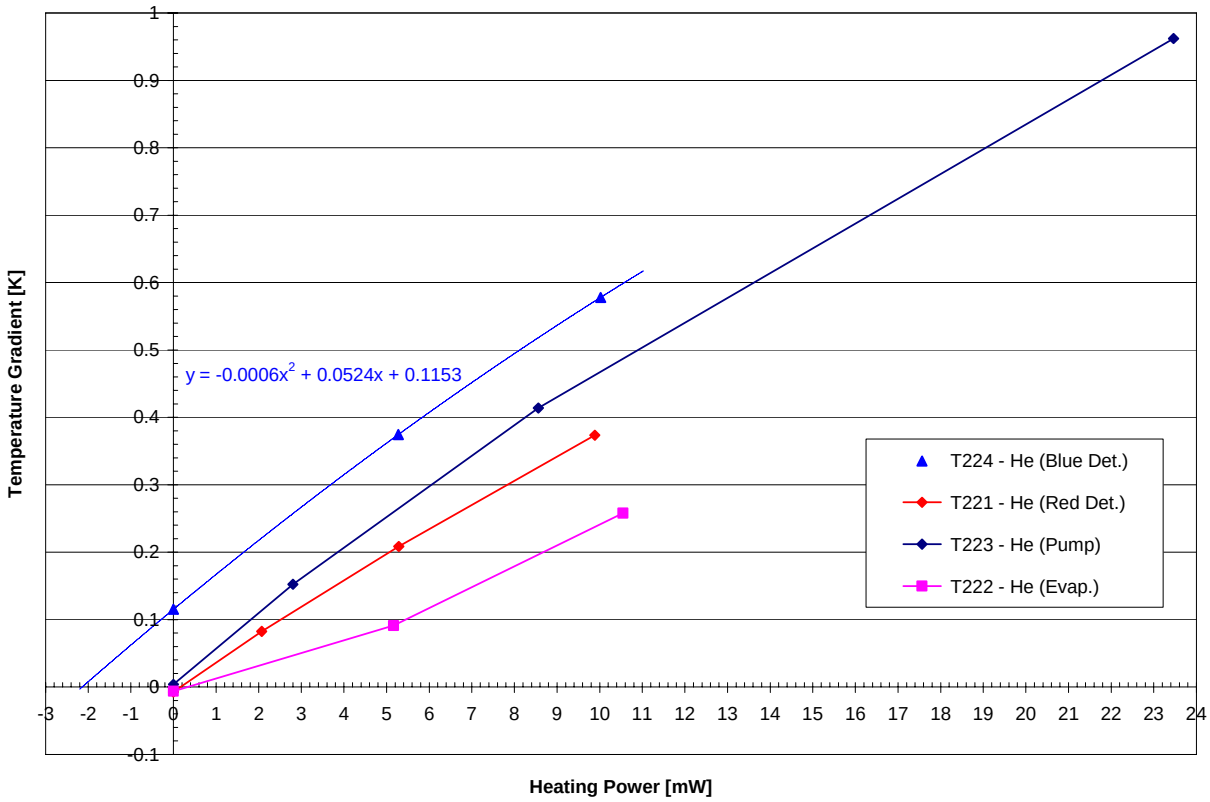

Figure 3.2-7: PACS L0 Temperature Gradients versus Electrical Heating Power

3.3 SPIRE

The temperature sensors for SPIRE L0 are located on top of Invar plates near the L0 rigid and open pods, see **Figure 3.3-1** and **Figure 3.3-2**.

The SPIRE L0 I/F temperature evolution is shown in **Figure 3.3-3** (thicker lines) together with the MTD temperatures (thinner lines).For the instrument interfaces the FM sensors T225, T226 and T227 are the relevant ones. The Helium temperature as an average of the four DLCM sensors (T101, T102, T103, T104) is also shown in **Figure 3.3-3**. The corresponding electrical power (thick lines) applied at the L0 MTD's is given in **Figure 3.5-5** together with the "transient" thermal conductance between the instrument I/F's and liquid helium (thin lines, see y-axis at the right hand side). An extra test has been conducted for the pump which is shown in **Figure 3.3-5** and **Figure 3.3-6**.

Figure 3.3-7 shows the temperature gradients across the L0 thermal links versus electrical heating power. The curves are almost linear and all curves end nearly in the origin; i.e. parasitic heat loads can be considered as negligible. The derived thermal conductance of all SPIRE L0 interfaces is shown in **Figure 3.5-14**. A compilation of all L0 I/F conductance values is also given in **Table 3.6-1**.

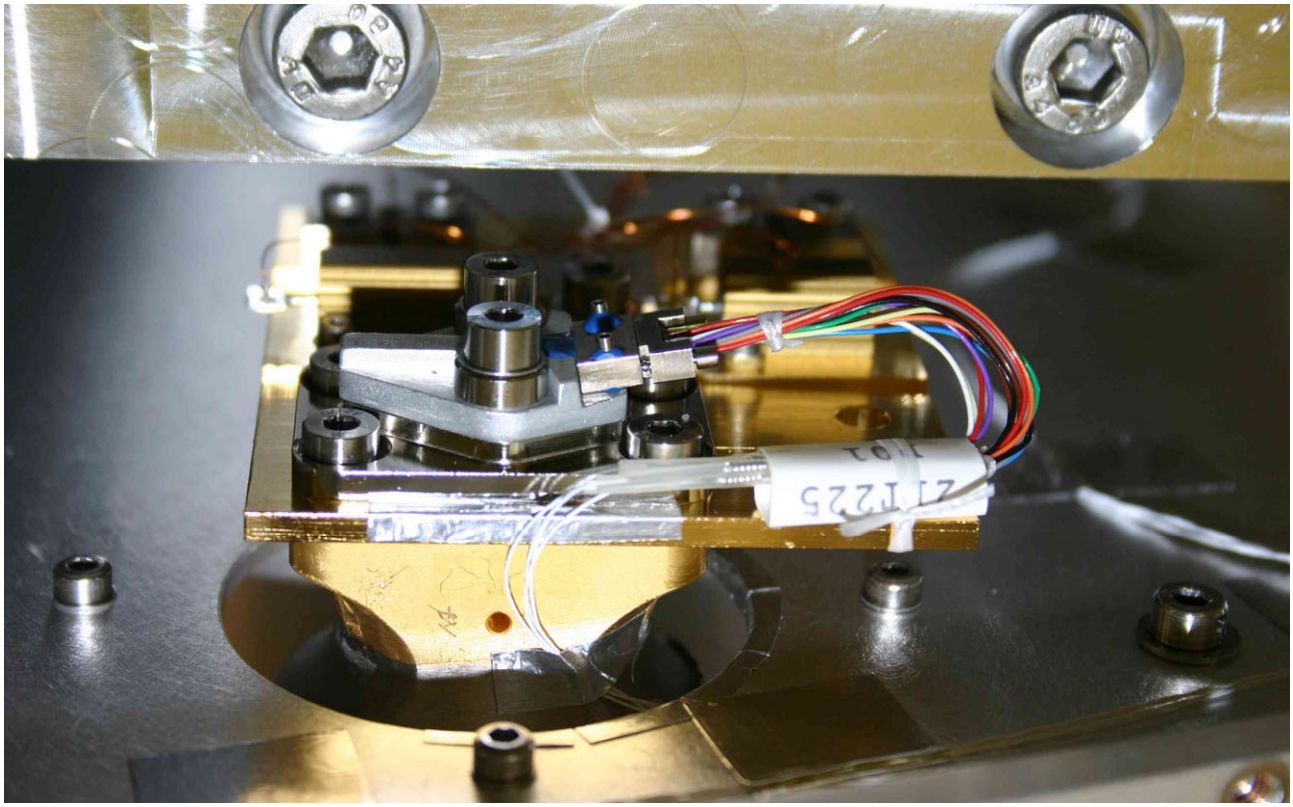

Figure 3.3-1: Temperature Sensor T225 – SPIRE Detector Rigid Pod I/F

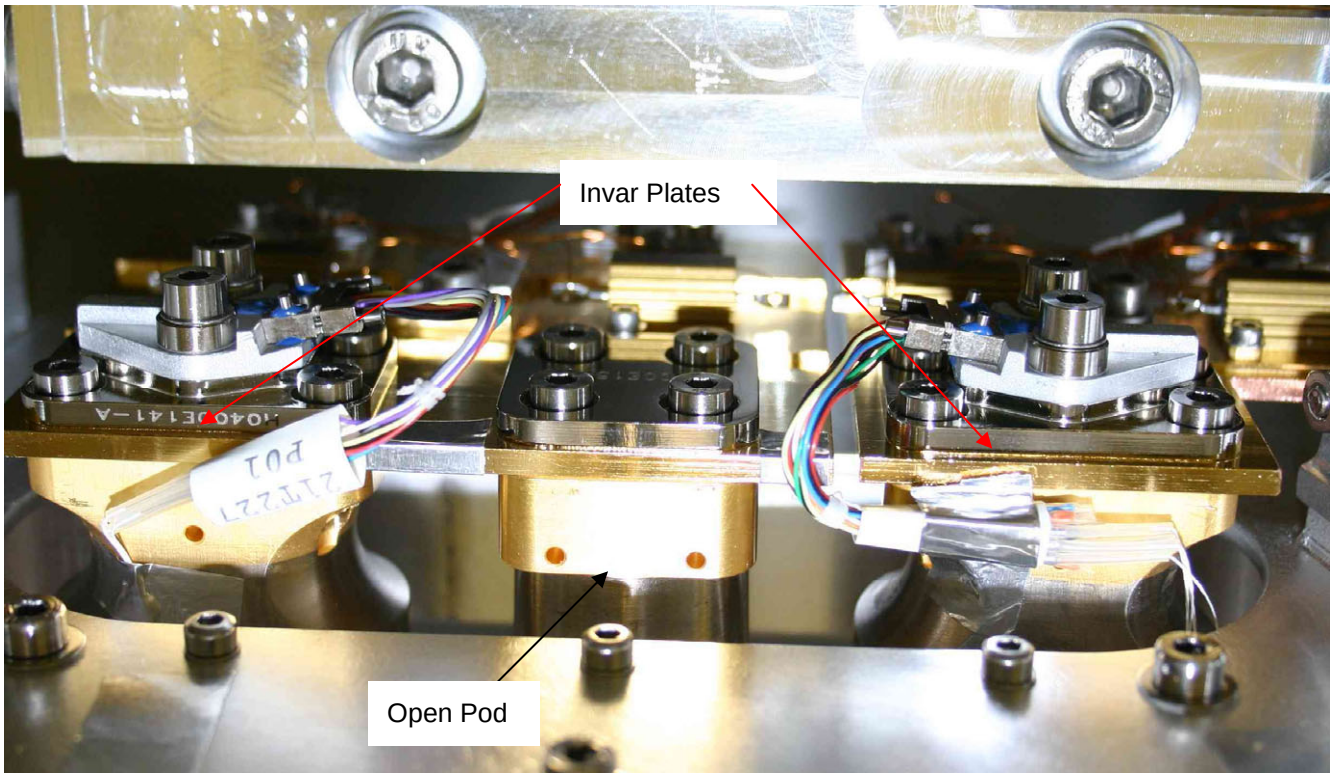

Figure 3.3-2: Temperature Sensors T226 and T227 – SPIRE Pump and Evaporator Rigid Pod I/F

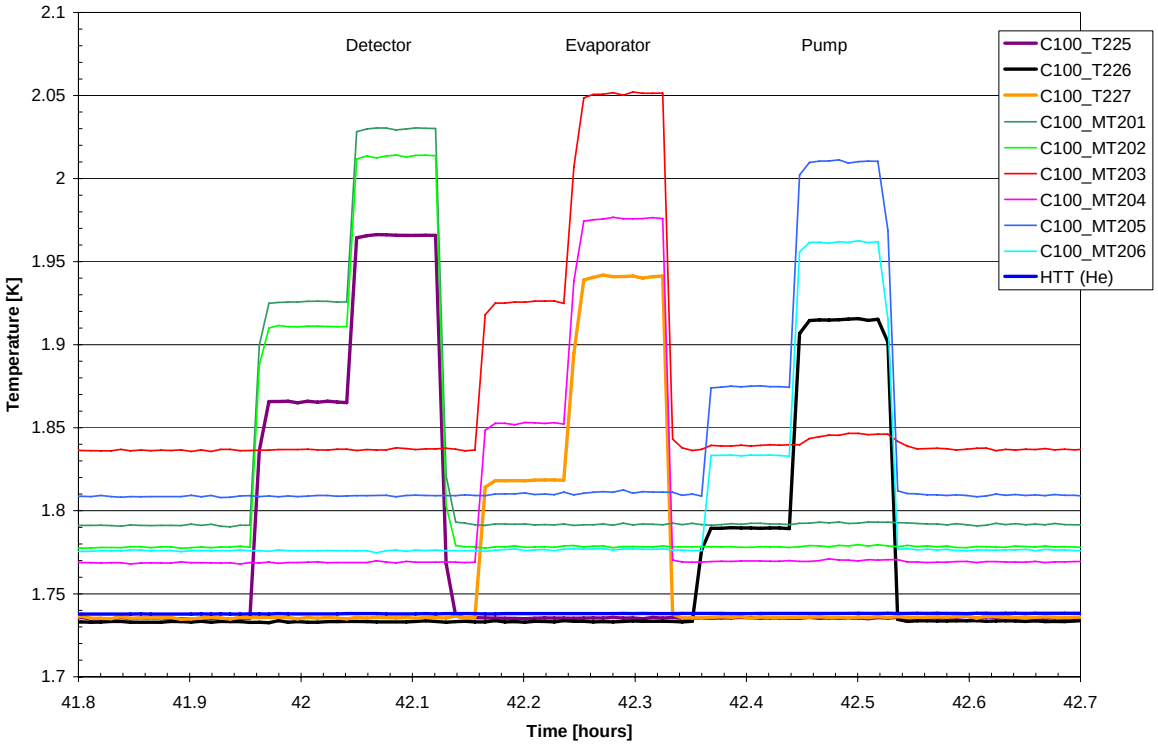

Figure 3.3-3: Temperature Evolution of SPIRE L0 Interfaces

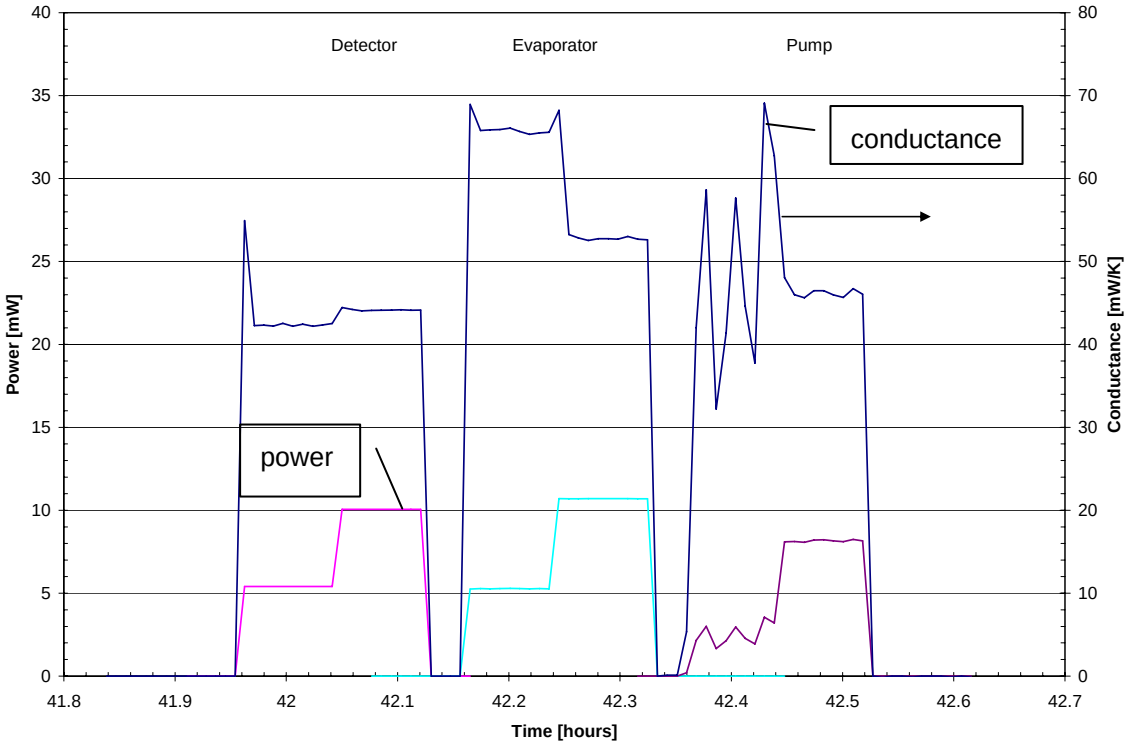

Figure 3.3-4: Electrical Heating Power and Thermal Conductance at SPIRE L0 Interfaces

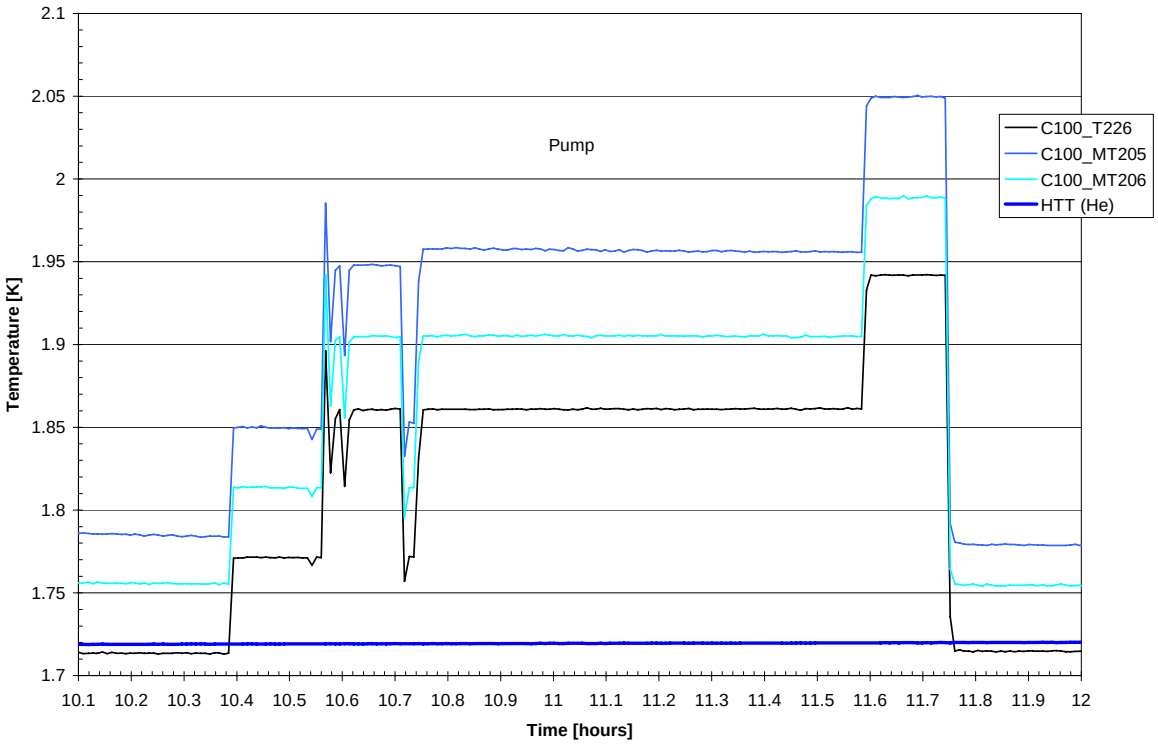

Figure 3.3-5: Temperature Evolution of .SPIRE L0 Pump Interface – Extra Test

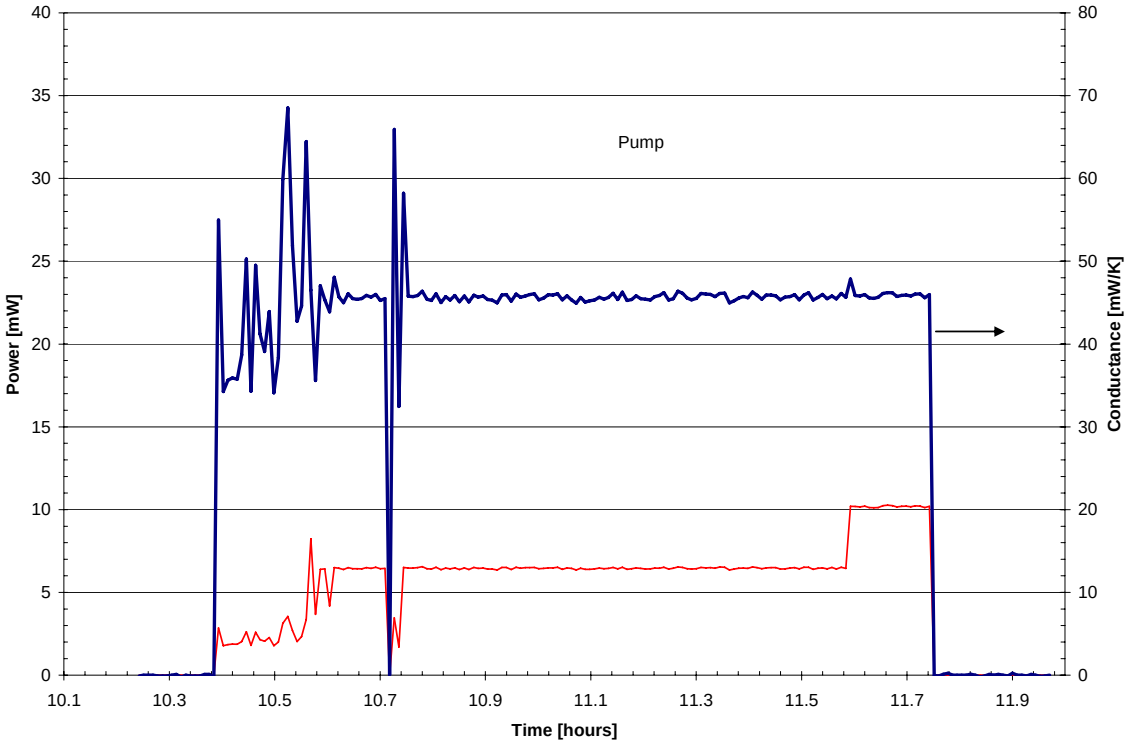

Figure 3.3-6: Electrical Heating Power and Thermal Conductance at SPIRE L0 Pump I/F – Extra Test

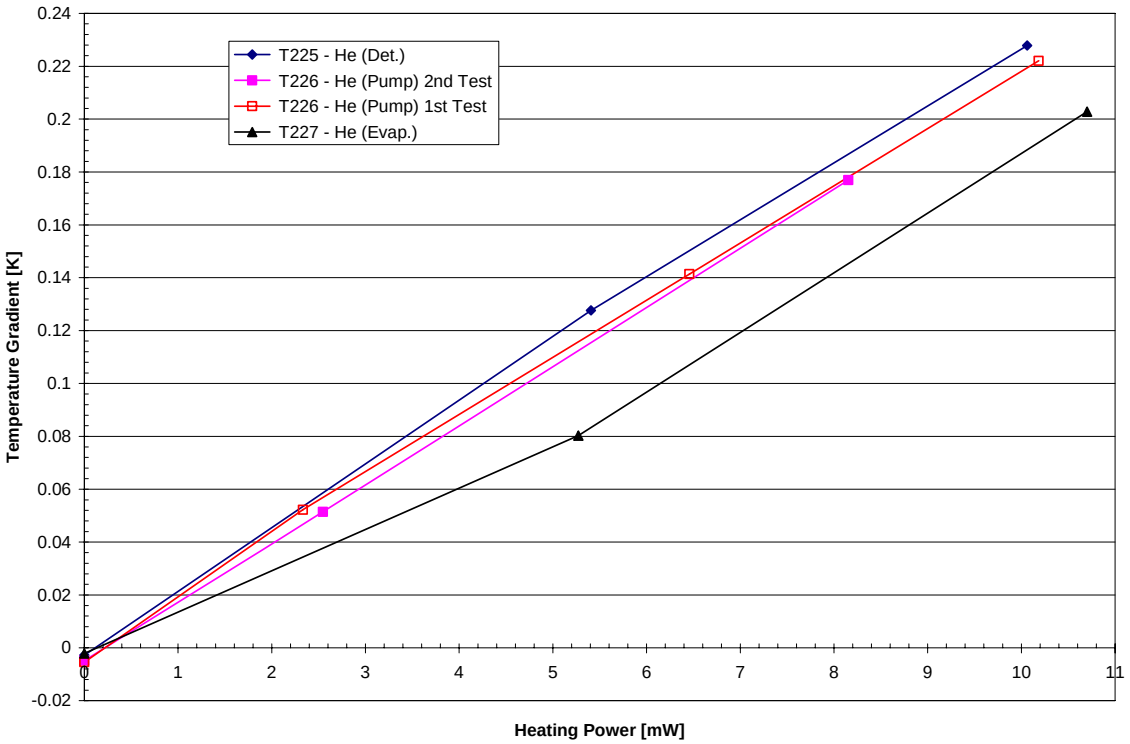

Figure 3.3-7: SPIRE L0 Temperature Gradients versus Electrical Heating Power

3.4 HIFI

Due to updated I/F mass requirements the thickness of the flexible copper strap has been reduced from 3.5 mm to 2.5 mm. For the same reason the temperature sensor T228 for HIFI L0 has been shifted from the end of the copper strap close to the instrument side to the rigid pod, see **Figure 3.4-1**. For the actual I/F temperature therefore the MTD sensors MT101 and MT102 need to be used.

The HIFI L0 I/F temperature evolution is shown in **Figure 3.4-2** together with the corresponding electrical power applied (y-axis at the right hand side). The MTD sensors are out of range at temperatures higher than 2.108 K. **Figure 3.4-3** shows the temperature gradient across the L0 thermal link versus electrical heating power. The curves are almost linear and the curve for the sensor T228 at the rigid pod I/F ends nearly in the origin; for the MTD I/F (MT101, MT102) a parasitic heat load of about 0.6 mW can be derived. The HIFI L0 I/F conductance versus mean temperature is shown in **Figure 3.4-4**.

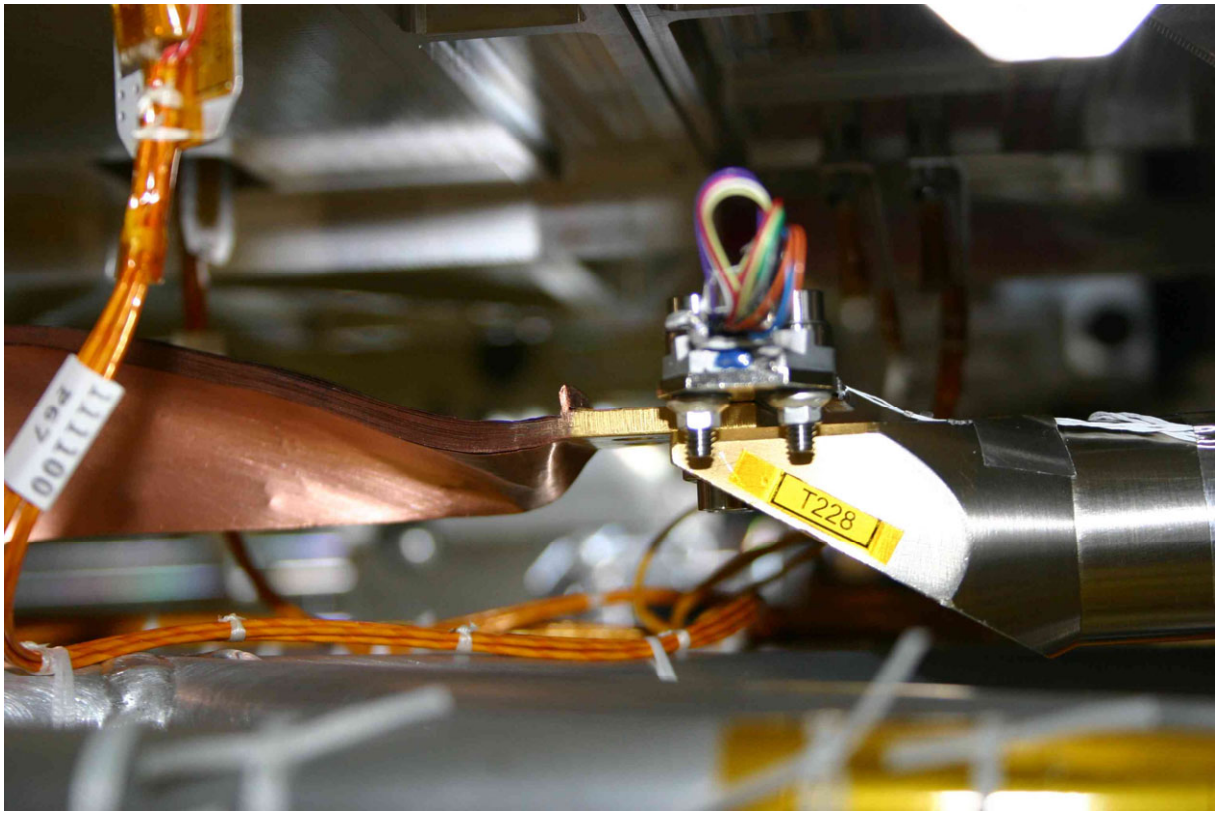

Figure 3.4-1: Temperature Sensor T228 – HIFI Rigid Pod I/F

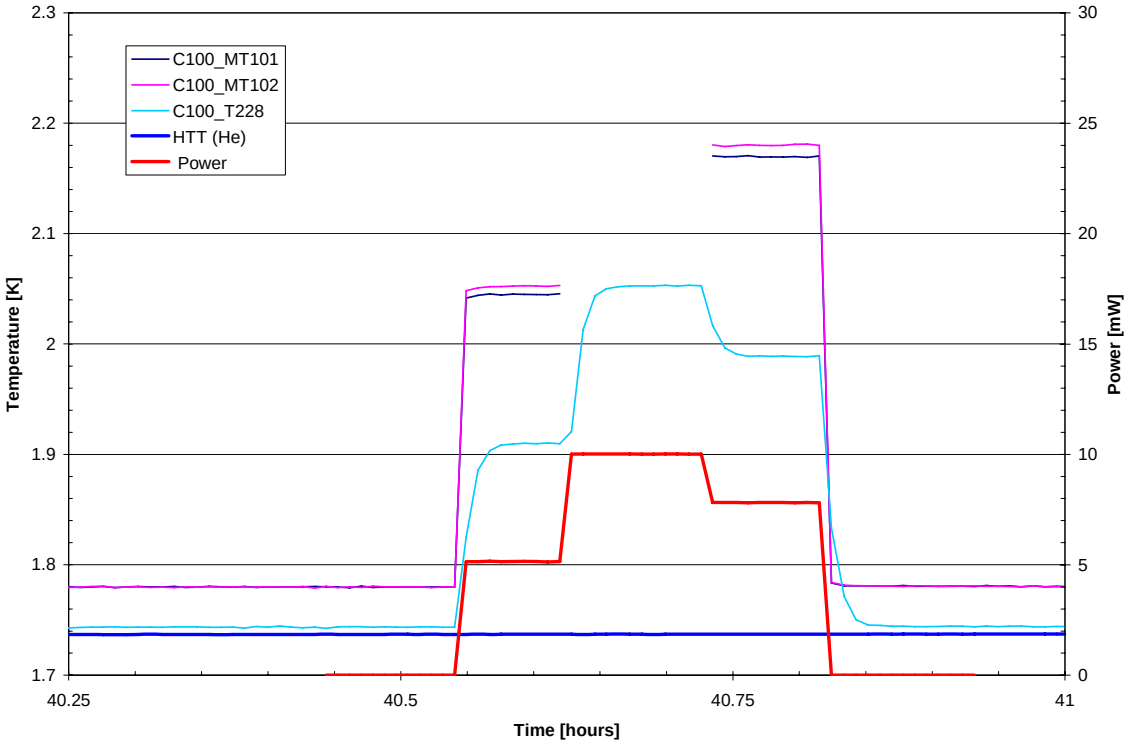

Figure 3.4-2: Temperature Evolution of HIFI L0 Interface

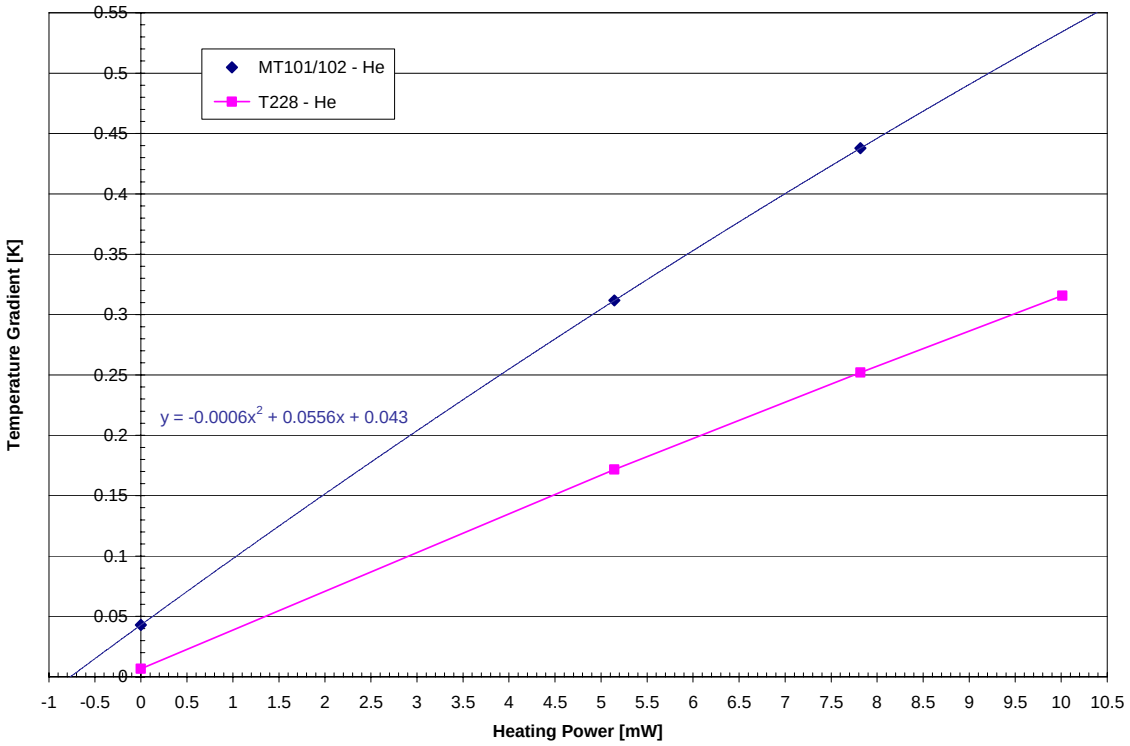

Figure 3.4-3: HIFI L0 Temperature Gradient versus Electrical Heating Power

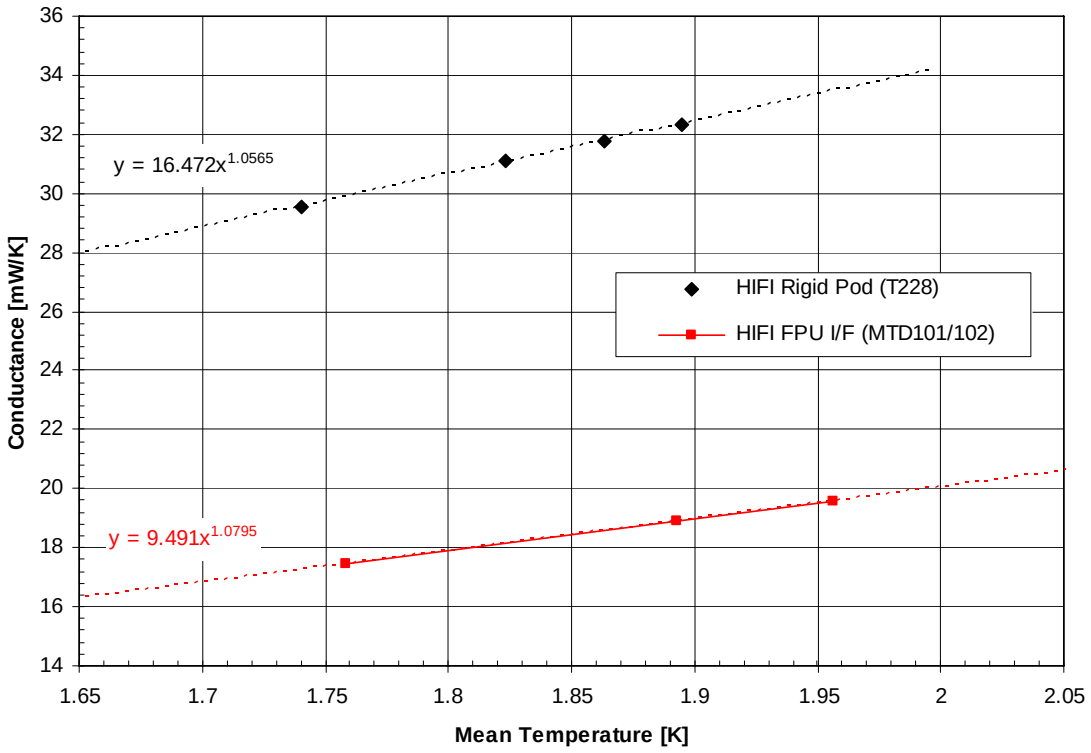

Figure 3.4-4: Thermal Conductance versus Mean Temperature for HIFI L0 I/F to Helium

3.5 PACS and SPIRE L0 Performance Tests outside LSS

Since the open pods of the PACS and SPIRE Evaporator interfaces could not be immersed with liquid helium using the set-up inside the LSS an extra test has been conducted outside the LSS. Therefore the CVV has been tilted by 90° and then rotated by +20° and -20° to enable immersion of the PACS and SPIRE open pods with liquid helium as shown in **Figure 3.5-1** and **Figure 3.5-2**, respectively. This extra L0 test has been conducted on the 5.January 2006 at ESTEC premises.

During the extra test the opportunity has been taken to measure again the L0 performance of the PACS Pump, the PACS Red Detector, the SPIRE Pump and the SPIRE Detector for a completely wetted internal pod. This allows extrapolating the performance of those interfaces for in orbit conditions. The temperature evolution of all relevant L0 temperatures is shown in **Figure 3.5-4**. For the helium temperature the average of the two DLCM sensors T101 and T105 has been taken, the other two DLCM sensors were not inside the liquid during this test.

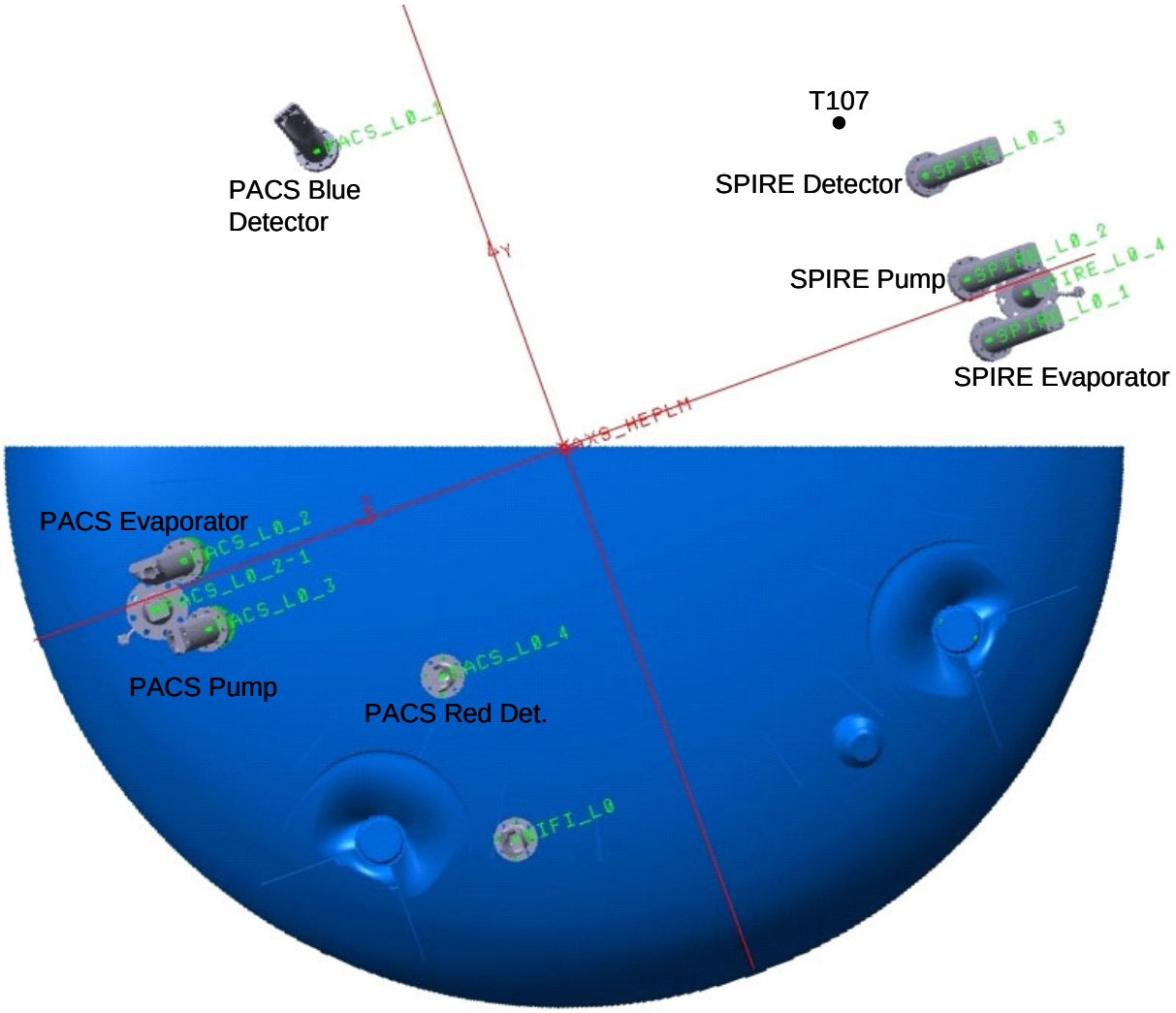

Horizontal CVV counter-clockwise rotated by 20° with 50% Filling Charge in the HTT

Figure 3.5-1: Helium Liquid Level Line during PACS L0 Testing

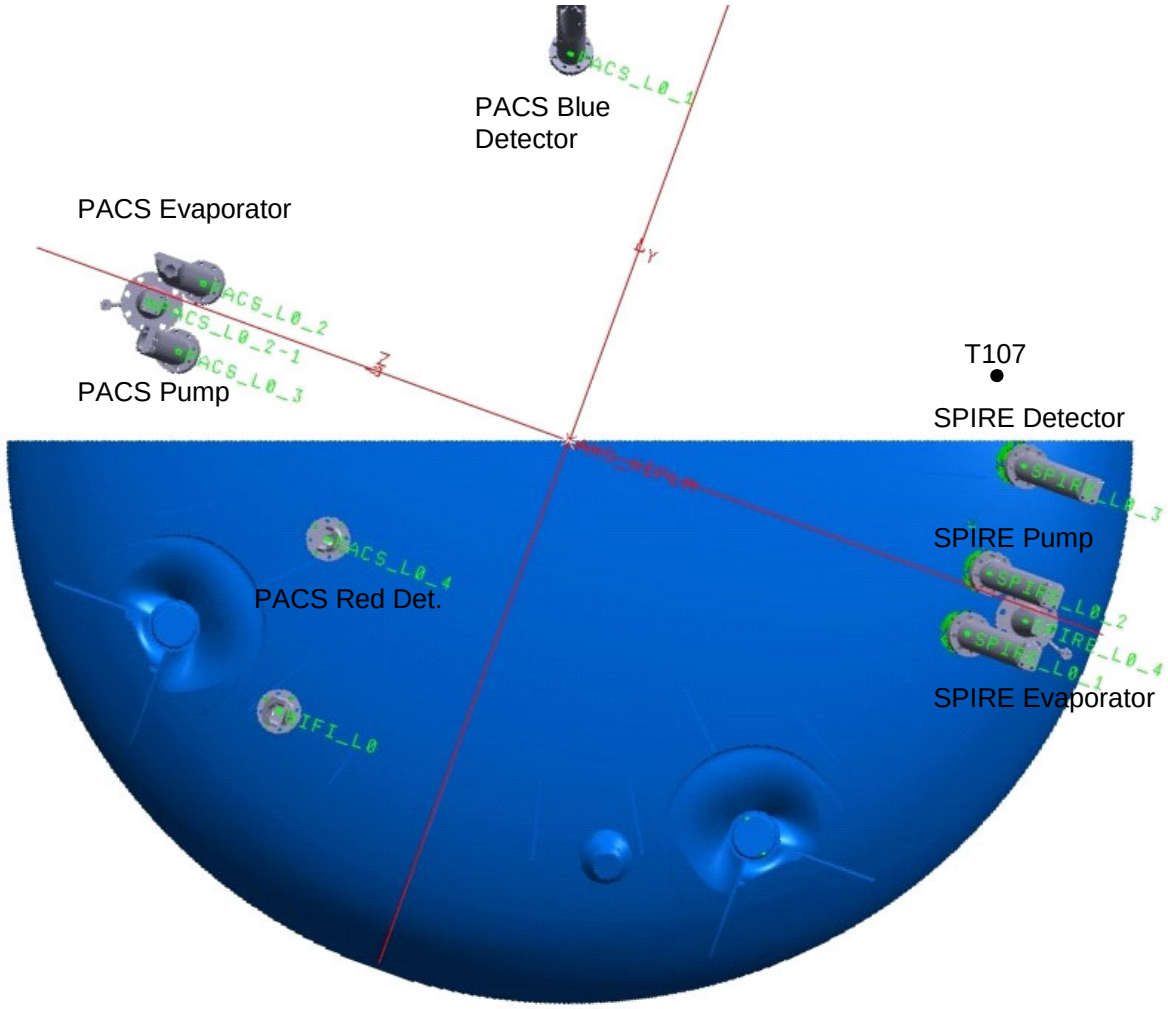

Horizontal CVV clockwise rotated by20° with 50% Filling Charge in the HTT

Figure 3.5-2: Helium Liquid Level Line during SPIRE L0 Testing

The evaluation of the thermal conductance values has been conducted in the same way as described in the previous section. The temperature gradients across the L0 thermal links versus electrical heating power are shown for each I/F separately. None of the curves ends in the origin; which indicates parasitic heat load for all the tested interfaces. To determine the parasitic heat more accurately, a best fit regression has been applied for the respective measurement data. The regression formula is included in the relevant figure. The largest parasitic heat of about 11 mW obviously existed for the SPIRE Evaporator I/F. The reason is not understood yet.

The derived PACS L0 thermal conductance values are shown in **Figure 3.5-8** versus mean temperature. Mathematical regression formulas are applied for the relevant conductance data to allow extrapolation to lower operating temperatures. The derived conductance values for SPIRE L0 are shown in **Figure 3.5-14** in comparison to the data obtained during the LSS TB/TV test.

All derived L0 I/F conductance values obtained from this extra test are also included in **Table 3.6-1**.

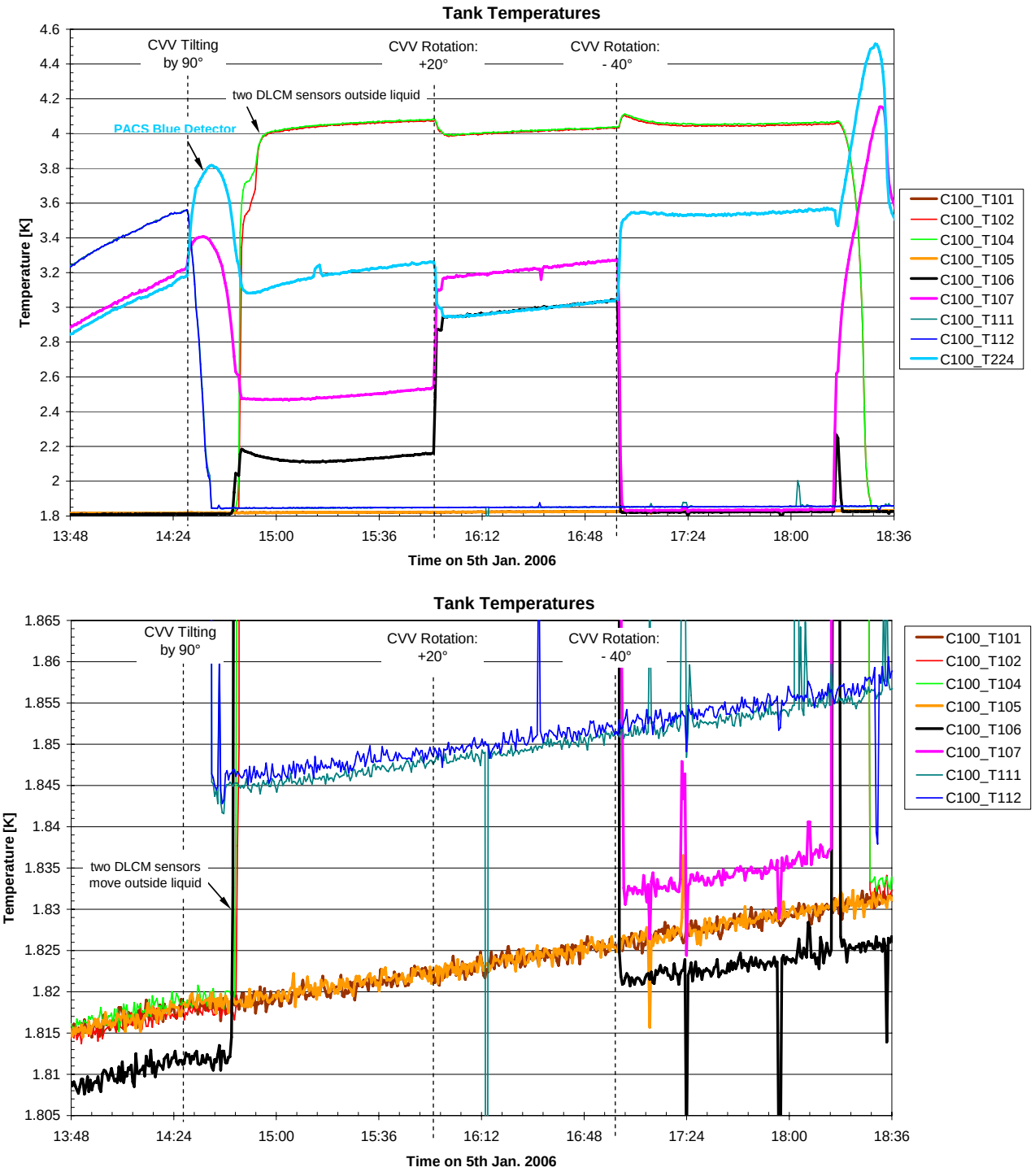

Figure 3.5-3: Temperature Evolution of all HTT Sensors during Test

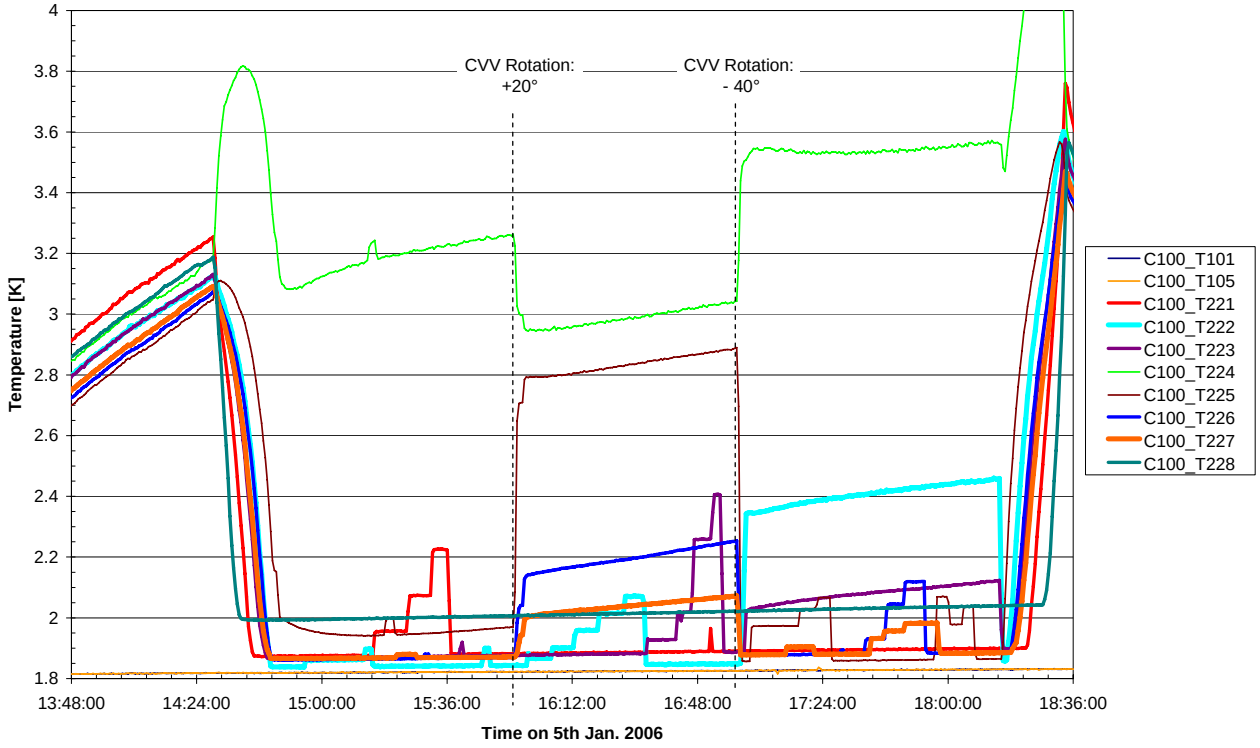

Figure 3.5-4: Temperature Evolution of all L0 Interfaces during Test

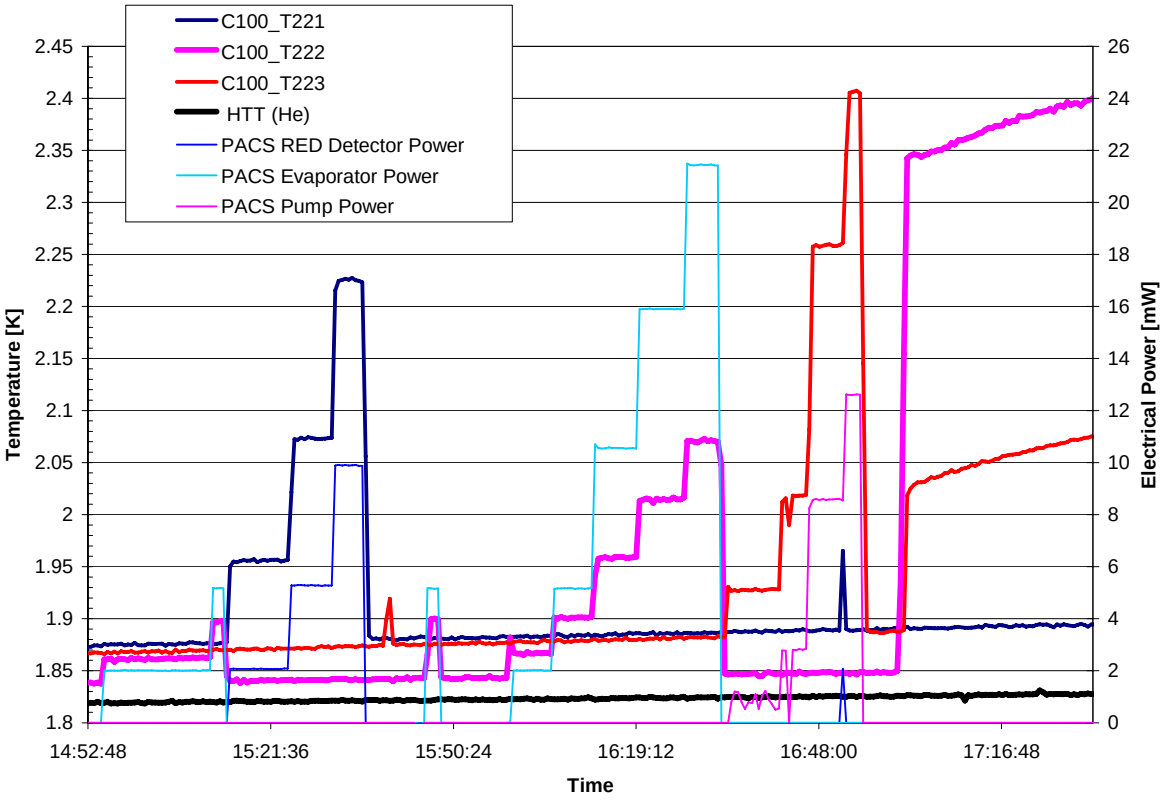

Figure 3.5-5: Power and Temperature Evolution of PACS L0 Interfaces

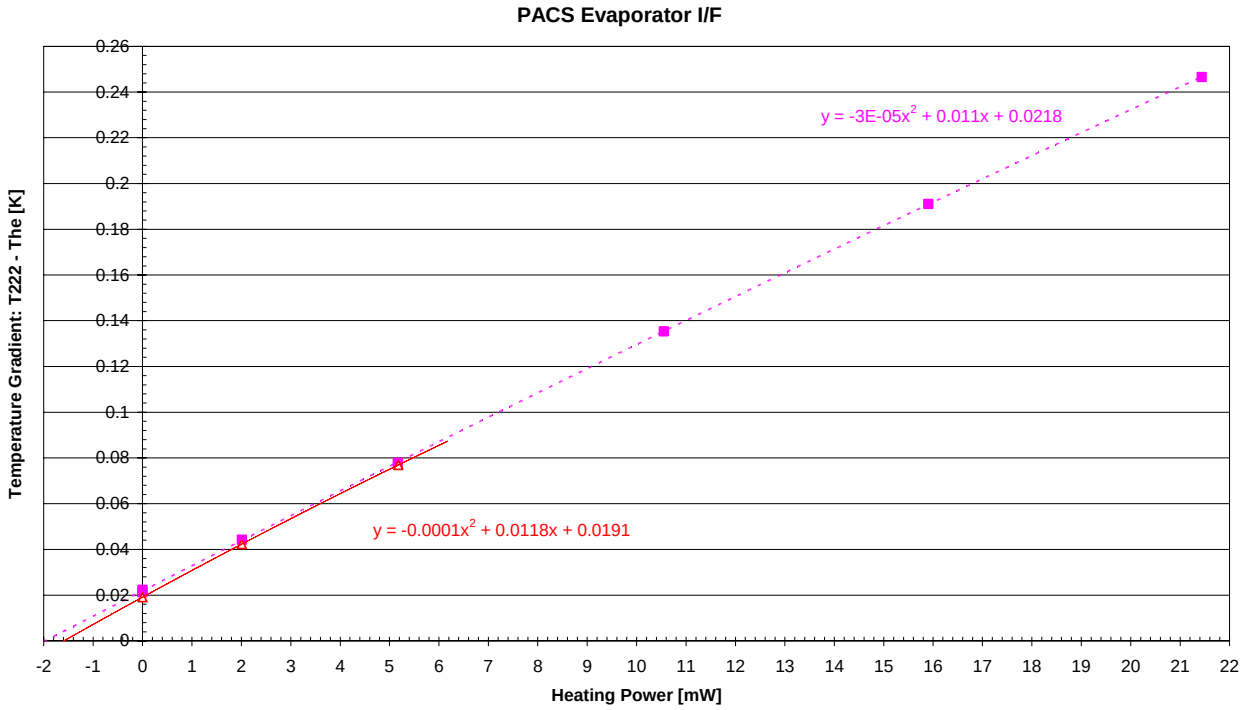

Figure 3.5-6: Temperature Gradient versus Electr. Heating Power at PACS Evaporator I/F (Open Pod)

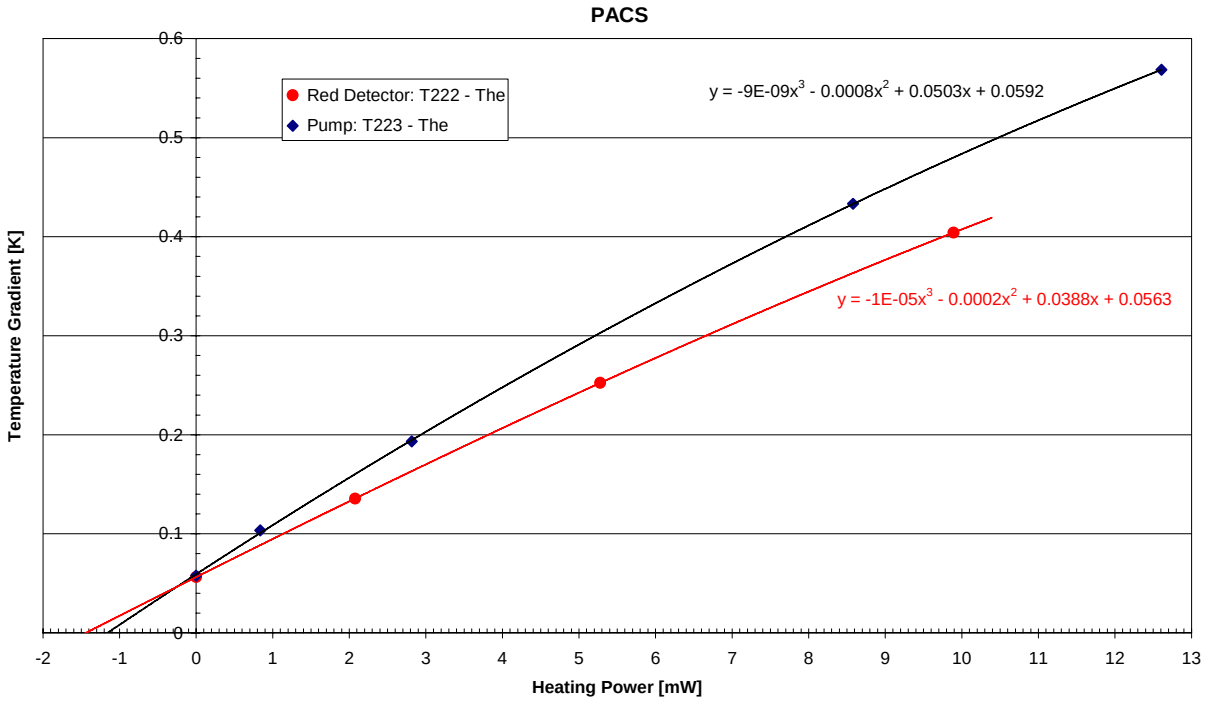

Figure 3.5-7: Temperature Gradient versus Electr. Heating Power at PACS Detector and Pump I/F

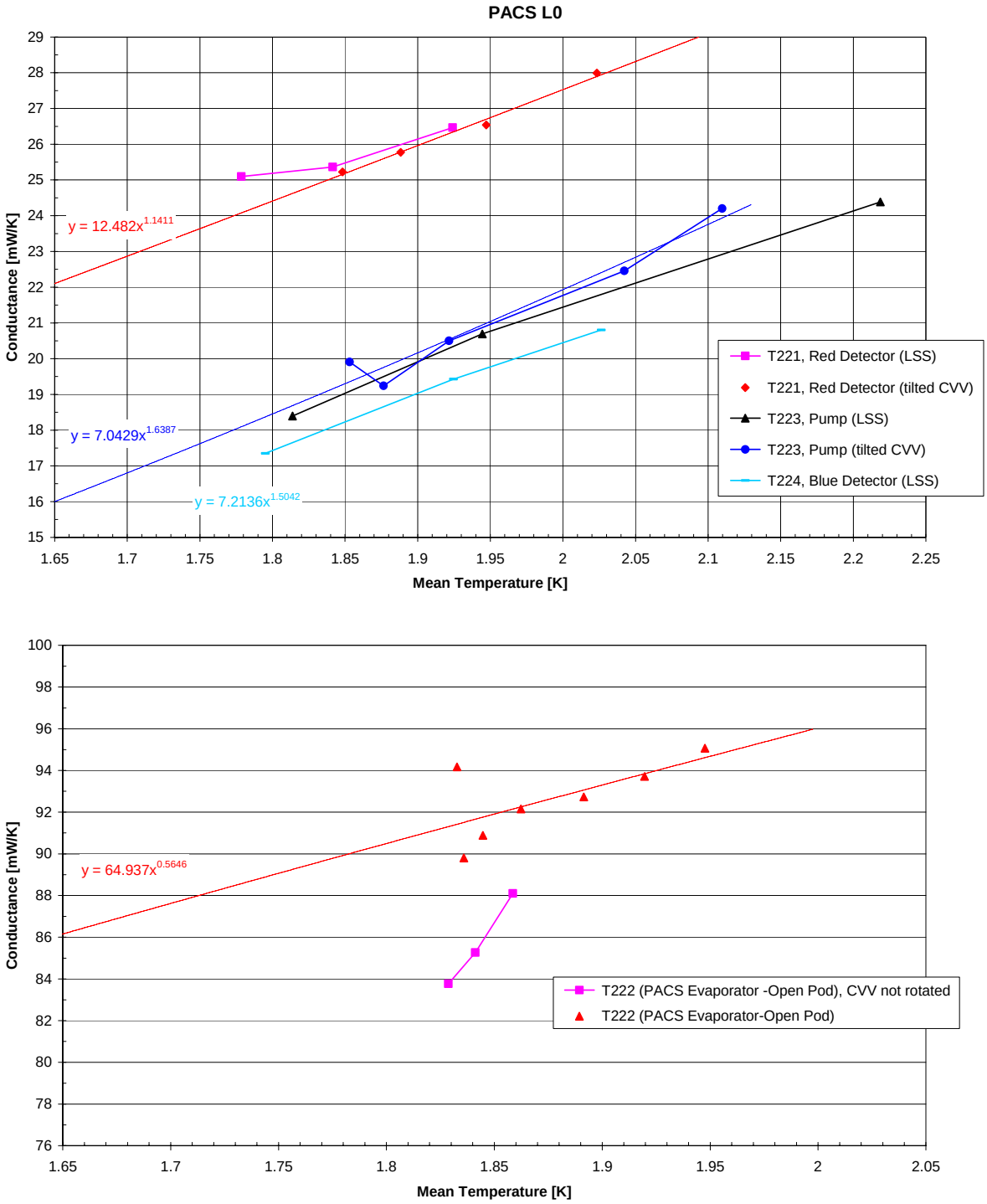

Figure 3.5-8: Thermal Conductance versus Mean Temperature for PACS L0 I/F to Helium

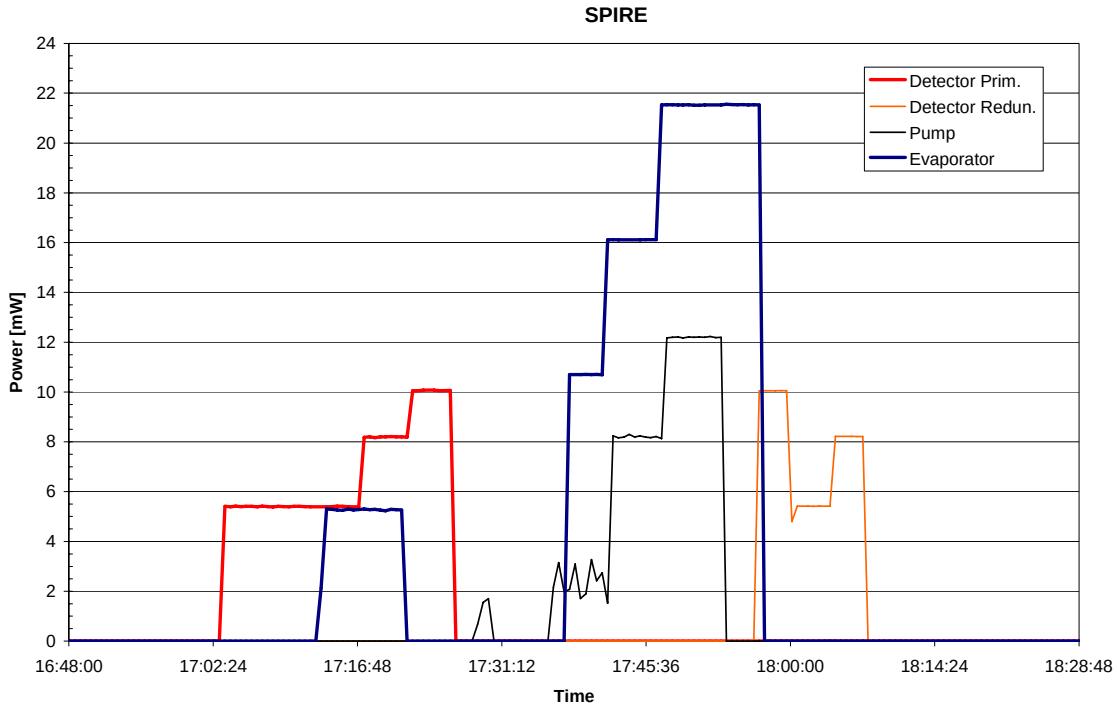

Figure 3.5-9: Electrical Power on SPIRE L0 Interfaces

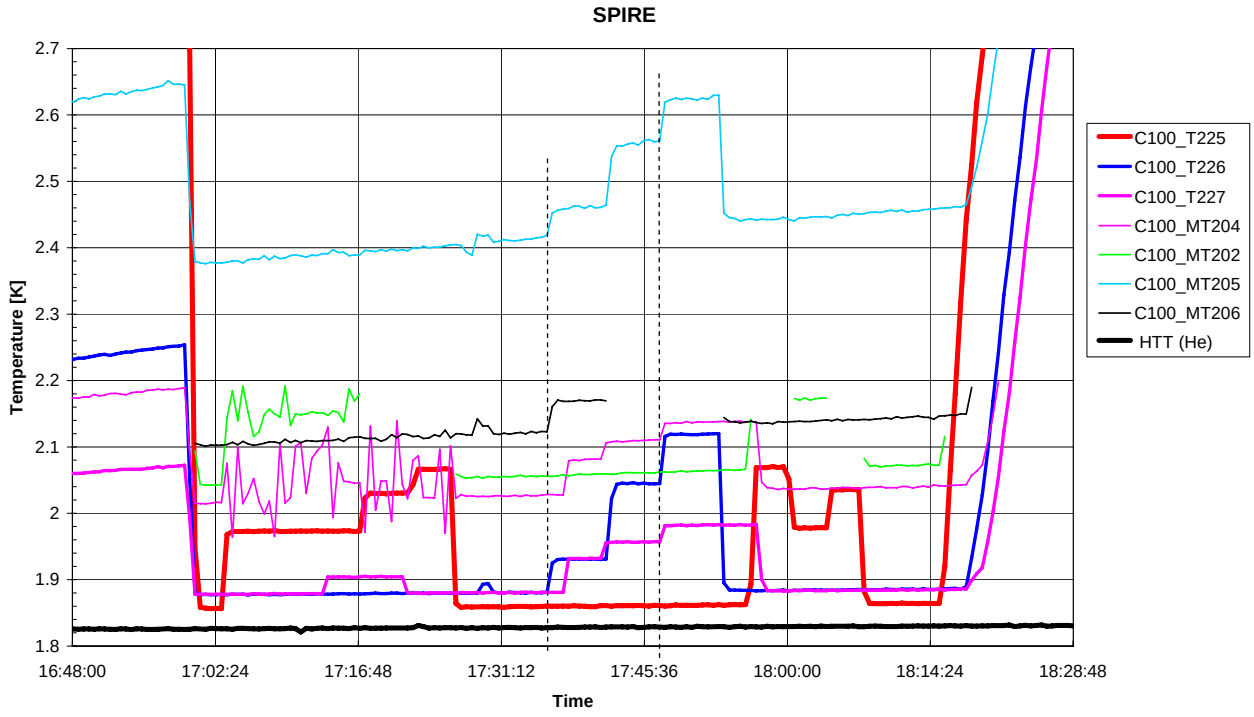

Figure 3.5-10: Temperature Evolution of SPIRE L0 Interfaces

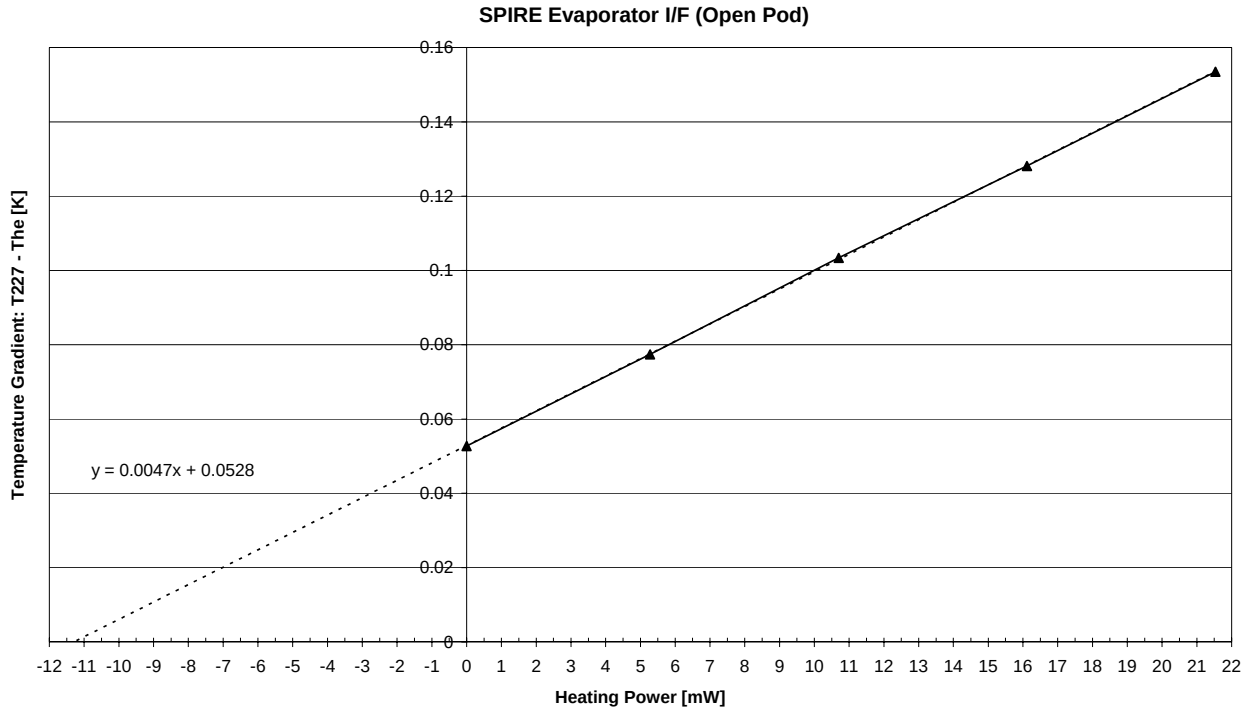

Figure 3.5-11: Temperature Gradient versus Electr. Heating Power at SPIRE Evaporator I/F (Open Pod)

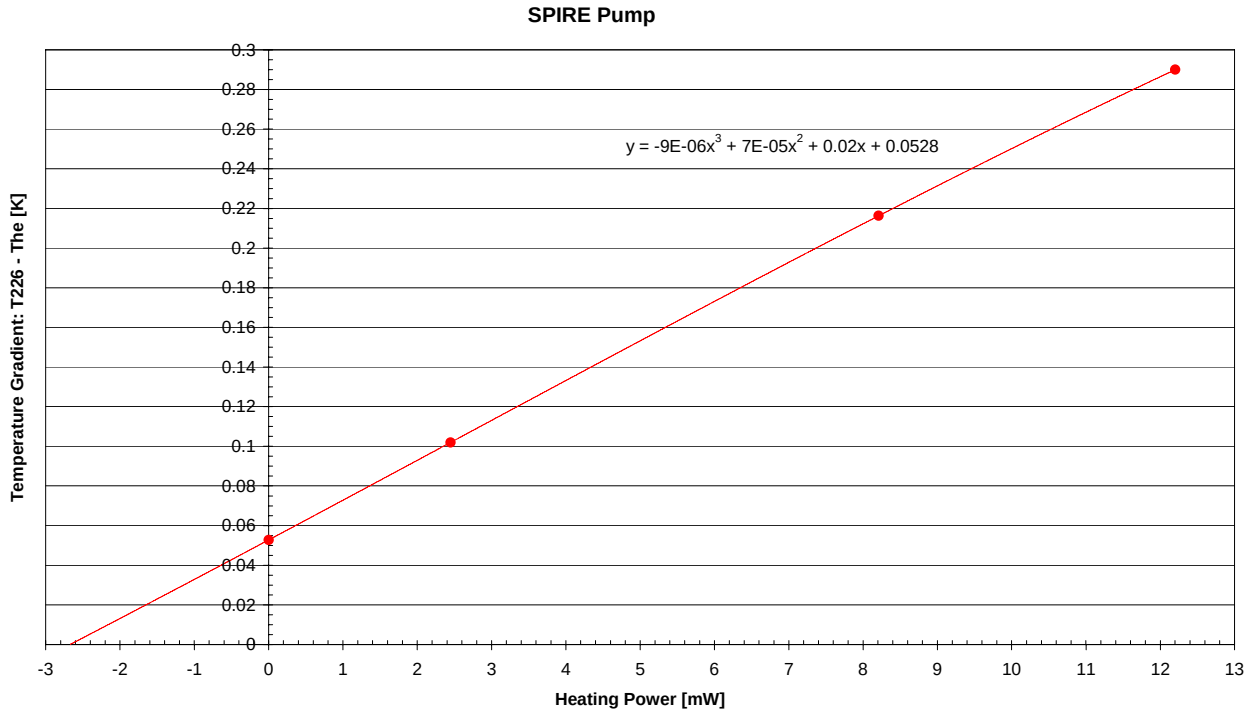

Figure 3.5-12: Temperature Gradient versus Electr. Heating Power at SPIRE Pump I/F

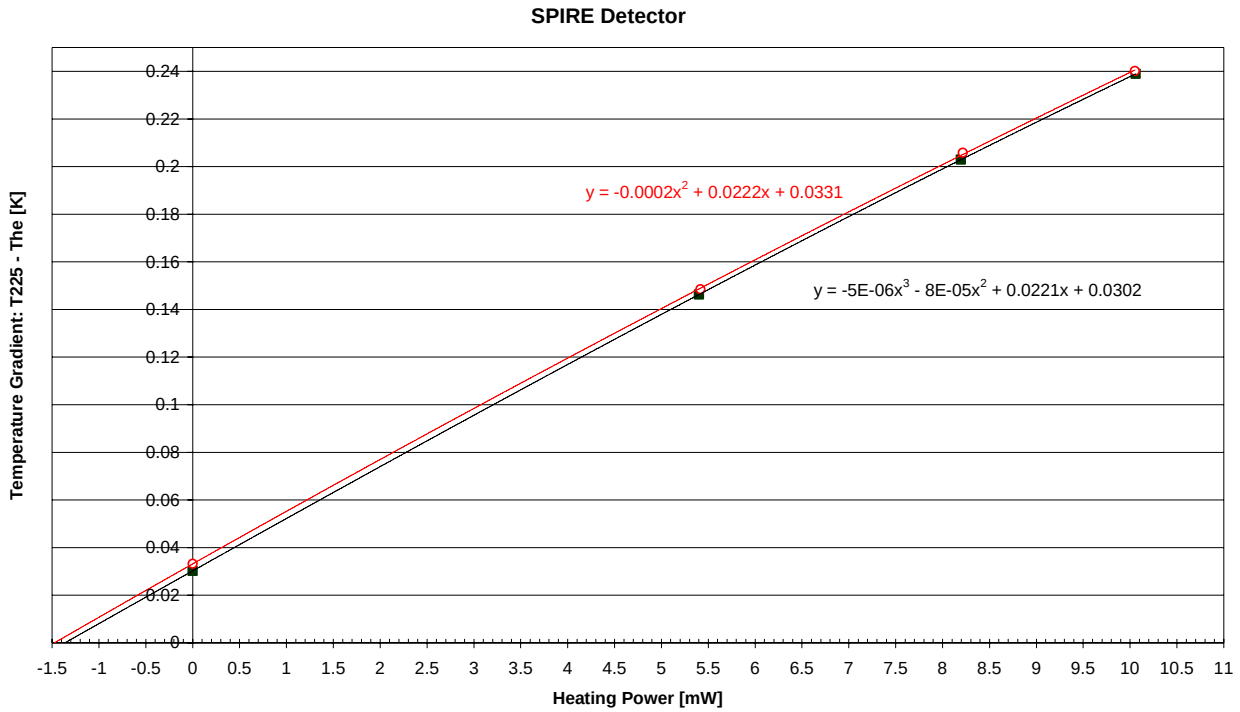

Figure 3.5-13: Temperature Gradient versus Electrical Heating Power at SPIRE Detector I/F

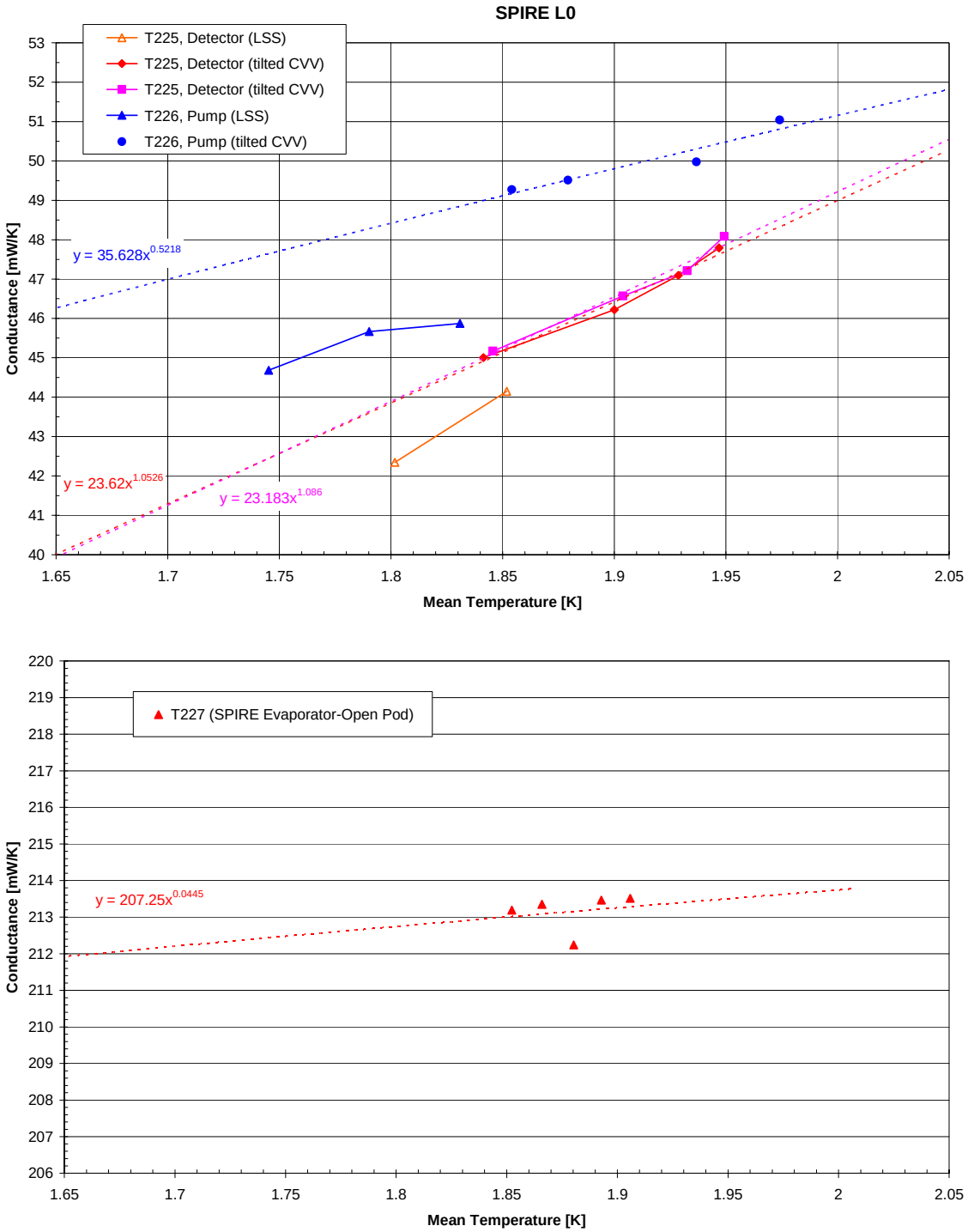

Figure 3.5-14: Thermal Conductance versus Mean Temperature for SPIRE L0 I/F to Helium

3.6 L0 Summary and Conclusion

Instrument Interface	Requirement AD 01 to AD 04	Derived Conductance		Measured Temperature in LSS	Measured Conductance in LSS	Measured Conductance with 90° tilted CVV	Conductance extrapolated to mean temperature	
		He @ 1.7K	He @1.65K				@1.70K	@1.65K
PACS Red Detector (T221)	1.75K @ 0.8mW	16 mW/K	8 mW/K	1.82K @ 2.1mW	25mW/K@1.737K He	26mW/K @1.821K He	23 mW/K	22 mW/K
PACS Blue Detect. (T224)	2.0K @ 2.0mW	6.7 mW/K	5.7 mW/K	2.11K @ 7.3mW	19mW/K@1.737K He	*not tested*	16 mW/K	15 mW/K
PACS Cooler Pump (T223)	5 K @ 2mW	0.6 mW/K	0.6 mW/K	1.89K @ 2.8mW	18mW/K@1.738K He	20mW/K @1.825K He	17 mW/K	16 mW/K
PACS Cooler Evap. (T222)	1.85K @ 15mW	100 mW/K	75 mW/K	2.0K @ 10.5mW	41mW/K@1.738K He	95mW/K @1.824K He	87 mW/K	86 mW/K
SPIRE Detector (T225)	2 K @ 4mW (1.71K@1mW)*	13.3 mW/K (100mW/K)*	11.4 mW/K (17mW/K)*	1.87K @ 5.4mW	42mW/K@1.738K He	47mW/K @1.827K He	41 mW/K	40 mW/K
SPIRE Pump (T226)	2 K @ 2mW	6.7 mW/K	5.7 mW/K	1.77K @ 2.3mW	45mW/K@1.719K He	50mW/K @1.828K He	47 mW/K	46 mW/K
SPIRE Evaporator (T227)	1.85K @ 15mW (1.75K@15mW)*	100 mW/K (300mW/K)*	75 mW/K (150 mW/K)*	1.94K @10.7mW	53mW/K@1.738K He	213mW/K @1.82K He	212mW/K	212mW/K
HIFI (MT101/102)**	2.02 K @ 6.8mW	21.3 mW/K	18.4 mW/K	2.05K @ 5.9mW** 2.17K @ 8.6 mW	19mW/K@1.737K He	*not tested*	17 mW/K	16 mW/K

*) defined as Goal

**) 10 Cu foils removed (thickness from 3.5mm to 2.5mm) as agreed by ASPI/ESA in HP-ASP-MN-6100, dated 28.02.2005

Table 3.6-1: L0 Test Data versus Instrument Requirements

All L0 thermal link performances are within the requirements except for the PACS cooler evaporator when operating at a mean temperature above 1.674K (corresponds to He @ 1.668K for 1mW heat flux) and HIFI. Note that the HIFI thermal link thickness was reduced by 28% due to instrument I/F mechanical load requirements.

4 Thermal Performance of L1 Interfaces

4.1 Conditions during L1 Performance Measurement

The L1 measurement has been performed during the test phase TP4 from 21.-23.October 2005 and during TP6 from 29.-31.October 2005 applying different electrical heating power on the L1 MTD's. During TP4 the spacecraft was tilted by 14° and the helium filling level was about 90%. The mass flow was routed via PPS (valve V106 open) and adjusted to about 2.3 mg/s, see **Figure 4.1-2**. For evaluation the average mass flow (red line) calculated by the excel AVERAGE routine has been used.

In TP6 L1 measurement has been performed with a higher mass flow of about 4.7 mg/s, see **Figure 4.1-5**. During TP6 the venting helium was not routed via PPS (valve V104 open) and therefore the spacecraft was not tilted.

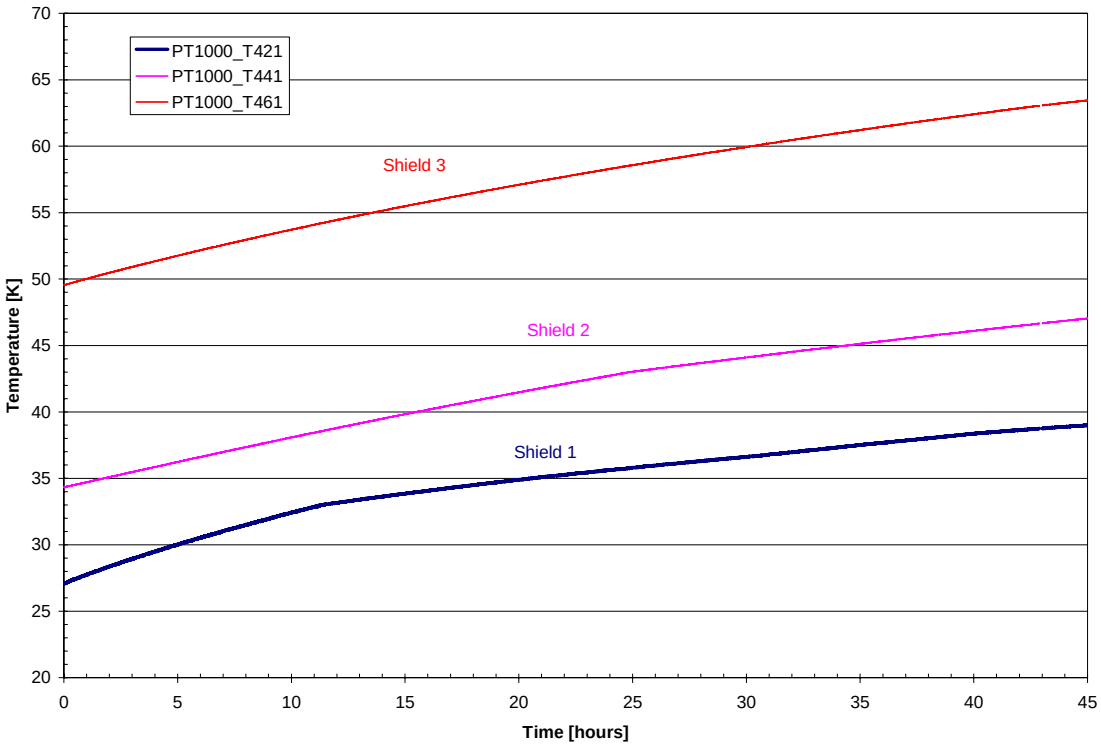

Figure 4.1-1: Temperature Evolution of the Thermal Shields during TP4

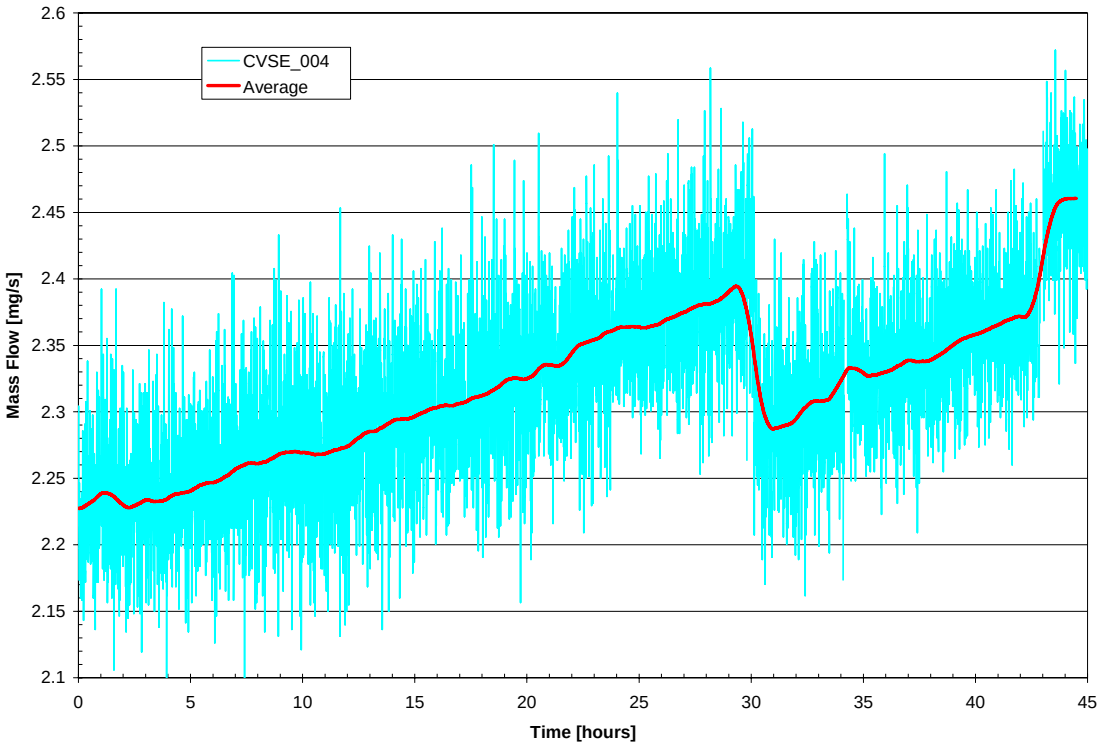

Figure 4.1-2: Mass Flow Evolution during TP4

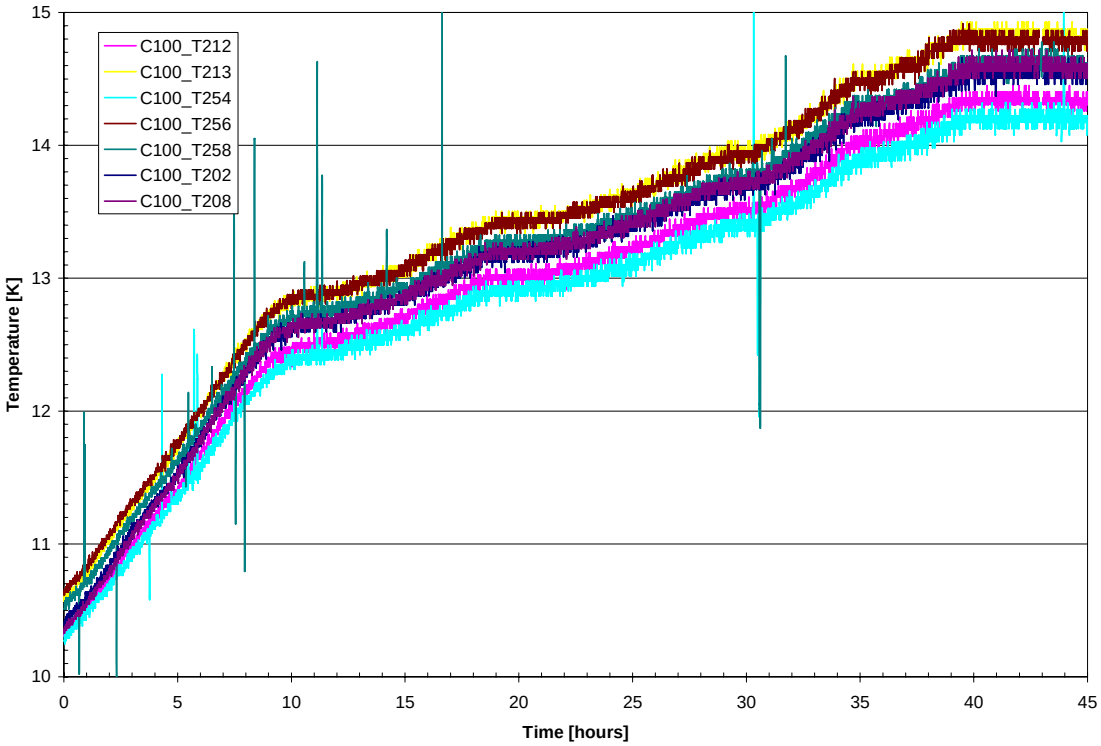

Figure 4.1-3: Temperature Evolution of Optical Bench Plate (L2) during TP4

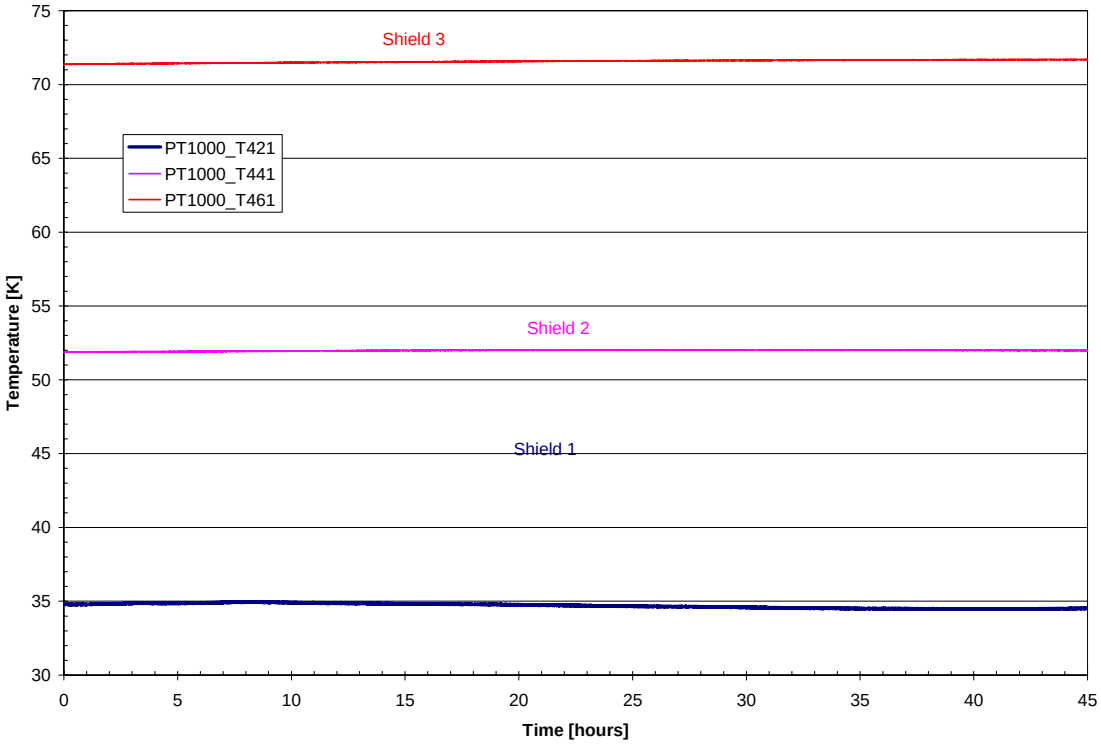

Figure 4.1-4: Temperature Evolution of the Thermal Shields during TP6

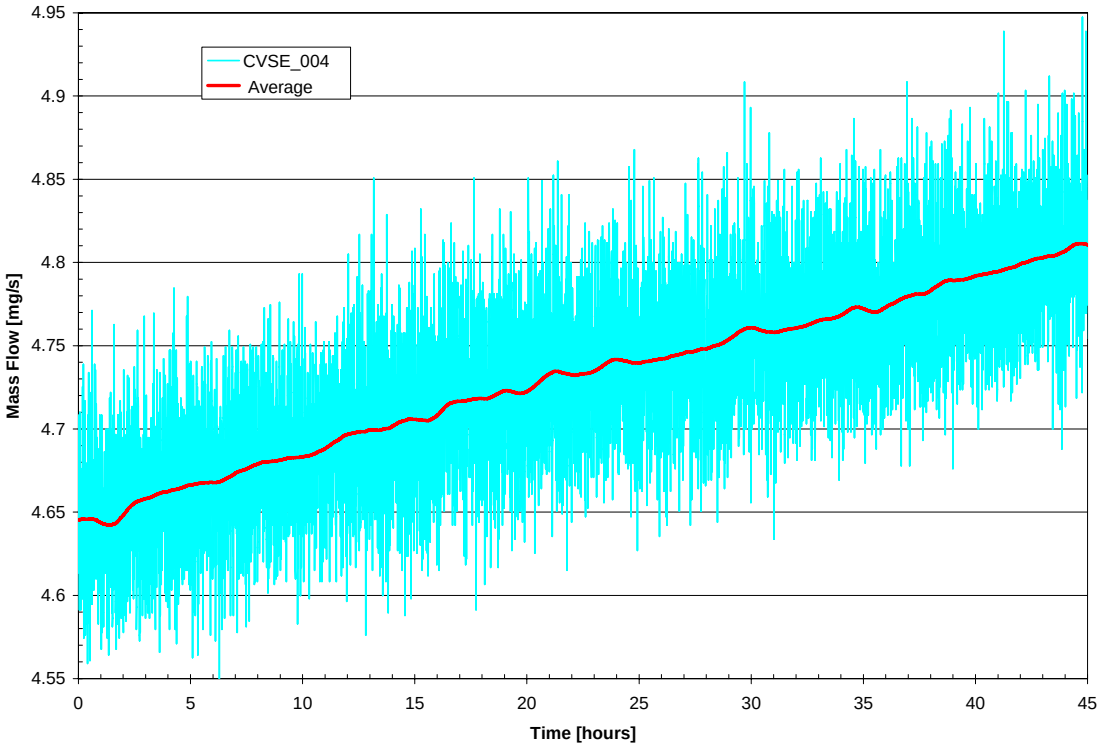

Figure 4.1-5: Mass Flow Evolution during TP6

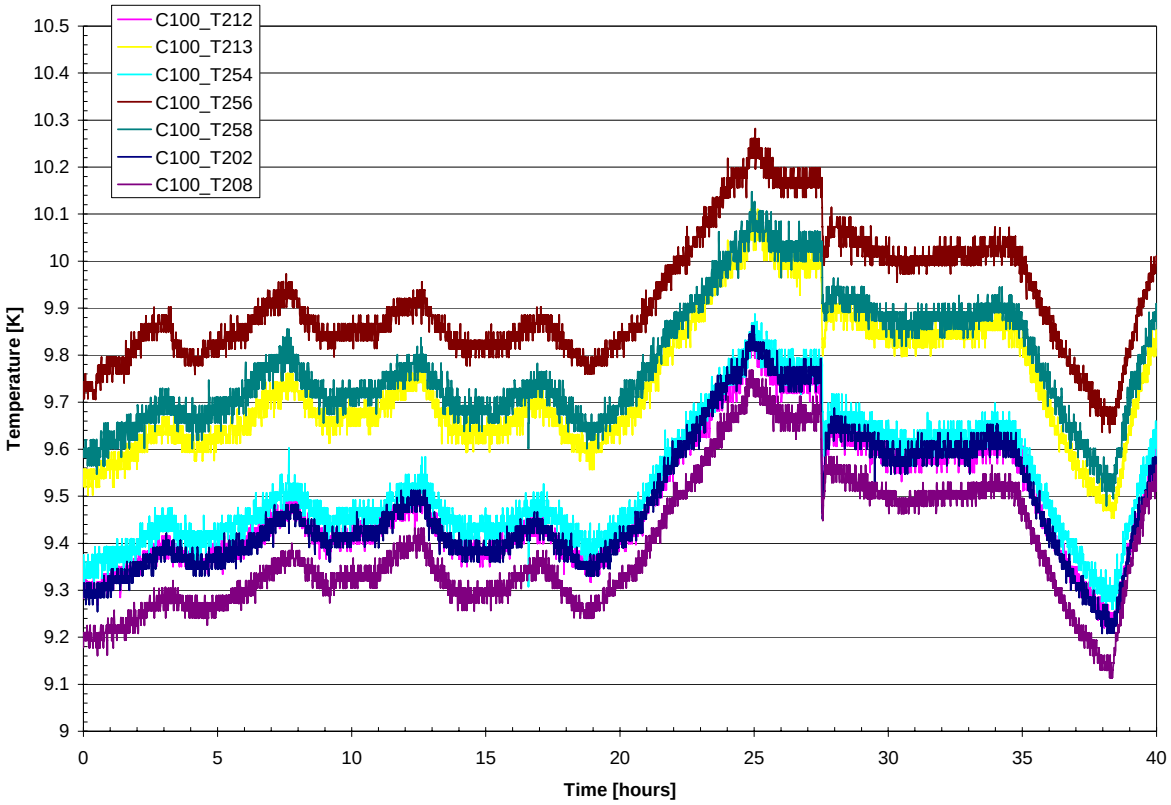

Figure 4.1-6: Temperature Evolution of Optical Bench Plate (L2) during TP6

An unexpected temperature behaviour was observed on the ventline sensors during TP6, when the large mass flow (~2 times predicted in-orbit rate) was venting from the HTT via the HTT outlet valve V104 instead of via the PPS as in nominal flight operations. An overview on the applied MTD electrical power during TP6 and the corresponding response of the helium ventline temperature distribution is given in **Figure 4.1-7**: When the HIFI L1 heater was switched on, a response on all L1 ventline sensors (T231-T237) was observed, with the upstream sensors going to lower temperatures than before. This behaviour repeated during all L1 heating operations, most significantly on T231 when the PACS heaters were operated. To further assess the phenomenon, the SPIRE L1 heater was switched on in addition to the PACS heaters, which caused a further decrease of the T231 and also of the PACS L1 vent-line sensors T232-T235. Individual temperature peaks, reaching about the previous level, simultaneously occurred on the L1 sensors without an obvious cause. The HIFI L1 heater was switched on in addition, but this showed no further impact. HIFI and SPIRE L1 heaters were then switched off again.

Such behaviour was not observed during TP4 when the nominal mass flow rate was routed via the nominal vent path including the PPS.

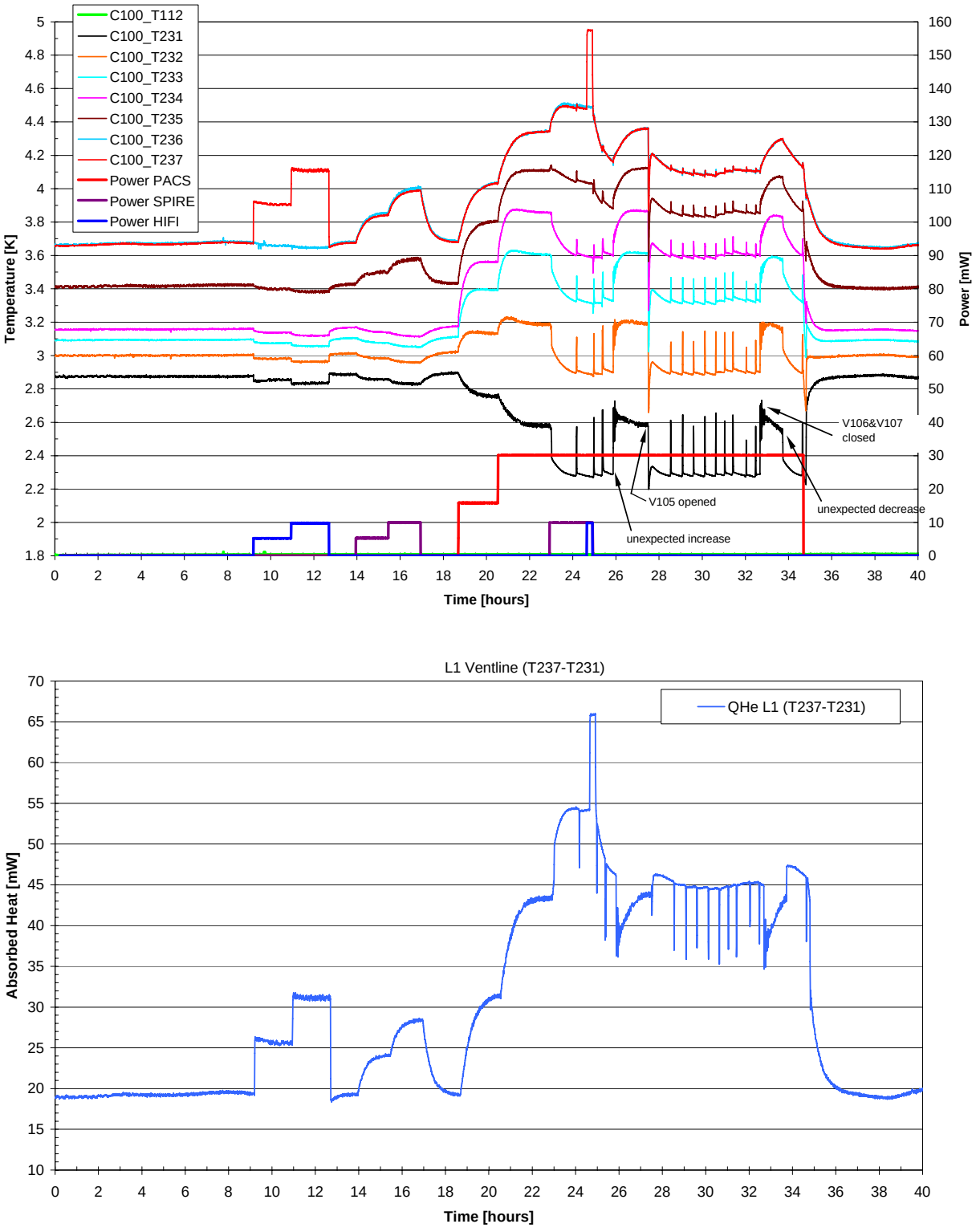

Figure 4.1-7: Temperature, Power and Absorbed Heat Evolution of L1 Ventline during TP6

4.2 PACS (TP4)

The PACS L1 I/F consists of three flexible copper straps attached to the helium ventline. The first copper strap (so called Photometer I/F) is attached near the L1 inlet and is equipped with an FM temperature sensor (T242) as shown in **Figure 4.2-1**. Since the other two copper straps don't have FM sensors the installed MTD sensors are taken for thermal conductance evaluation.

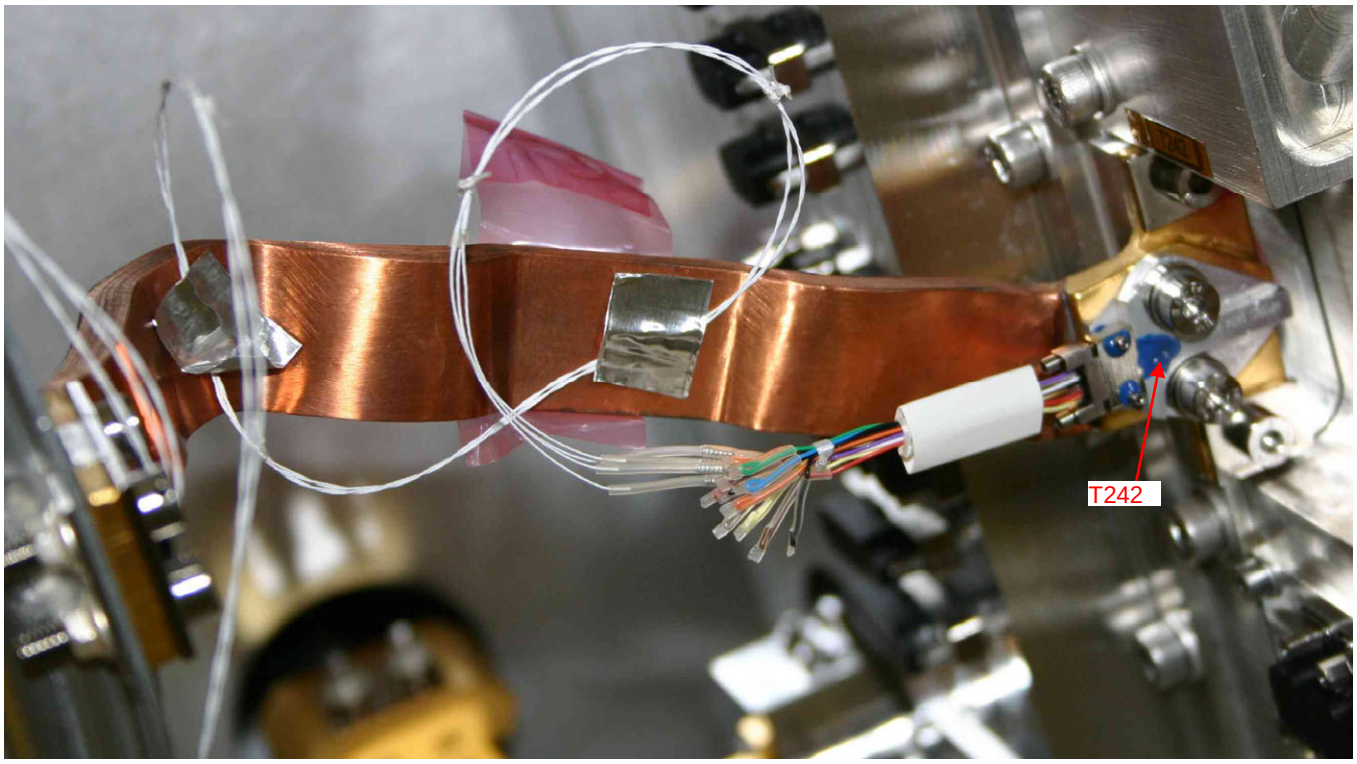

Figure 4.2-1: Temperature Sensor T242 – PACS L1 FPU I/F (Photometer)

The PACS L1 electrical power and temperature evolution is shown in **Figure 4.2-2**. Because the temperature readouts of the ventline inlet sensor T231 were not available during TP4 (NCR 1649) the temperature data obtained from sensor T112 (PPS) have been used instead. The temperature gradients along the ventline as well as between PACS MTD (L1) and ventline are shown in **Figure 4.2-3**. Considering the three individual copper straps and the intermediate ventline sensors no straight curves are achieved. The reason is, that due to the conductivity of the MTD itself (Al 6061) part of the electrical power applied on one I/F is rejected to the ventline via the two other interfaces (copper straps). However, using the total gradient between PACS outlet and inlet (represented by T112) lead to a straight line which allows a determination of about 6.7 mW parasitic heat load to the L1 ventline from HTT to the last PACS L1 I/F upstream (T234). Due to the short venting path through the HTT tubing via PPS and V106, the most significant part of this parasitic heat is considered to be coming via the PACS mounting feet attached to the warmer Optical Bench Plate (OBP).

The heat absorbed by the helium mass flow can be calculated by multiplying this gradient with the heat capacity of the helium gas (i.e. 5.2 kJ/kg/K). This absorbed heat is shown in **Figure 4.2-4** versus the electrical power applied at the MTD. This demonstrates a good correspondence between the heat absorbed

by the helium and the heat flow across the MTD L1 I/F consisting of the electrical power plus 6.7 mW parasitic, also shown in **Figure 4.2-4**.
The calculated L1 I/F conductance related to the PACS ventline outlet (T234) is shown in **Figure 4.2-5** versus mean temperature (average of MT313/314 and T234).

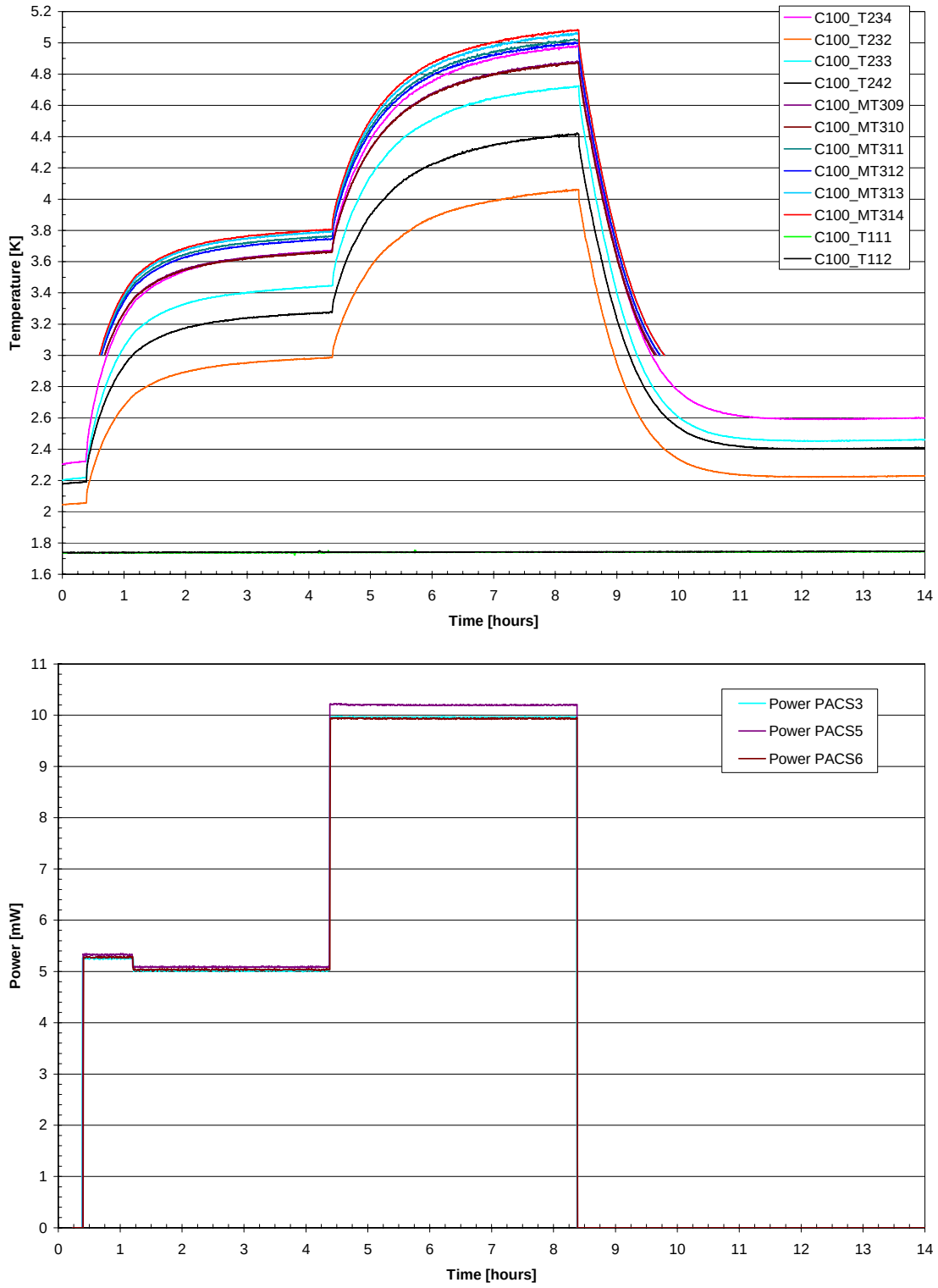

Figure 4.2-2: PACS L1 Electrical Power and Temperature Evolution during TP4

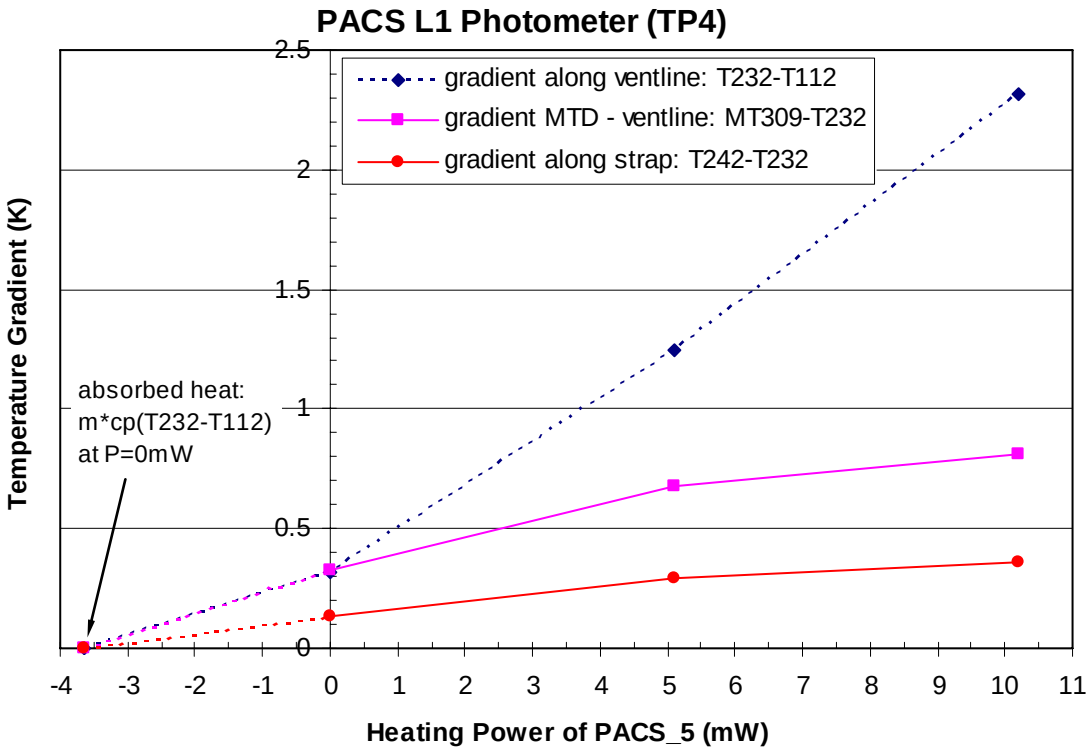
PACS L1 Photometer (TP4)
gradient along ventline: T232-T112
gradient MTD - ventline: MT309-T232
gradient along strap: T242-T232
absorbed heat:
m*cp(T232-T112)
at P=0mW
Temperature Gradient (K)
Heating Power of PACS_5 (mW)
2.5
2
1.5
1
0.5
0
-4 -3 -2 -1 0 1 2 3 4 5 6 7 8 9 10 11

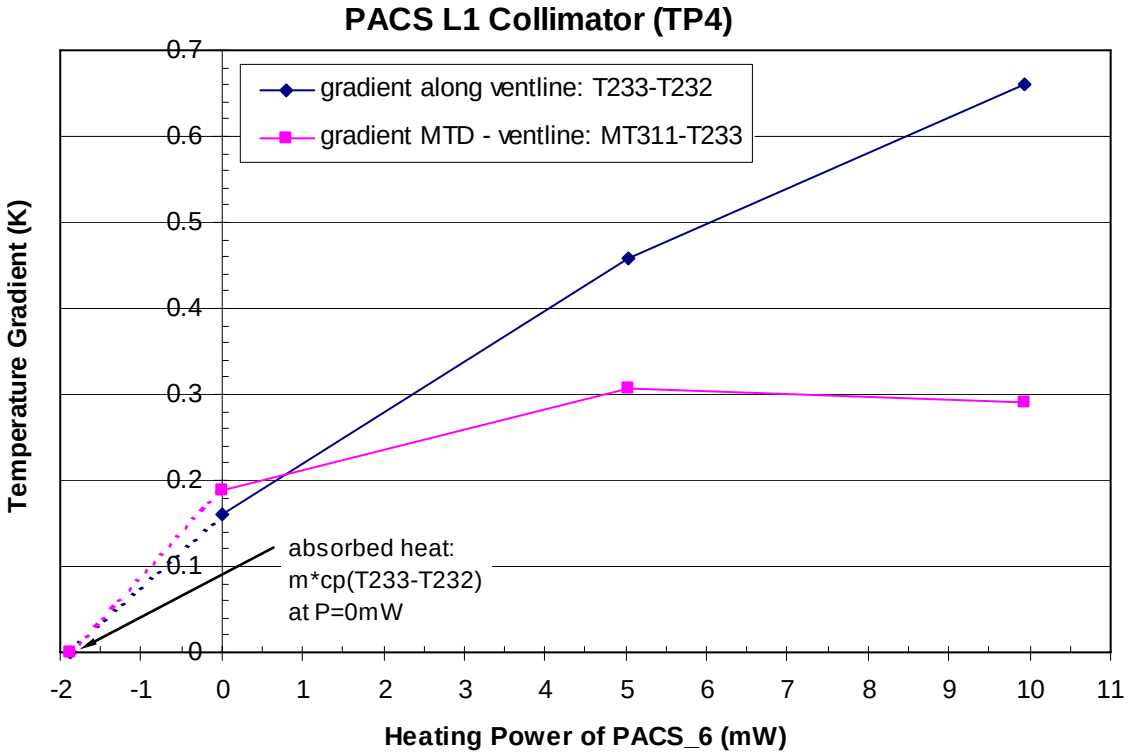
PACS L1 Collimator (TP4)
gradient along ventline: T233-T232
gradient MTD - ventline: MT311-T233
absorbed heat:
m*cp(T233-T232)
at P=0mW
Temperature Gradient (K)
Heating Power of PACS_6 (mW)
0.7
0.6
0.5
0.4
0.3
0.2
0.1
0
-2 -1 0 1 2 3 4 5 6 7 8 9 10 11

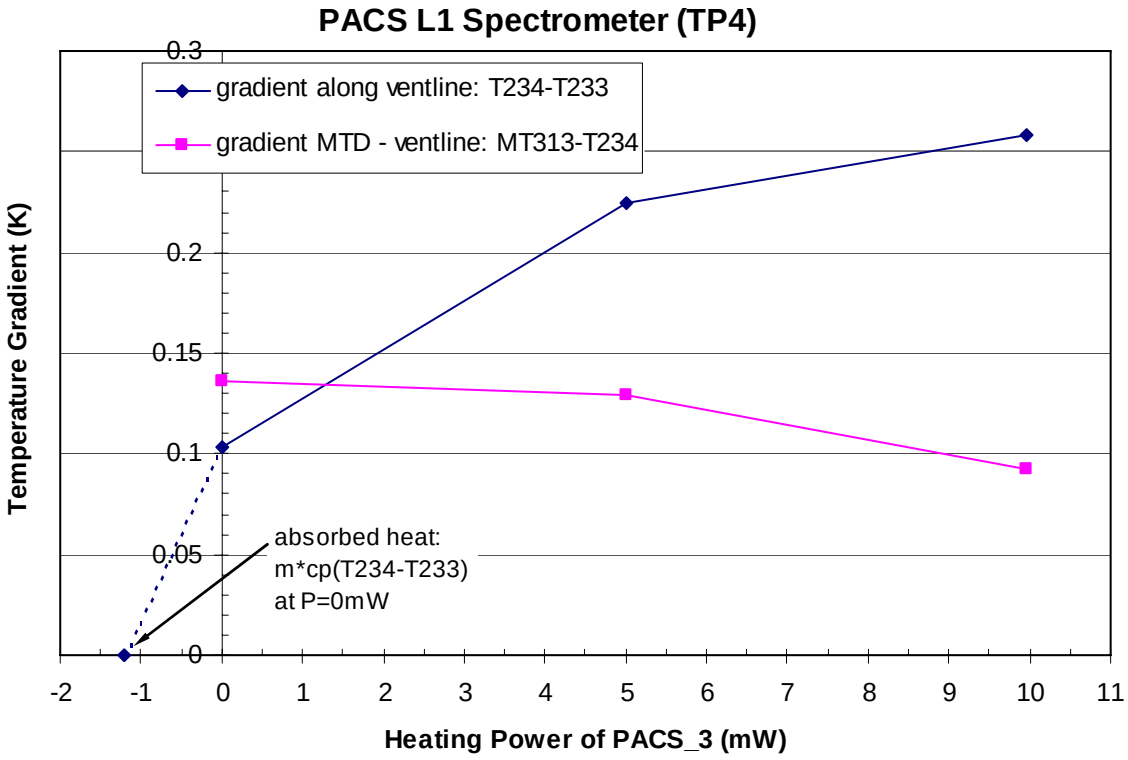

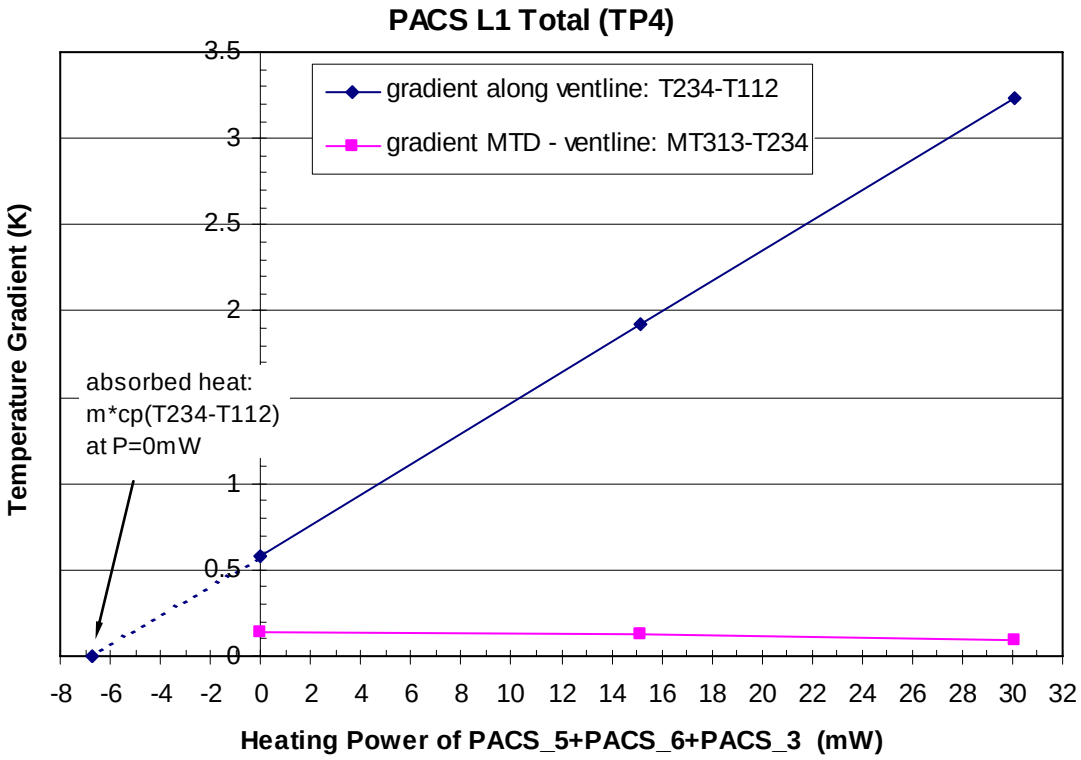

Figure 4.2-3: PACS Temperature Gradients versus Heating Power (TP4)

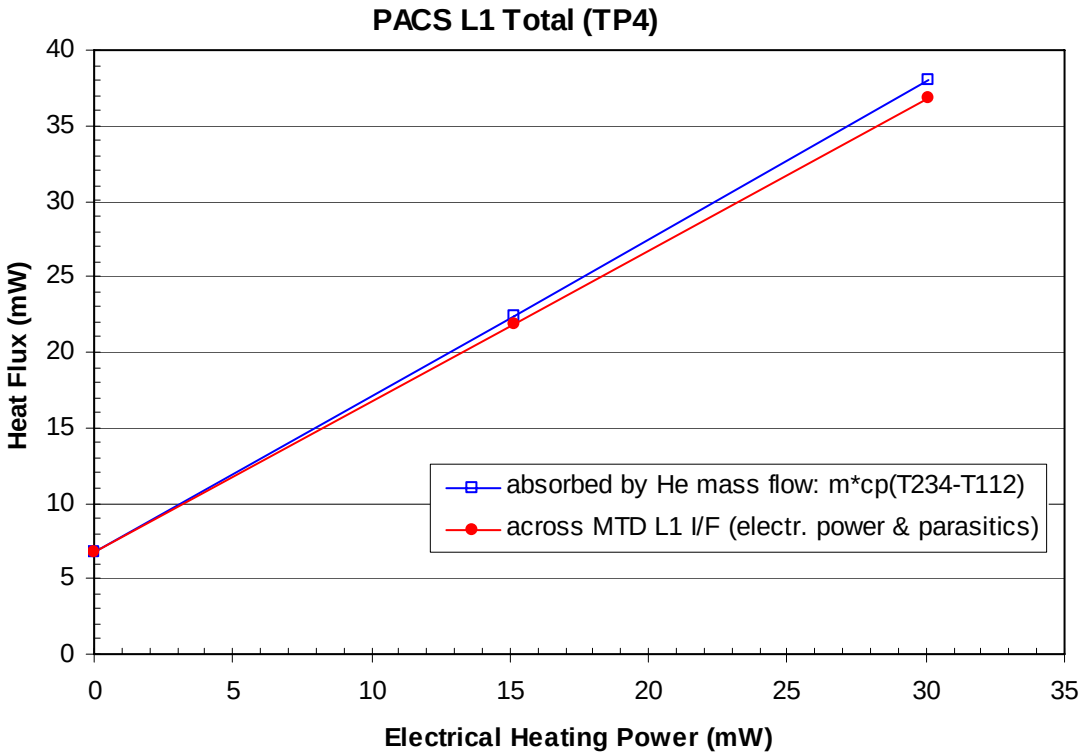

Figure 4.2-4: PACS L1 Interface Heat Flows (TP4)

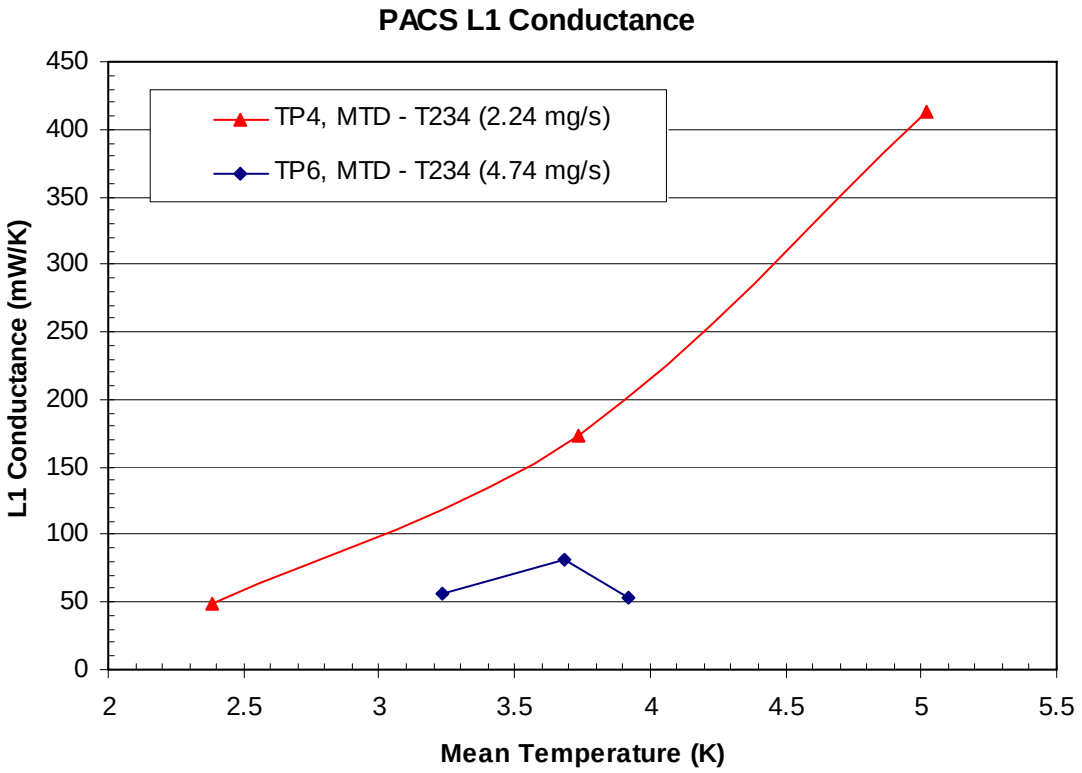

Figure 4.2-5: PACS L1 Thermal Interface Conductance (TP4 and TP6)

4.3 SPIRE (TP4)

The SPIRE L1 I/F consists of two flexible copper straps attached to the helium ventline close together. One of the copper straps is equipped with the FM temperature sensor T248 as shown in **Figure 4.3-1** together with the SPIRE ventline outlet sensor T236.

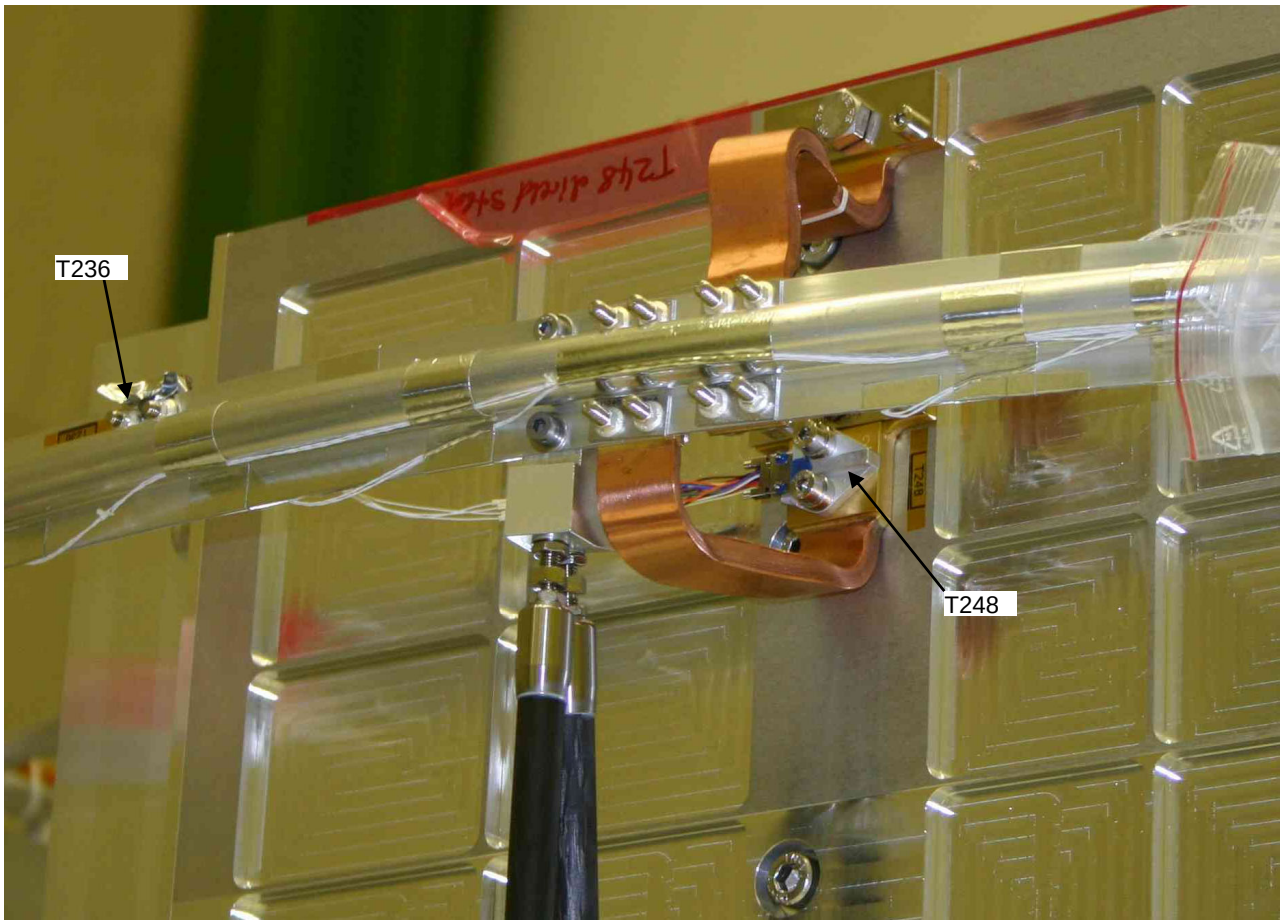

Figure 4.3-1: Temperature Sensor T248 – SPIRE L1 FPU I/F

The SPIRE L1 temperature evolution is shown in **Figure 4.3-2** for the whole TP4 test phase and in **Figure 4.3-3** for the SPIRE operational phase. **Figure 4.3-2** shows, that the PACS operation is clearly seen by the SPIRE sensors.

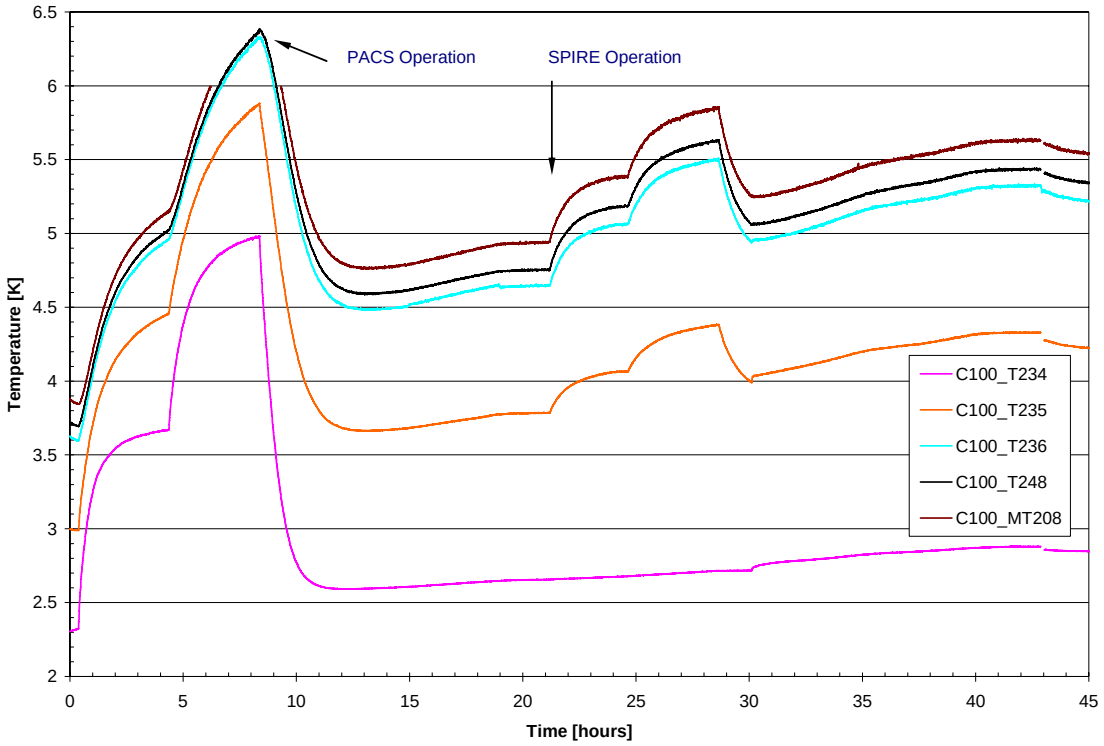

Figure 4.3-2: SPIRE L1 Temperature Evolution during TP4

The temperature gradient along the ventline as well as between SPIRE MTD (L1) and ventline is shown in **Figure 4.3-4**. The temperature gradient between SPIRE outlet (T236) and inlet (T234) along the ventline show a straight line that allows a determination of about 24 mW parasitic heat load to the L1 ventline via the SPIRE mounting feet attached to the warmer Optical Bench Plate (OBP). The parasitic heat load of SPIRE is more than 3 times higher compared to PACS, because the steel feet of SPIRE have a higher thermal conductance than the CFRP feet of PACS. Note, that for the SPIRE inlet the sensor T234 is taken, because the sensor T235 already shows a temperature increase in case of SPIRE heating, see **Figure 4.3-2**. This means that heat from the SPIRE L1 copper straps is conducted upstream along the ventline wall material towards the sensor T235 which is located about 150 mm apart from the SPIRE strap I/F (for temperature sensors location see also **Figure 5.1-1**).

The heat absorbed by the helium mass flow is shown in **Figure 4.3-5** versus the electrical power applied at the MTD. This demonstrates a good correspondence between the heat absorbed by the helium and the heat flow across the MTD L1 I/F consisting of the electrical power plus 24.2 mW parasitic, also shown in **Figure 4.3-5**.
The calculated L1 I/F conductance related to the SPIRE ventline outlet (T236) is shown in **Figure 4.3-6** versus mean temperature (average of MT207/208 and T236). For comparison the conductance between copper strap I/F at MTD side (T248) and ventline outlet (T236) is shown, too.

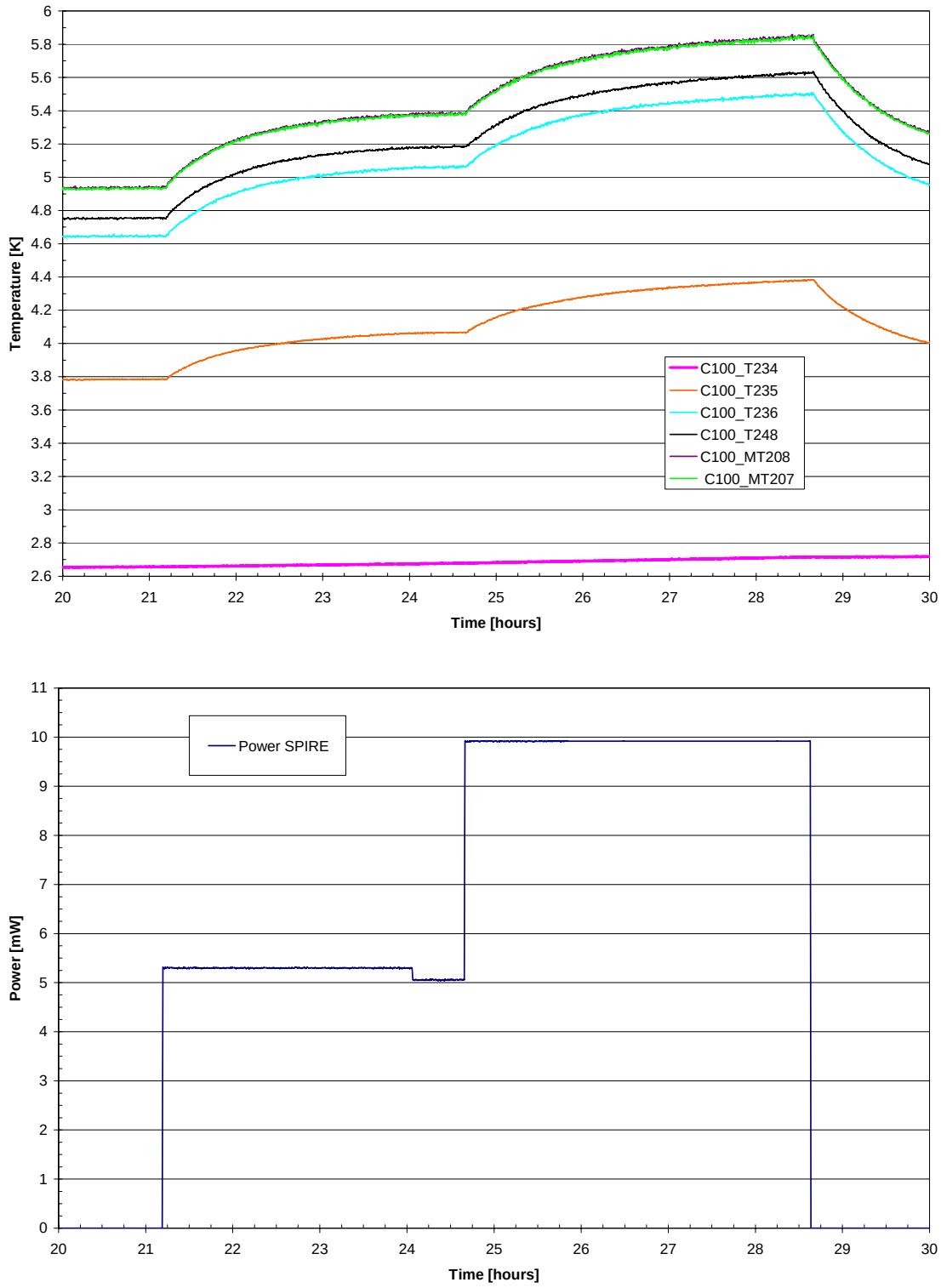

Figure 4.3-3: SPIRE L1 Power and Temperature Evolution during Operation TP4

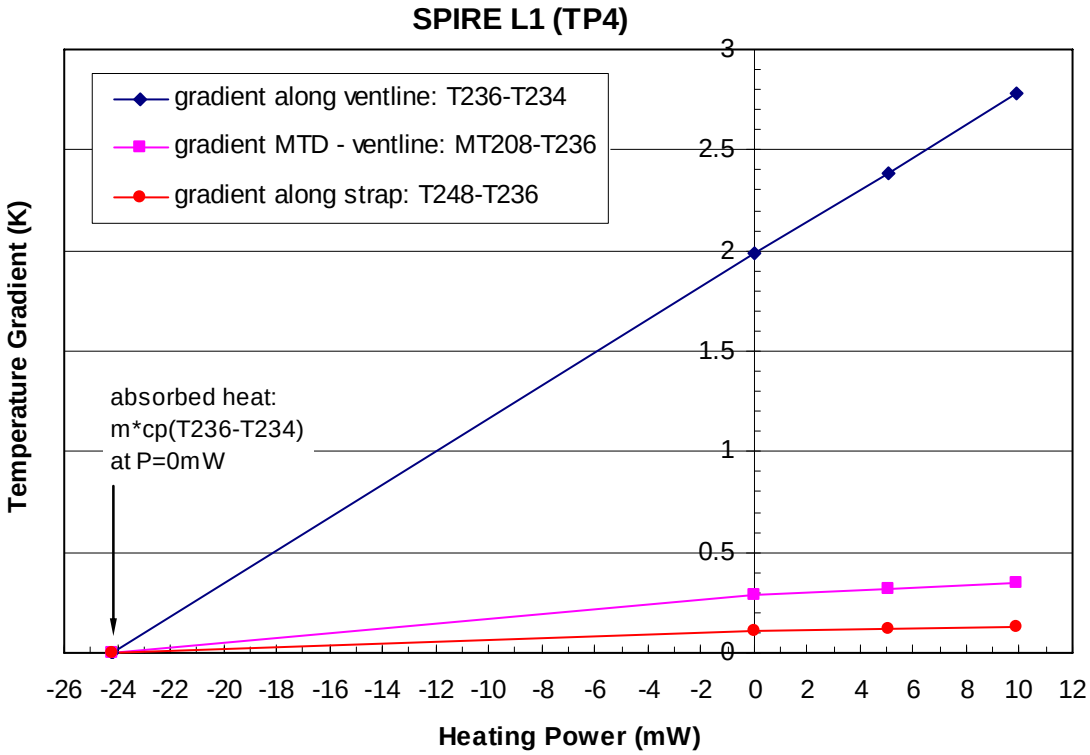

Figure 4.3-4: SPIRE Temperature Gradients versus Heating Power (TP4)

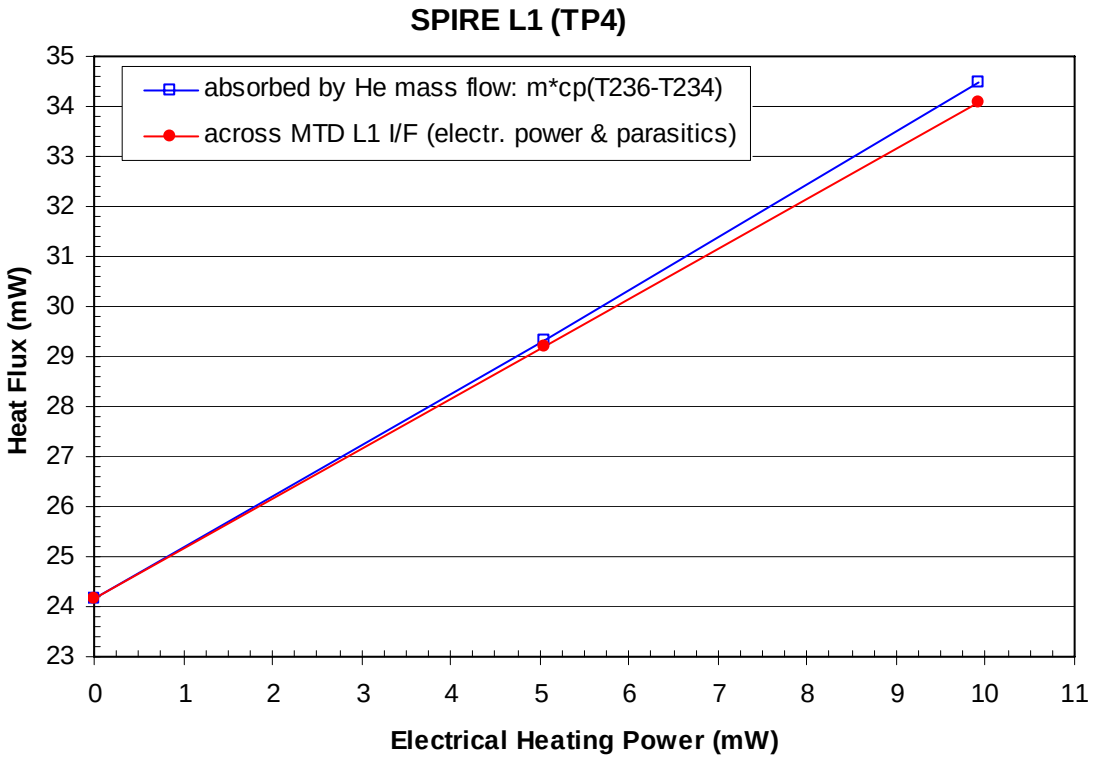

Figure 4.3-5: SPIRE L1 Interface Heat Flows (TP4)

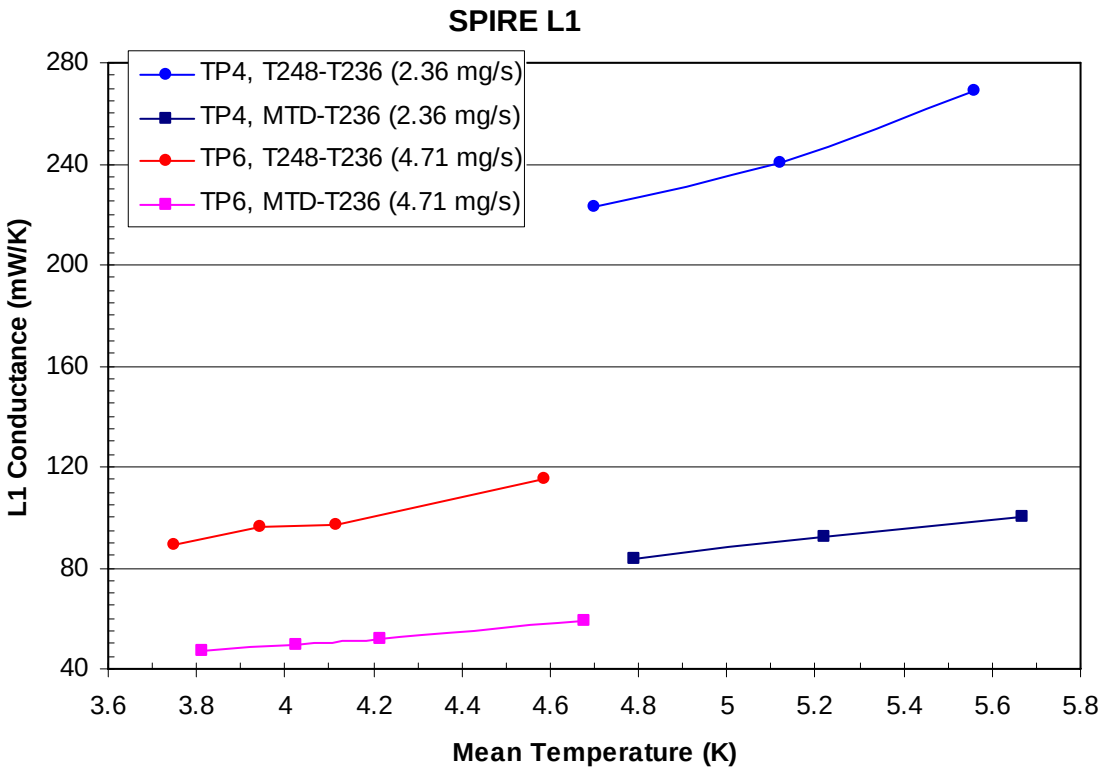

Figure 4.3-6: SPIRE L1 Interface Conductance (TP4 and TP6)

4.4 HIFI (TP4)

The HIFI L1 I/F is represented by one copper cooling strap. **Figure 4.4-1** shows the relevant FM sensor T244 attached to the copper strap near the HIFI MTD I/F.

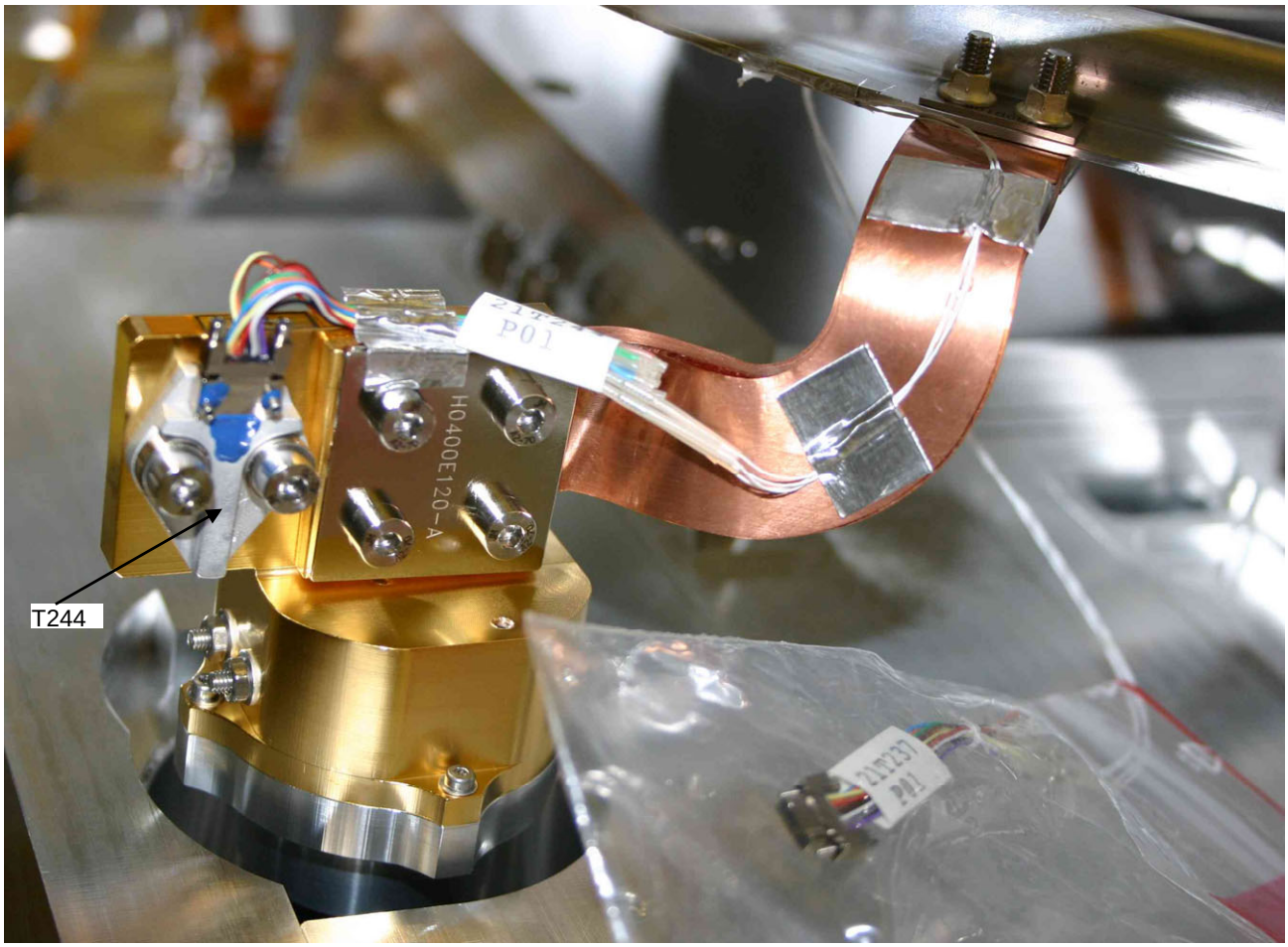

Figure 4.4-1: Temperature Sensor T244 – HIFI L1 FPU I/F

The HIFI L1 temperature evolution is shown in **Figure 4.4-2** for the whole TP4 test phase and in **Figure 4.4-3** for the HIFI operational phase. **Figure 4.4-2** shows, that the PACS and SPIRE operation is clearly seen by the HIFI L1 sensors.

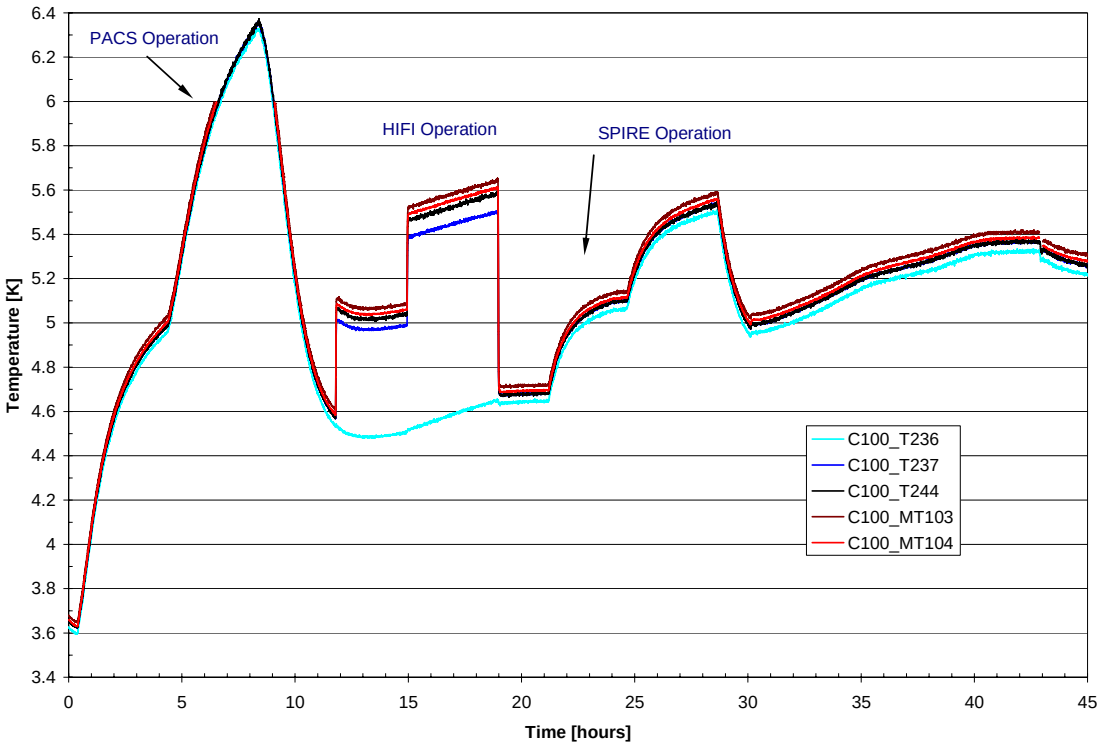

Figure 4.4-2: HIFI L1 Temperature Evolution during TP4

The temperature gradient along the ventline as well as between HIFI MTD (L1) and ventline is shown in **Figure 4.4-4**. The temperature gradient between HIFI outlet (T237) and inlet (T236) along the ventline show a straight line that allows a determination of a small parasitic heat load of about 0.4 mW to the L1 ventline.

The heat absorbed by the helium mass flow is shown **Figure 4.4-5** versus the electrical power applied at the MTD. This demonstrates a good correspondence between the heat absorbed by the helium and the heat flow across the MTD L1 I/F consisting of the electrical power plus 0.4 mW parasitic, also shown in **Figure 4.4-5**.
The calculated L1 I/F conductance related to the HIFI ventline outlet (T237) is shown in **Figure 4.4-6** versus mean temperature (average of MT103/104 and T237). For comparison the conductance between copper strap I/F at MTD side (T244) and ventline outlet (T237) is shown, too.

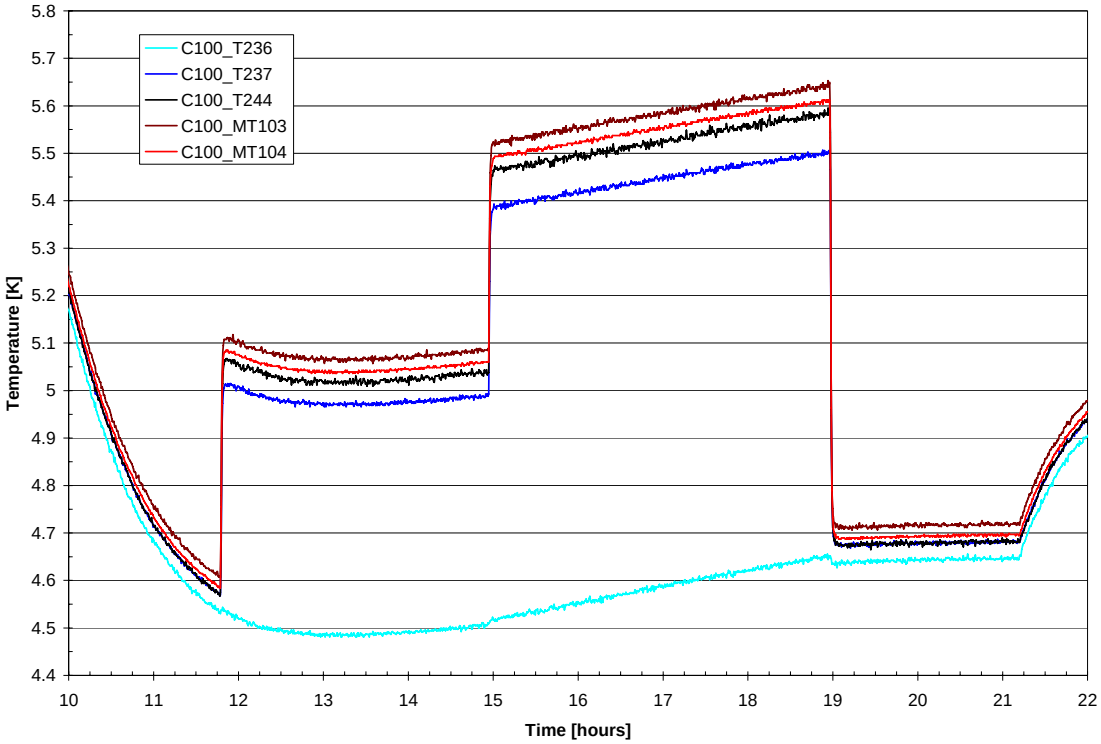

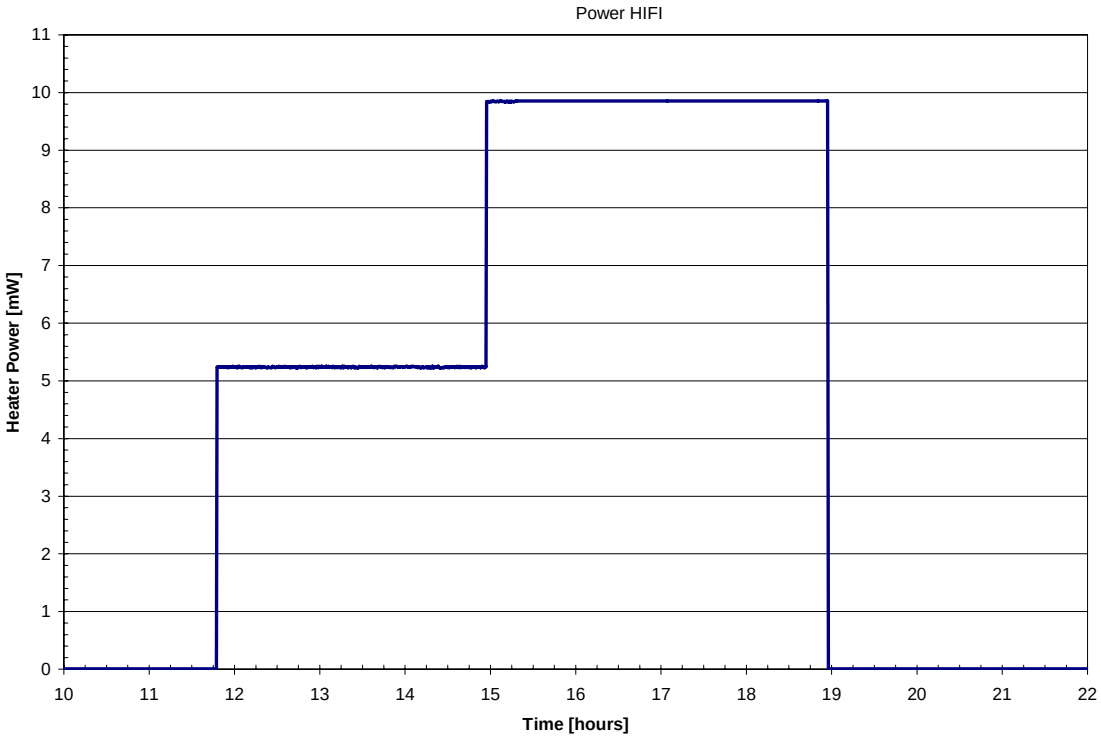

Figure 4.4-3: HIFI L1 Power and Temperature Evolution during Operation (TP4)

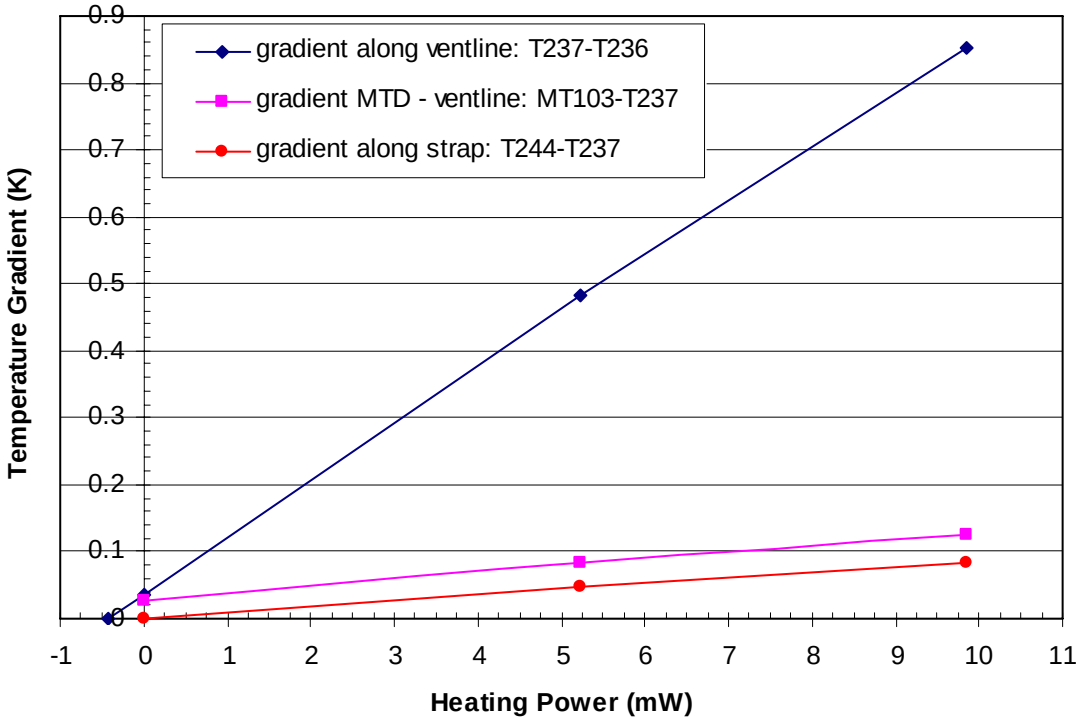

Figure 4.4-4: HIFI L1 Temperature Gradients versus Heating Power (TP4)

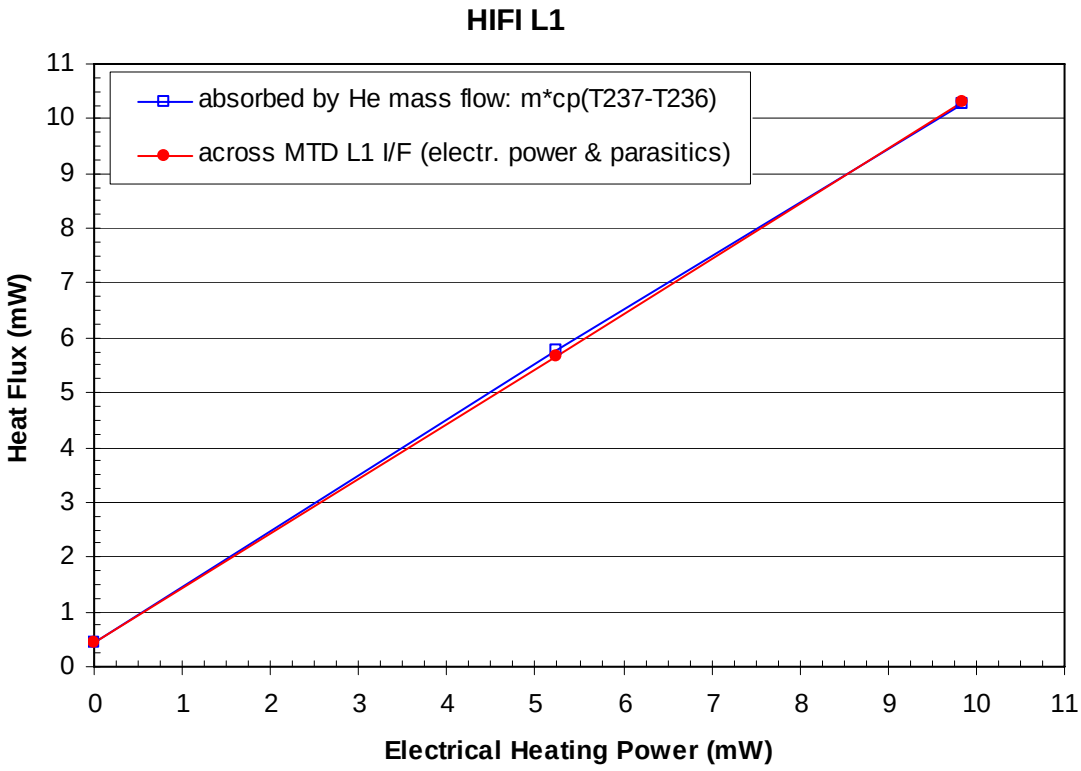

Figure 4.4-5: HIFI L1 Interface Heat Flows (TP4)

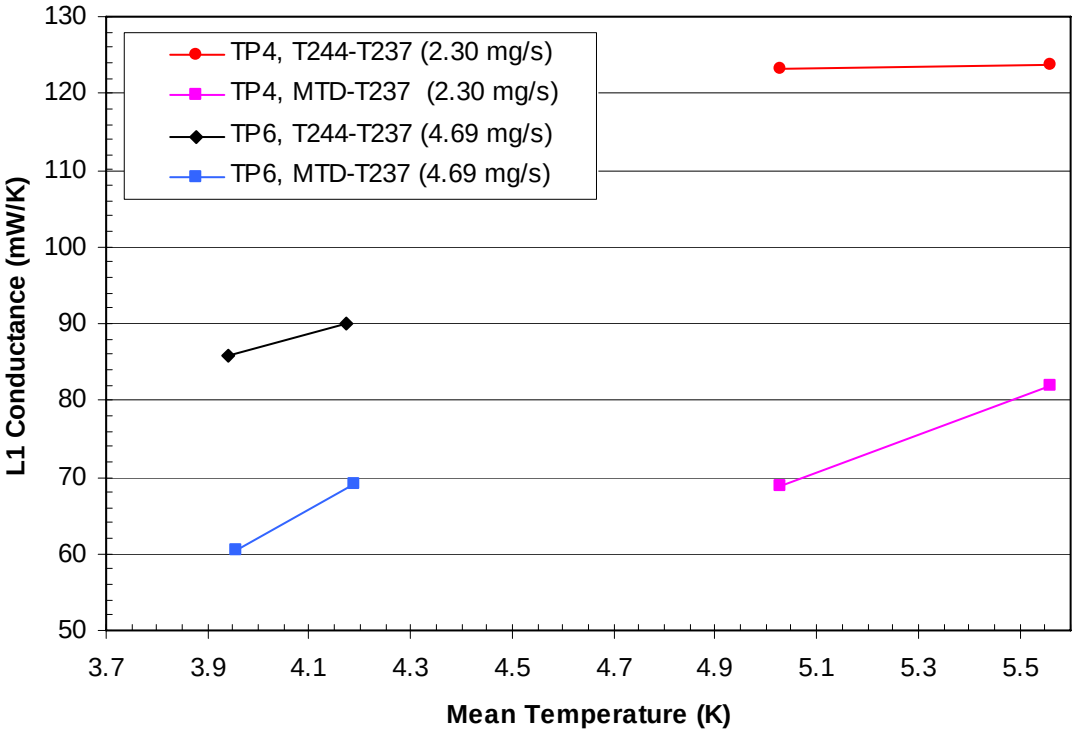

Figure 4.4-6: HIFI L1 Interface Conductance (TP4 and TP6)

4.5 PACS (TP6)

As already mentioned in section 4.1 the temperature evolution of the ventline behaves strange during TP6. Despite this, evaluation has been performed in the same principle as done for TP4. The relevant PACS L1 power and temperature curves are shown in Figure 4.5-1. For the evaluation of the thermal conductance at 3x 10mW the lower temperature levels are taken, i.e. about 2.3 K for T231 (PACS ventline inlet) and 3.6 K for T234 (PACS ventline outlet).

Looking at the total gradient between PACS outlet (T234) and HTT outlet (T112) no linear behaviour has been measured. Calculation of the heat absorbed by the helium mass flow taking the gradient no electrical heating (0 mW heating power) yields about 34 mW, see Figure 4.5-2. In TP4 the behaviour was linear and the corresponding absorbed heat was 6.7 mW. Probably just by chance the gradient between PACS outlet and inlet (T234-T231) shows a linear behaviour with 6.8 mW absorbed heat at no electrical heating.

The heat absorbed by the helium mass flow (T234-T231) in comparison to the MTD electrical power is shown in Figure 4.5-3. The difference between the two curves represent the parasitic heat across the MTD L1 I/F. The originally 6.8 mW parasitic heat at zero power drops to about 4.4 mW at 30 mW electrical power.

The calculated L1 I/F conductance related to the PACS ventline outlet (T234) is shown in **Figure 4.2-5** together with the TP4 results. However, due to the non-flight representative helium routing which probably led to the not yet explainable temperature evolution of the ventline the TP6 results are considered as not reliable.

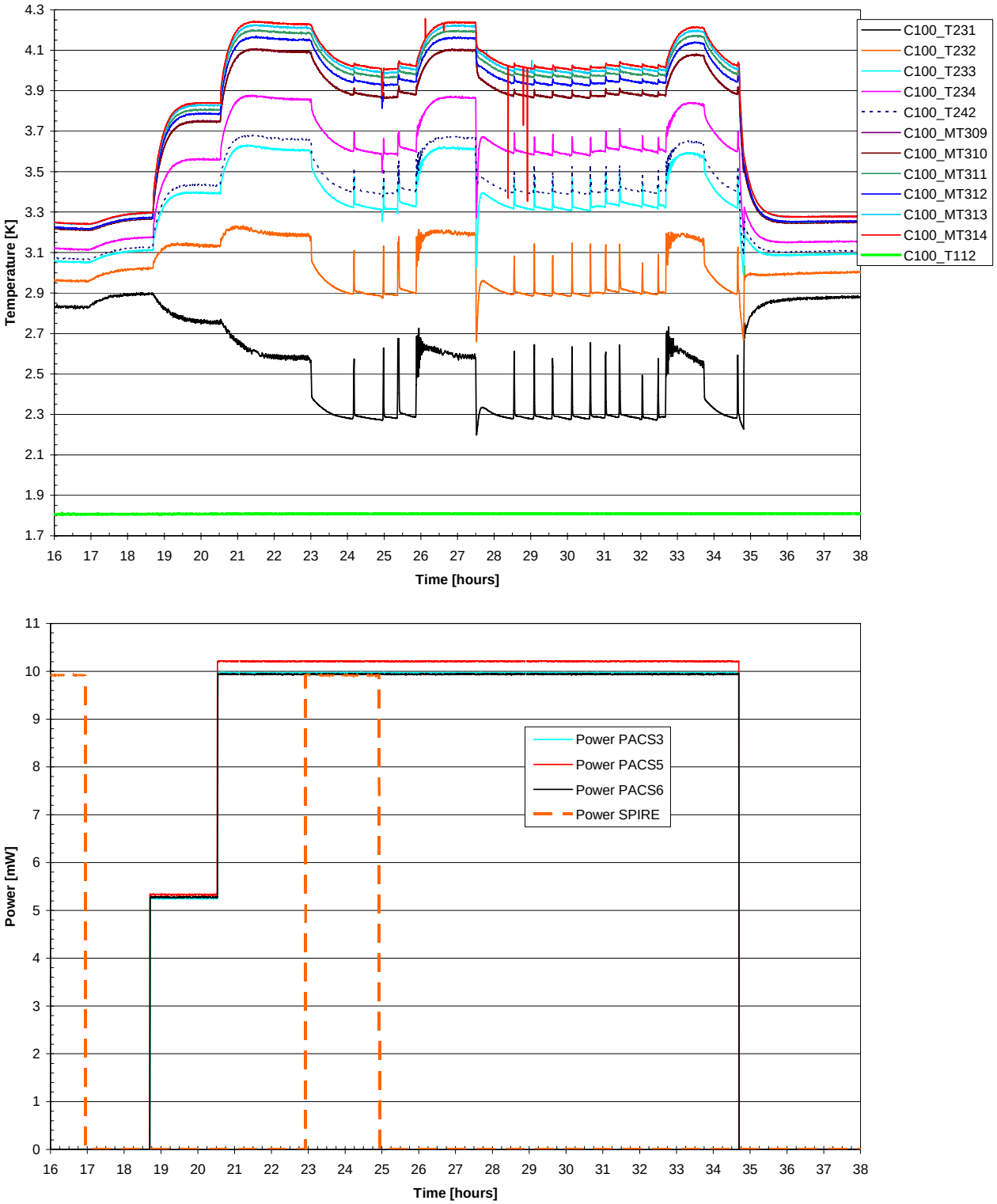

Figure 4.5-1: PACS L1 Power and Temperature Evolution during Operation (TP6)

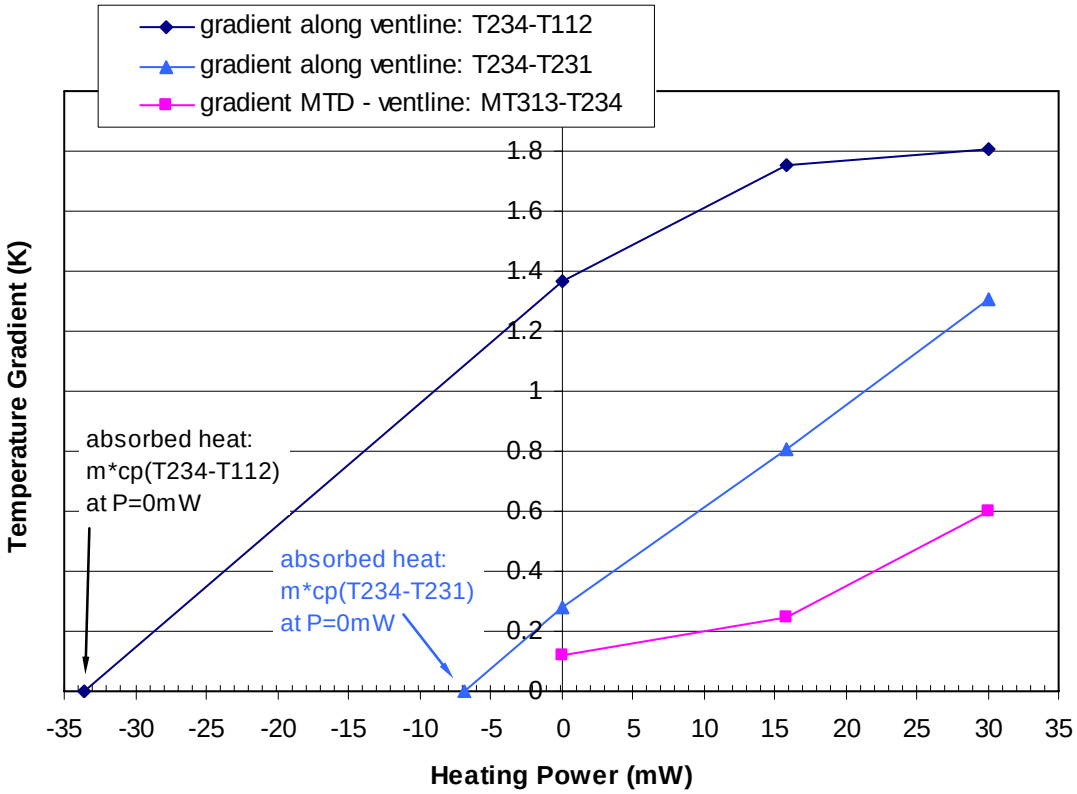

Figure 4.5-2: PACS L1 Temperature Gradients versus Heating Power (TP6)

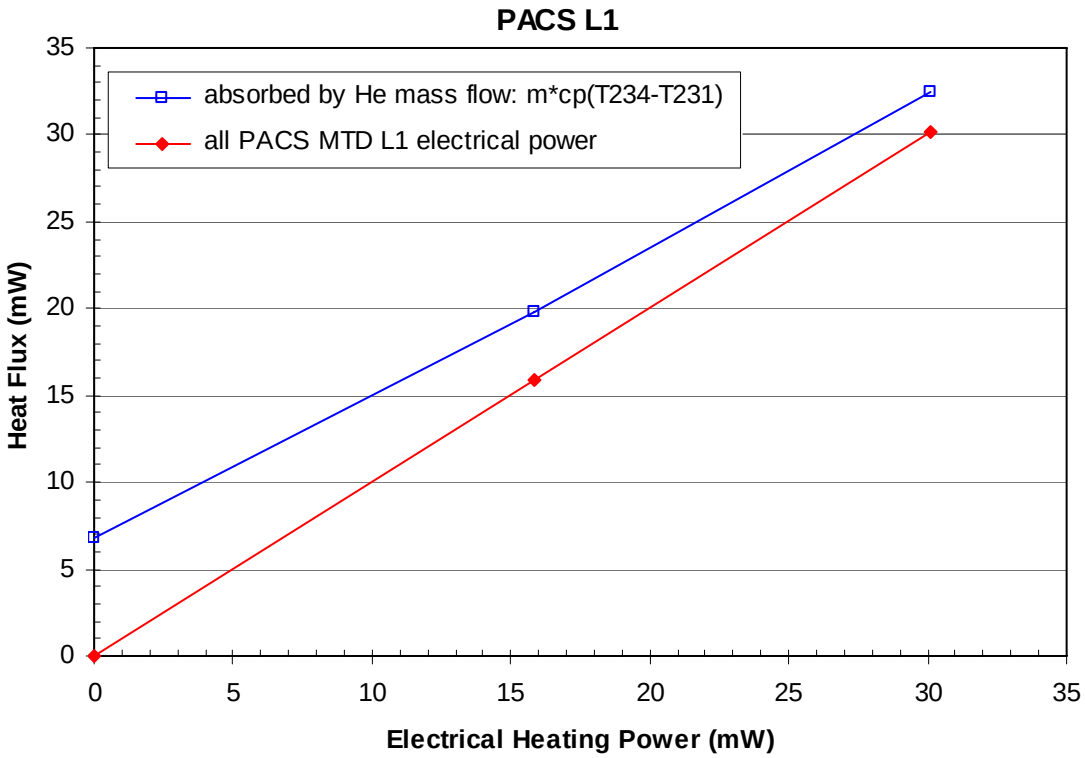

Figure 4.5-3: PACS L1 Heat Flow absorbed by Helium compared to Electrical Power (TP6)

4.6 SPIRE (TP6)

The SPIRE L1 temperature evolution is shown in **Figure 4.6-1** for nominal SPIRE operation and in **Figure 4.6-2** for the SPIRE switch on during PACS nominal operation. **Figure 4.6-1** shows, that the SPIRE heating is already seen by the sensor T235, which was also the case in TP4.

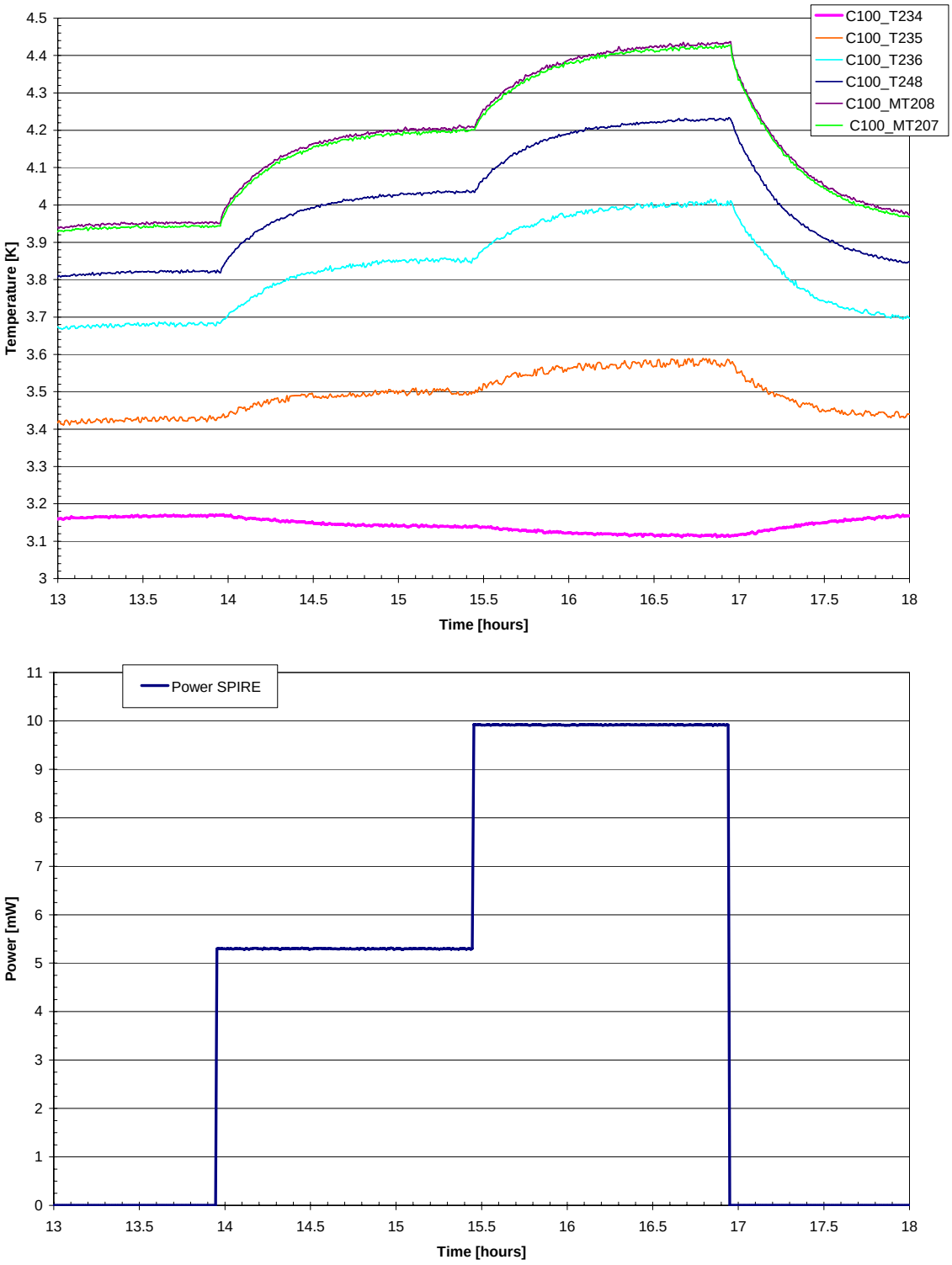

Figure 4.6-1: SPIRE L1 Power and Temperature Evolution during Operation (TP6)

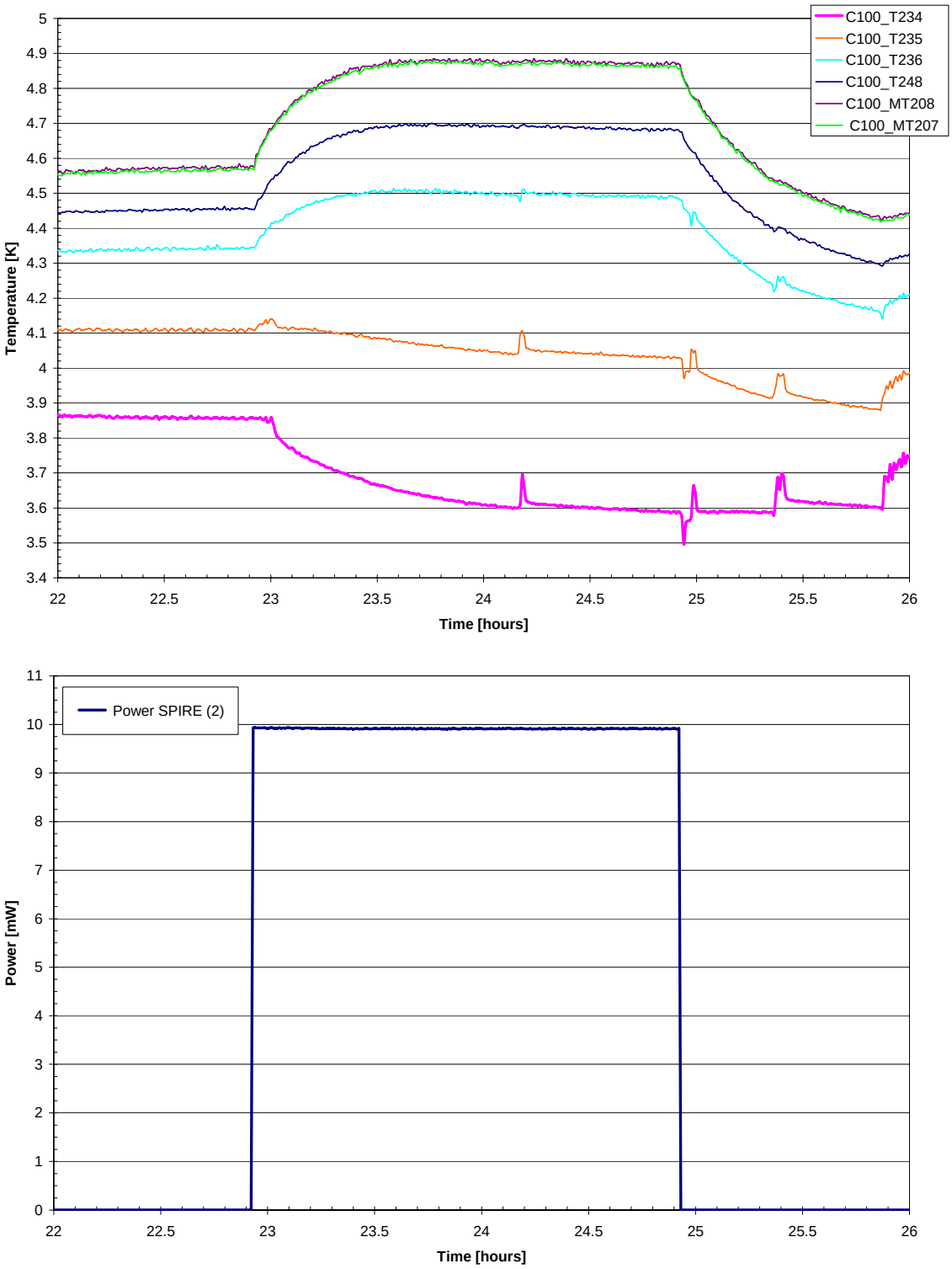

Figure 4.6-2: SPIRE L1 Additional Measurement during PACS Operation (TP6)

The temperature gradient along the ventline as well as between SPIRE MTD (L1) and ventline is shown in **Figure 4.6-3**. The additional points at 10 mW heating power belong to the SPIRE switch on during PACS operation. The temperature gradient between SPIRE outlet (T236) and inlet (T234) along the ventline show a straight line that allows a determination of about 12.5 mW parasitic heat load to the L1 ventline via the

SPIRE mounting feet. The parasitic heat load in TP6 is smaller than in TP4 because the temperature gradient between OBP (L2) and SPIRE MTD (L1) is smaller and in addition the conductance of the mounting feet is smaller due to the lower temperature.
The heat absorbed by the helium mass flow is shown in **Figure 4.6-4** versus the electrical power applied at the MTD. This demonstrates a good correspondence between the heat absorbed by the helium and the heat flow across the MTD L1 I/F consisting of the electrical power plus 12.5 mW parasitic, also shown in **Figure 4.6-4**.

The calculated L1 I/F conductance related to the SPIRE ventline outlet (T236) is shown in **Figure 4.3-6** versus mean temperature (average of MT207/208 and T236) together with the results obtained for TP4. The conductance between the copper strap I/F at MTD side (T248) and ventline outlet (T236) is shown, too.

Both conductance values obtained in TP6 are roughly a factor of 2 smaller in comparison to TP4. This indicates that the thermal conductance of the link materials, which is lower at lower temperatures, is dominating the total L1 I/F conductance much more than the heat transfer coefficient between ventline wall and helium gas (which is expected to be higher at the higher mass flow rate).

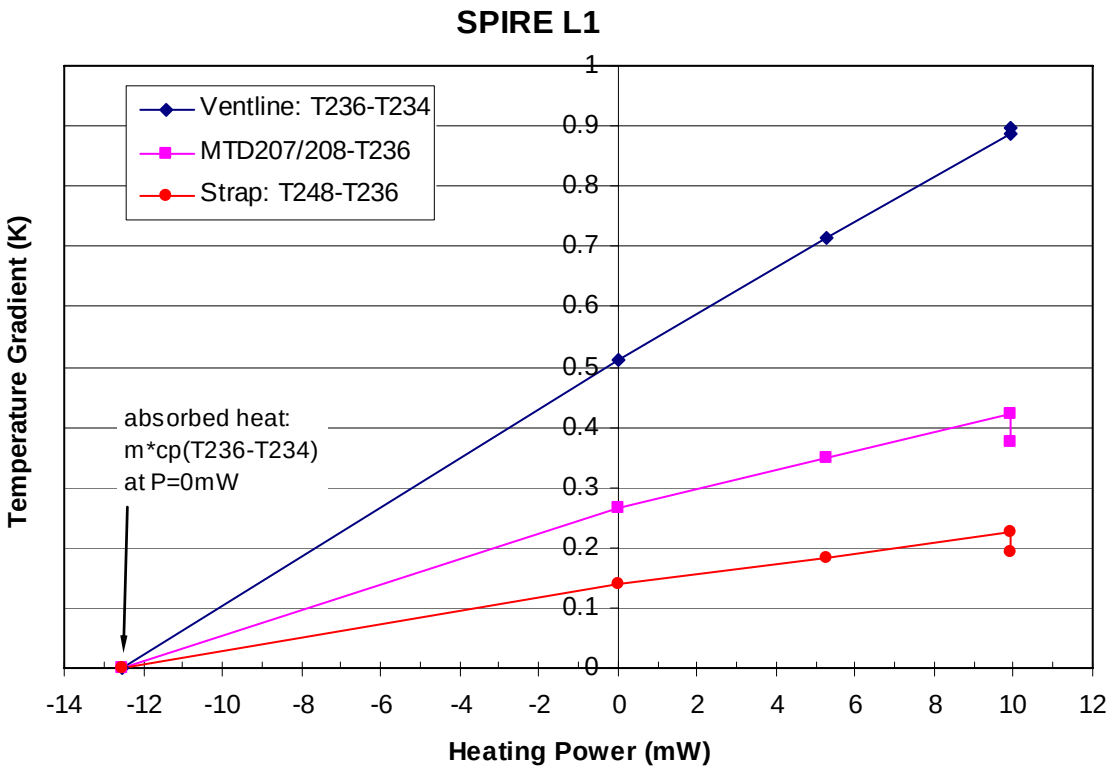

Figure 4.6-3: SPIRE L1 Temperature Gradients versus Heating Power (TP6)

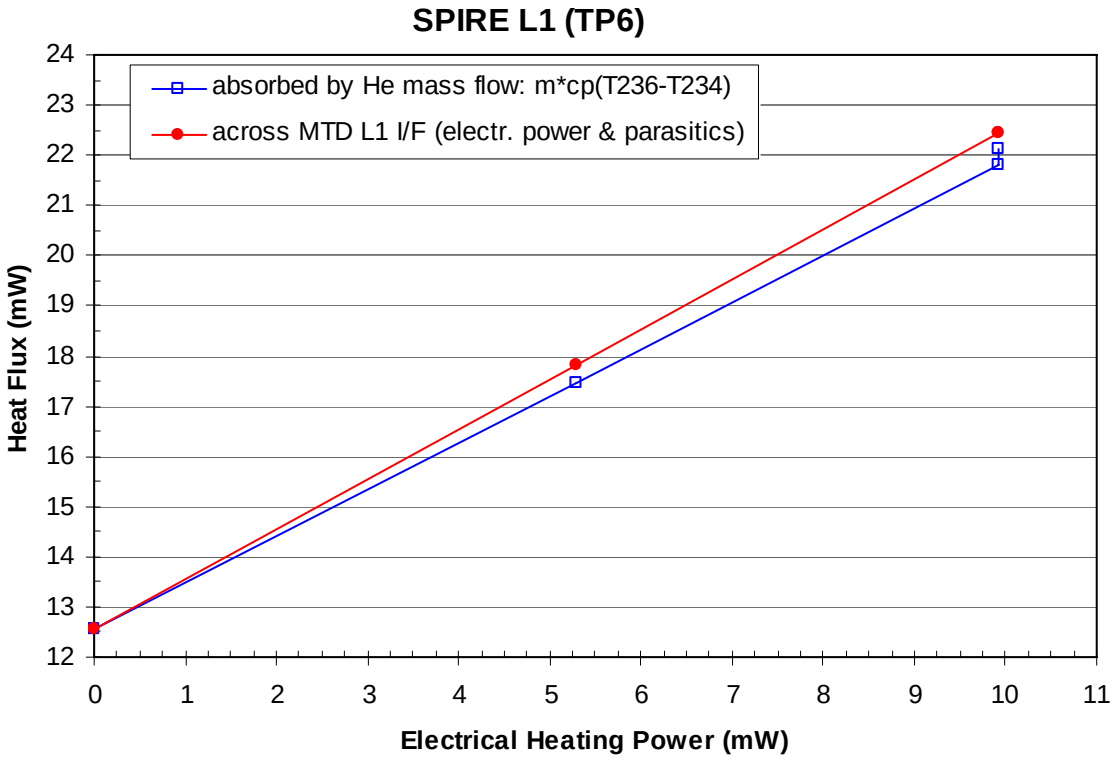

Figure 4.6-4: SPIRE L1 Interface Heat Flows (TP6)

4.7 HIFI (TP6)

The HIFI L1 temperature evolution is shown in **Figure 4.7-1** for the whole TP6 test phase and in **Figure 4.7-2** for the HIFI operational phase. **Figure 4.7-1** shows, that the PACS and SPIRE operation is clearly seen by the HIFI L1 sensors.

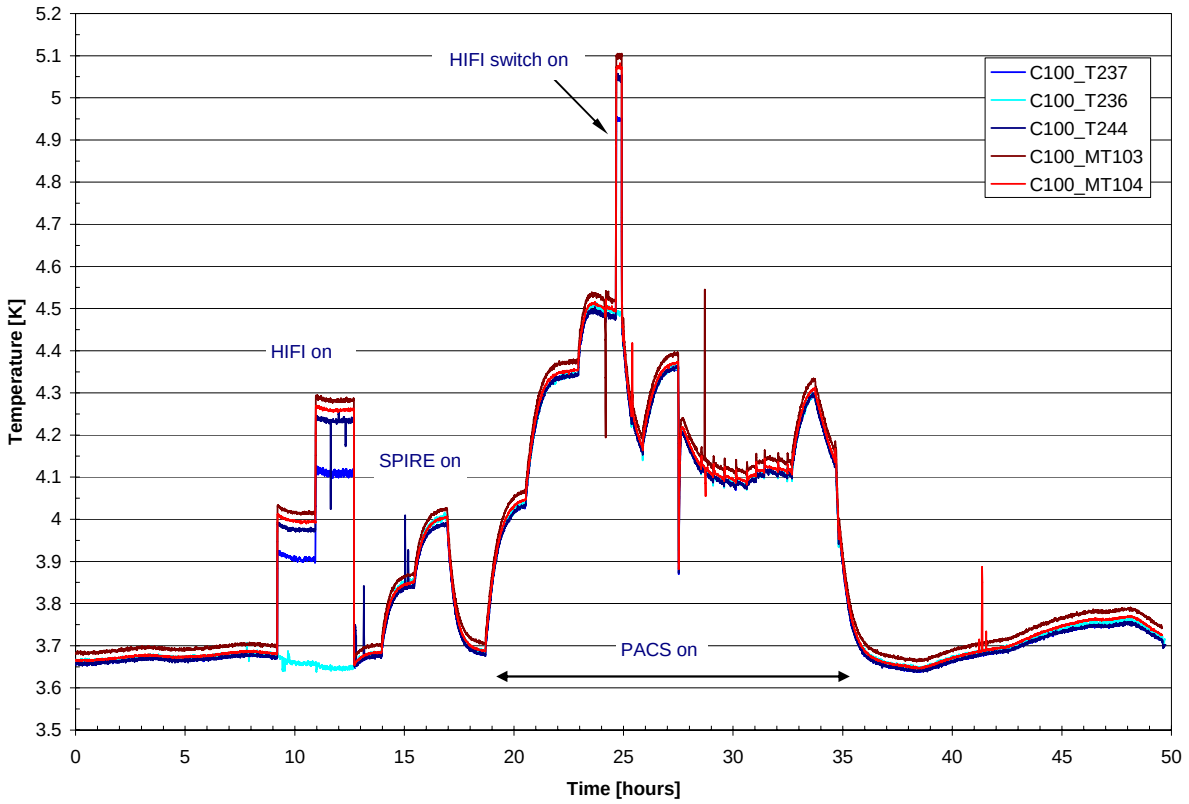

Figure 4.7-1: HIFI L1 Temperature Evolution during TP6

The temperature gradient along the ventline as well as between HIFI MTD (L1) and ventline is shown in **Figure 4.7-3**. The temperature gradient between HIFI outlet (T237) and inlet (T236) along the ventline show a straight line ending in the origin indicating that parasitic heat load to the L1 ventline is negligible.

The heat absorbed by the helium mass flow is shown **Figure 4.7-4** versus the electrical power applied at the MTD displaying the correspondence between the heat absorbed by the helium and the heat flow across the MTD L1 I/F consisting of the electrical power.

The calculated L1 I/F conductance related to the HIFI ventline outlet (T237) is shown in **Figure 4.4-6** versus mean temperature (average of MT103/104 and T237) together with the TP4 results. The conductance between copper strap I/F at MTD side (T244) and ventline outlet (T237) is shown, too. Both conductance values in TP6 with 4.69 mg/s are higher compared to TP4 with 2.3 mg/s. This indicates that the thermal conductance of the link materials, which is lower at lower temperatures, is dominating the total L1 I/F conductance much more than the heat transfer coefficient between ventline wall and helium gas (which is expected to be higher at the higher mass flow rate).

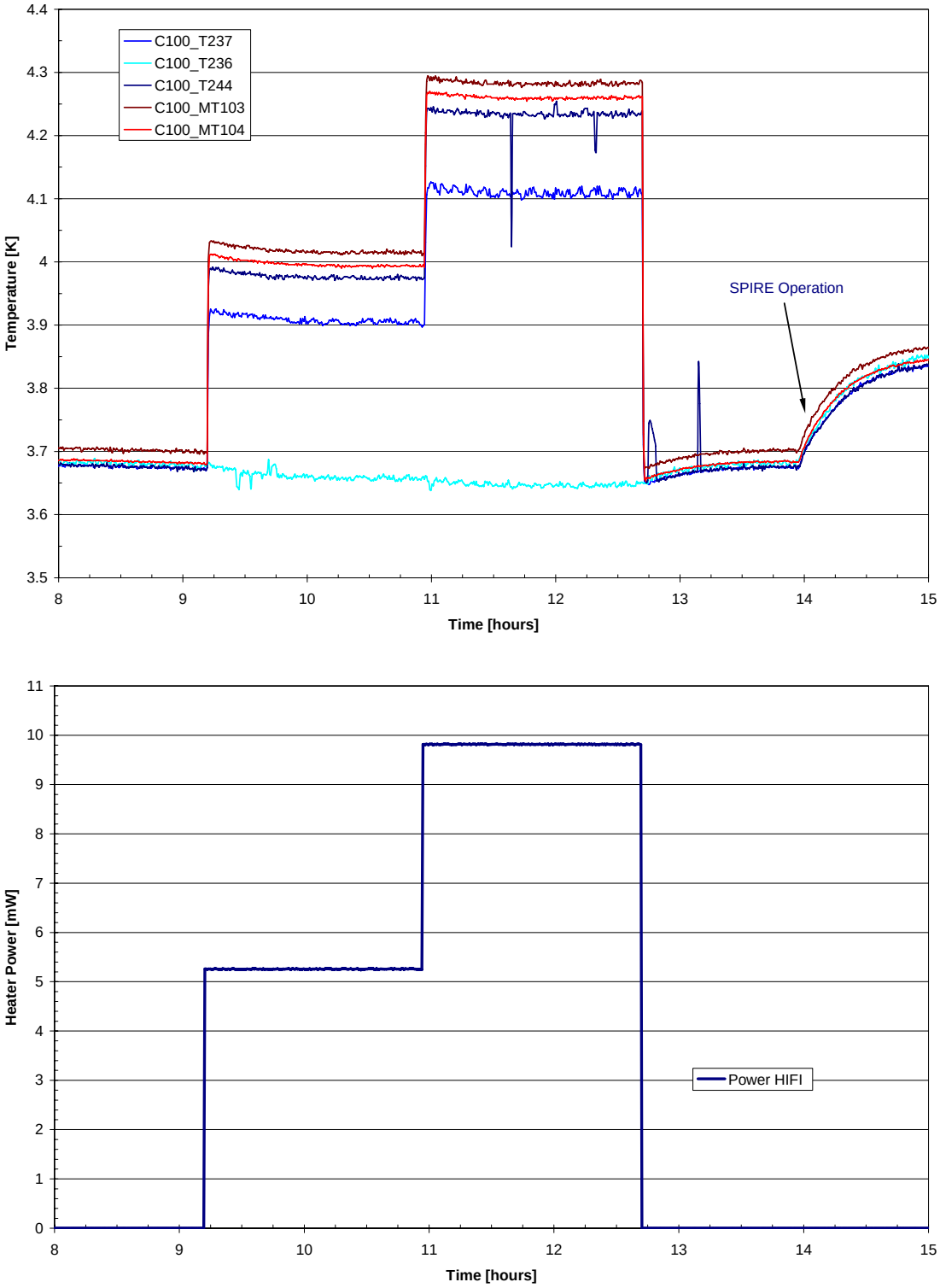

Figure 4.7-2: HIFI L1 Power and Temperature Evolution during Operation (TP6)

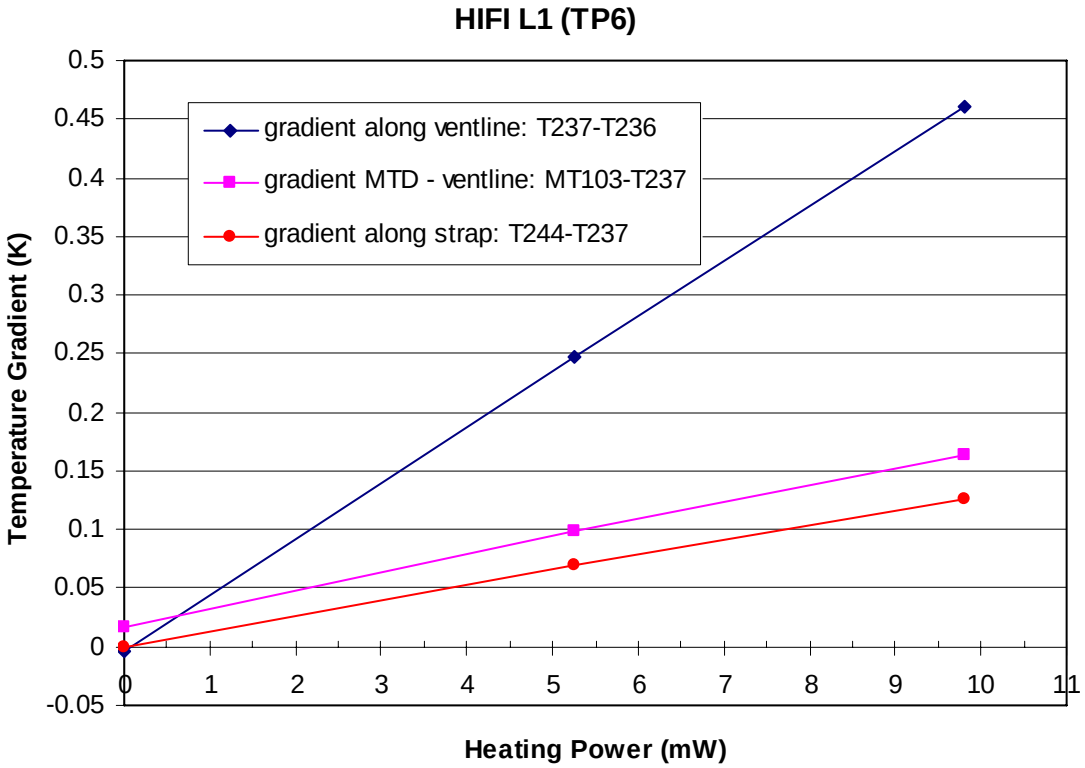

Figure 4.7-3: HIFI L1 Temperature Gradients versus Heating Power (TP6)

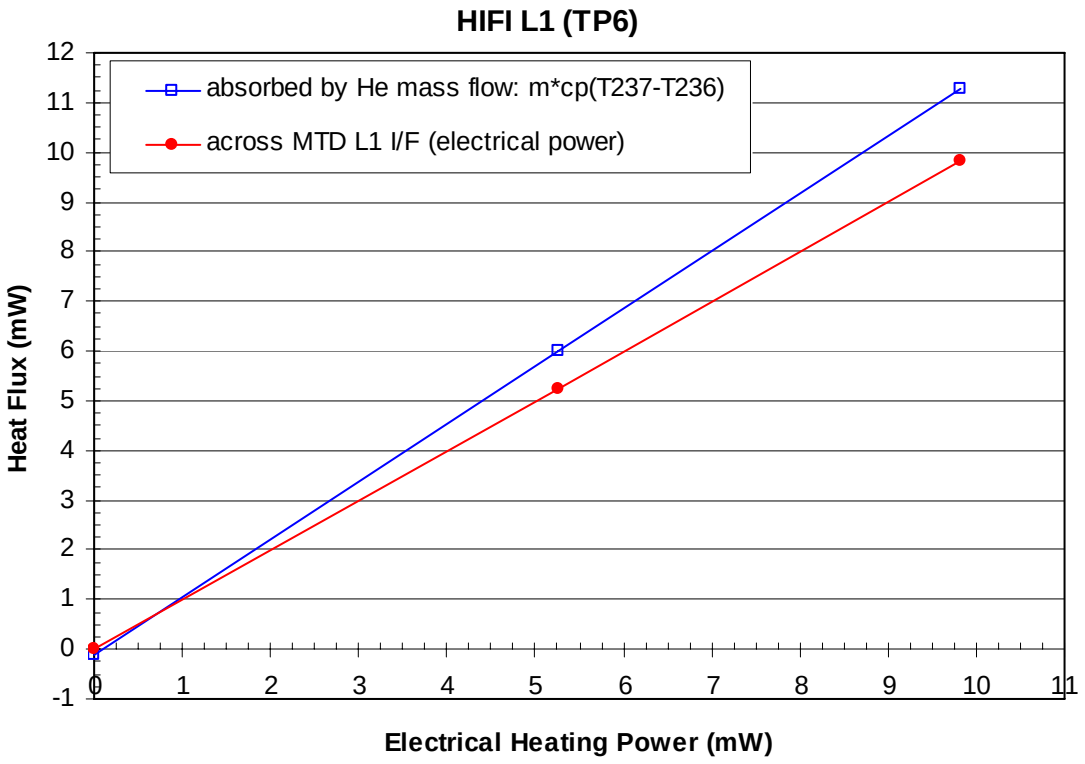

Figure 4.7-4: HIFI L1 Interface Heat Flows (TP6)

4.8 L1 Summary and Conclusion

Instrument Interface	Requirement	Measured Temperature in LSS (TP4)				Measured Temperature in LSS (TP6)			
	AD 01 to AD 03	MTD Temperature	Mass flow	OBP	Parasitic heat to L1	MTD Temperature	Mass flow	OBP	Parasitic heat to L1
PACS FPU *(MT313/314)*	5K @ 30 mW	3.80K @ 22mW 5.07K @ 37mW	2.24 mg/s 2.26 mg/s	11-12 K	6.7 mW	3.80K @ 23mW 4.22K @ 37mW	4.73 mg/s 4.77 mg/s	9.5-10 K	6.8 mW
SPIRE FPU *(MT207/208)*	5.5 K @ 15 mW (3.7K @ 13mW)*	4.93K @ 24mW 5.38K @ 29mW	2.34 mg/s 2.36 mg/s	13 K	24.2 mW	4.20K @ 18mW 4.43K @ 22mW	4.71 mg/s 4.72 mg/s	9.5 K	12.5 mW
HIFI *(MT103/104)*	6 K @ 15.5 mW	5.07K @ 6mW 5.62K @ 10mW *	2.30 mg/s 2.32 mg/s	13 K	0.4 mW	4.00K @ 5mW 4.27K @ 10mW	4.69 mg/s 4.70 mg/s	9.5 K	~ 0 mW

*) linear extrapolation of temperature gradient of curve "*MTD – ventline: MT103-T237*" in **Figure 4.4-4** yields 5.68K @15.5mW

Table 4.8-1: L1 MTD Test Data versus Instrument I/F Requirements

5 Thermal Performance of L2 and L3 Interfaces

5.1 Conditions during L2 and L3 Performance Measurement

The L3 performance measurements on JFET MTD's have been performed also in the test phase TP4 and TP6 as described in section 4.1. The L2 performance measurement by heating of the HIFI FPU MTD has been performed in TP6 only. The relevant FM temperature sensors on the Optical Bench Assembly are shown in **Figure 5.1-1**. The sensor T237 represents the L1 ventline outline, respectively the L2 inlet temperature of the helium mass flow. The sensor T258 mounted on the OBP represents the L2 outlet temperature, respectively the L3 ventline inlet temperature of the helium mass flow. Finally, the sensor T247 represents the L3 outlet temperature.

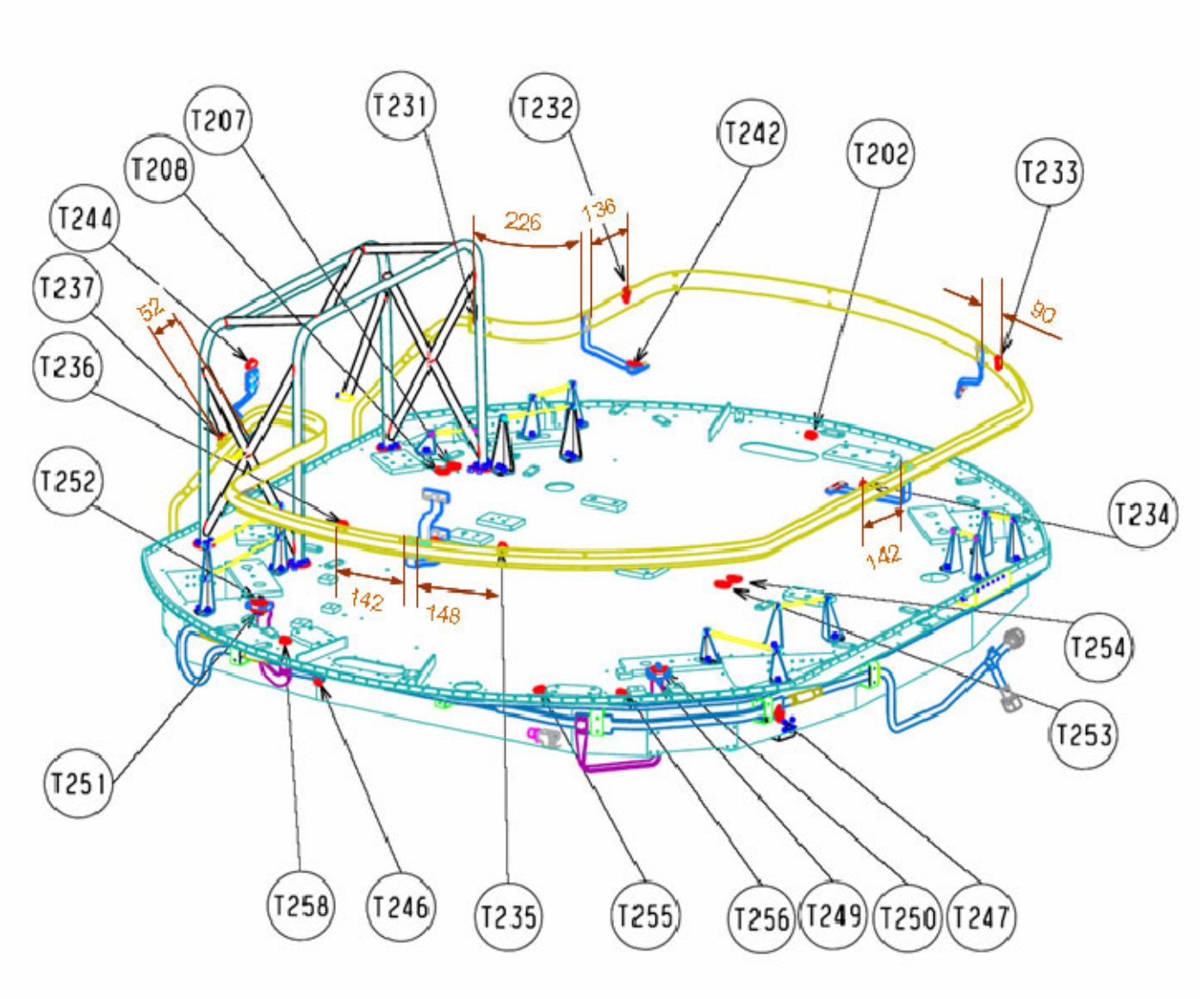

Figure 5.1-1: Distribution of Temperature Sensors on Optical Bench Assembly (L1, L2, L3)

5.2 Optical Bench Plate (TP4)

The temperature sensor distribution on the Optical Bench Plate (OBP) is given in **Figure 5.2-1** and the corresponding temperature evolution is presented in **Figure 5.2-2**. The maximum gradient on the OBP is about 0.8 K including Instrument Shield (T212 and T213) for a mass flow rate around 2.35 mg/s, see **Figure 4.1-2** at an average OPB temperature of about 14.5 K. The heat absorbed from the OBP by the helium mass flow is shown in **Figure 5.2-3** together with the heat absorbed by the L3 ventline.

Figure 5.2-1: Distribution of Temperature Sensors on the Optical Bench Plate (L2)

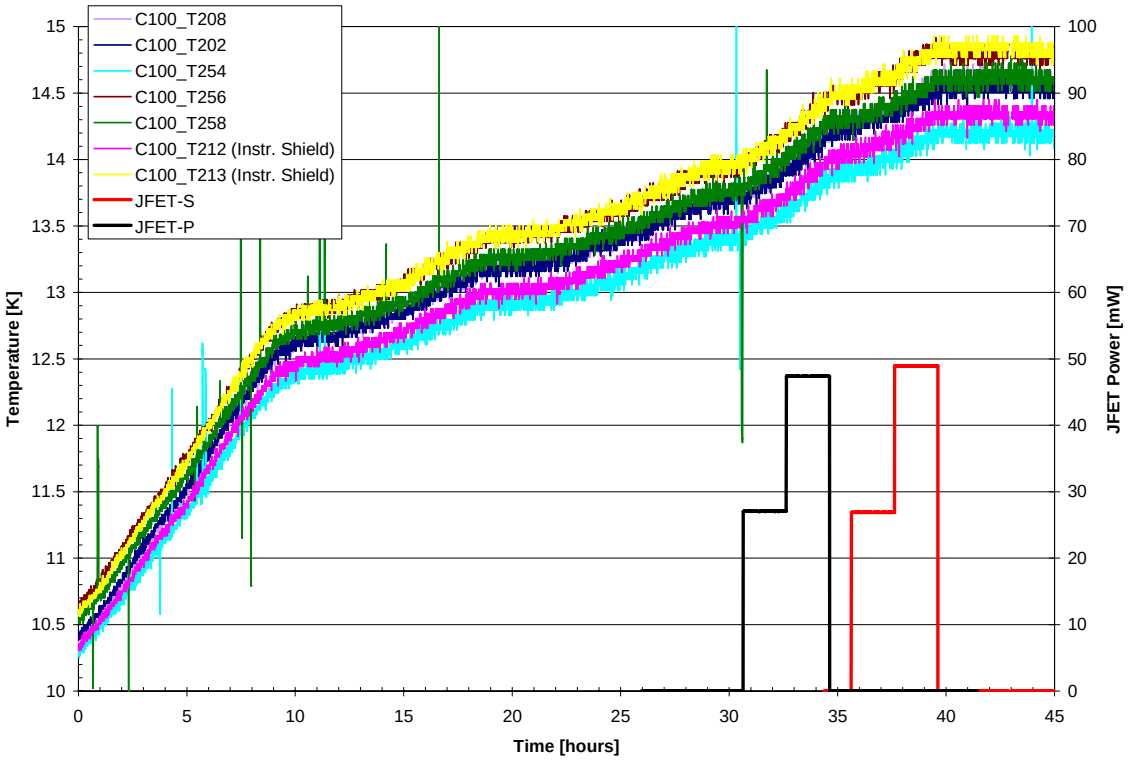

Figure 5.2-2: OBP (L2) Temperature Evolution during TP4

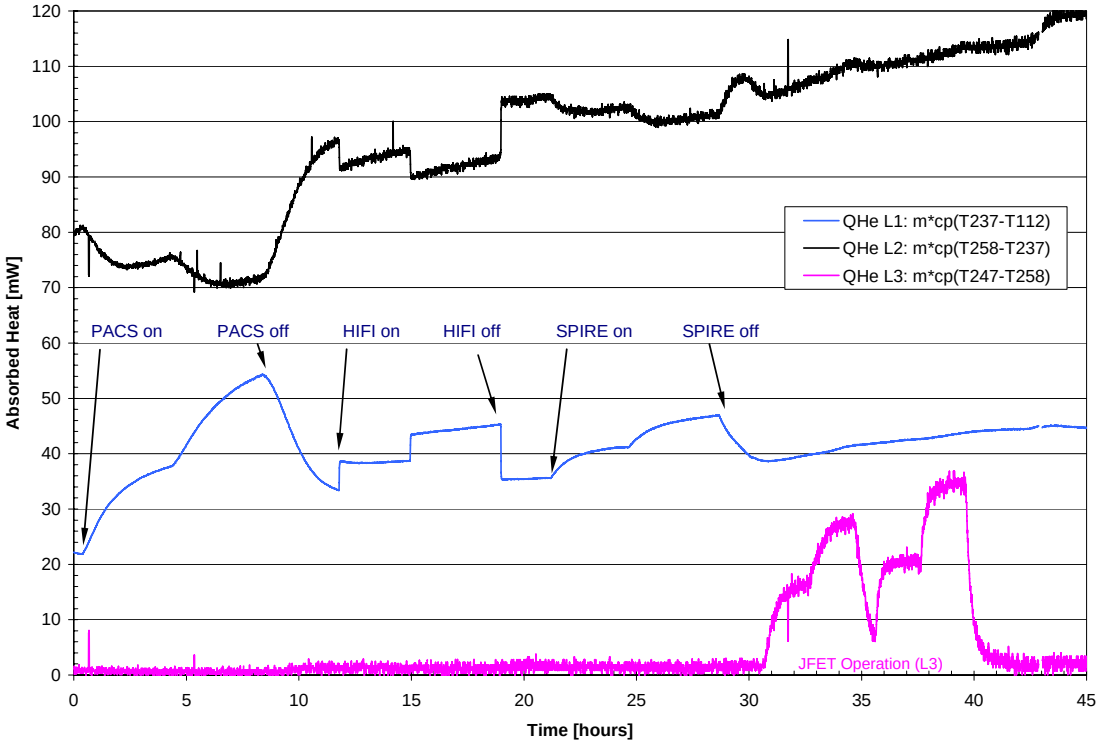

Figure 5.2-3: Absorbed Heat from OBP (L2) and L1 & L3 Ventline during TP4

5.3 Optical Bench Plate (TP6)

The temperature distribution on the Optical Bench Plate (OBP) is given in **Figure 5.3-1** showing a maximum gradient on the OBP of about 0.6 K including Instrument Shield (T212 and T213) for a mass flow rate around 4.75 mg/s, see **Figure 4.1-5** at an OBP average temperature of about 10 K. The heat absorbed from the OBP by the helium mass flow is shown in **Figure 5.3-2** together with the applied electrical heating power of the HIFI L2 MTD. The HIFI L2 MTD temperature evolution during electrical heating is shown in **Figure 5.3-3** and the evaluated gradient between HIFI MTD and OBP versus heating power is presented in **Figure 5.3-4**. The latter shows a straight line ending in the origin, which indicates that the conductive heat to the HIFI MTD via harness and coax cables is rather negligible and mostly absorbed directly by the OBP.

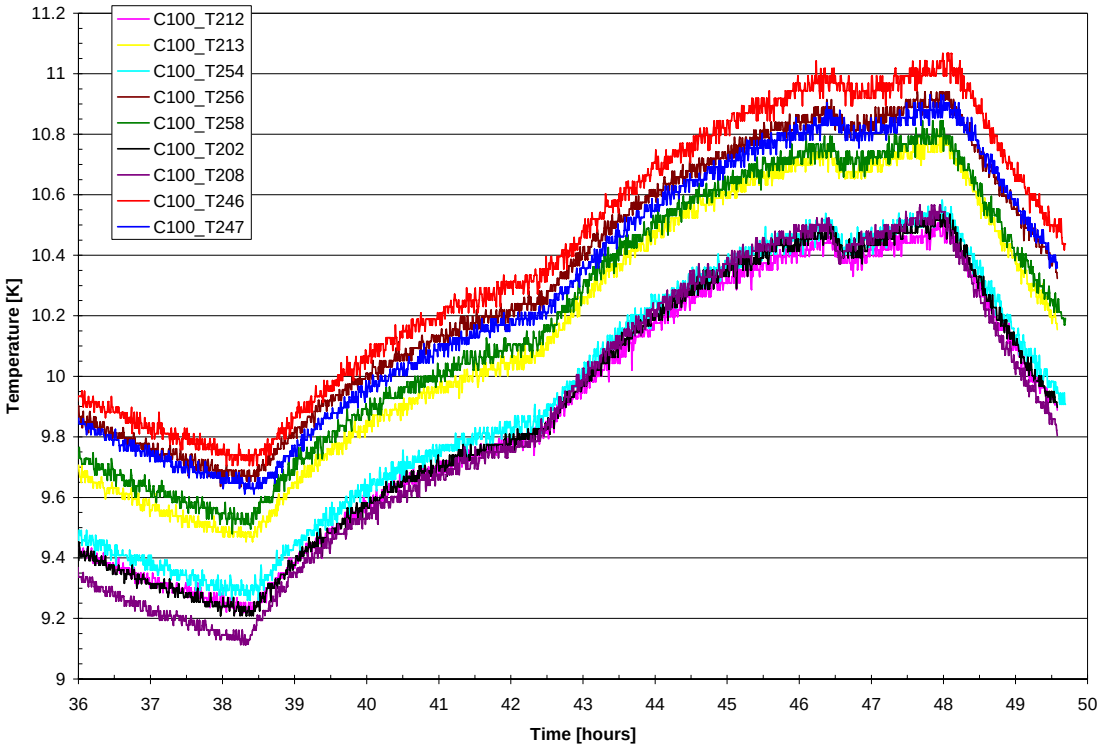

Figure 5.3-1: OBP (L2) Temperature Evolution during TP6

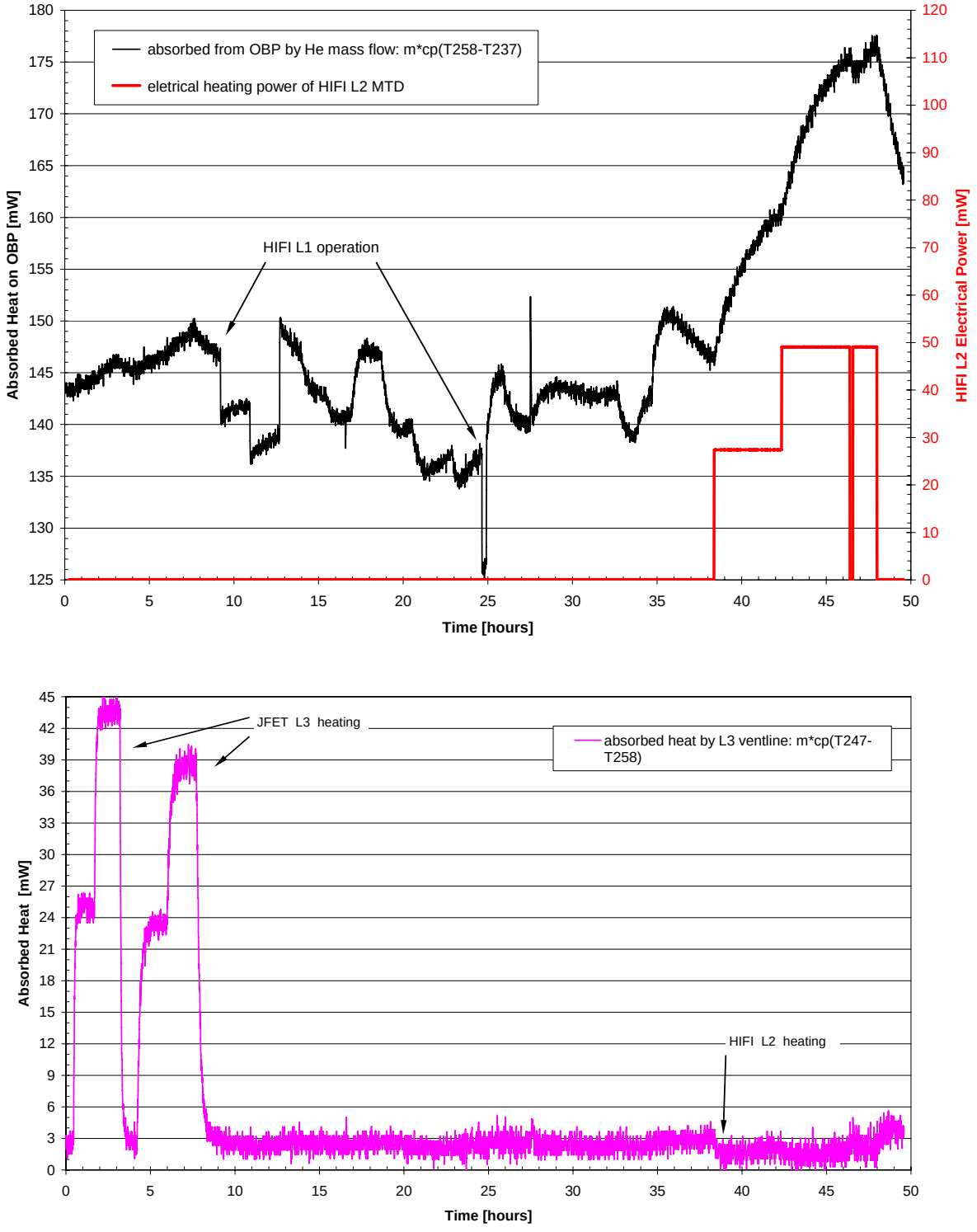

Figure 5.3-2: Absorbed Heat from L3 ventline, OBP (L2) and HIFI L2 Power during TP6

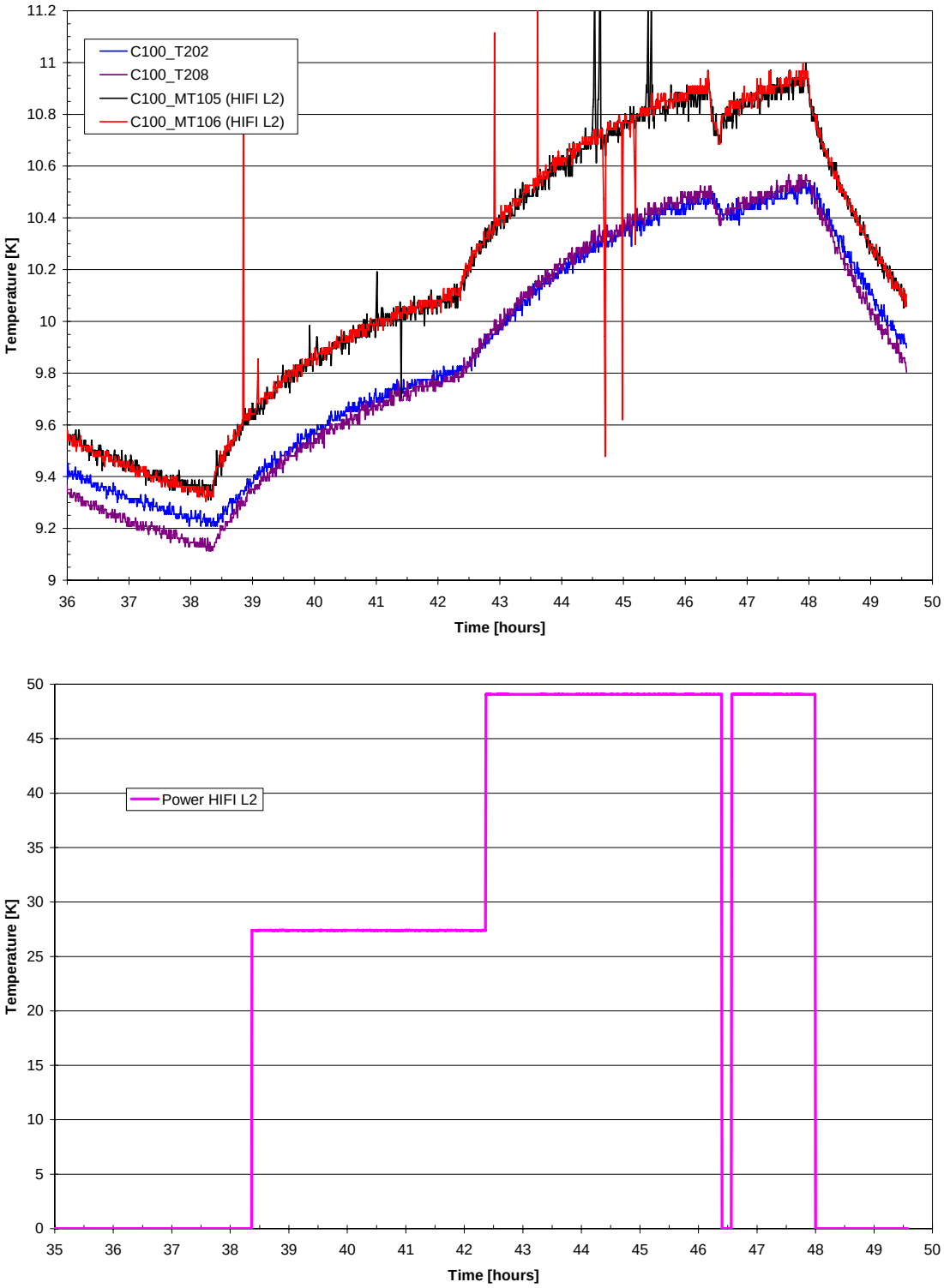

Figure 5.3-3: HIFI L2 Power and Temperature Evolution during Operation (TP6)

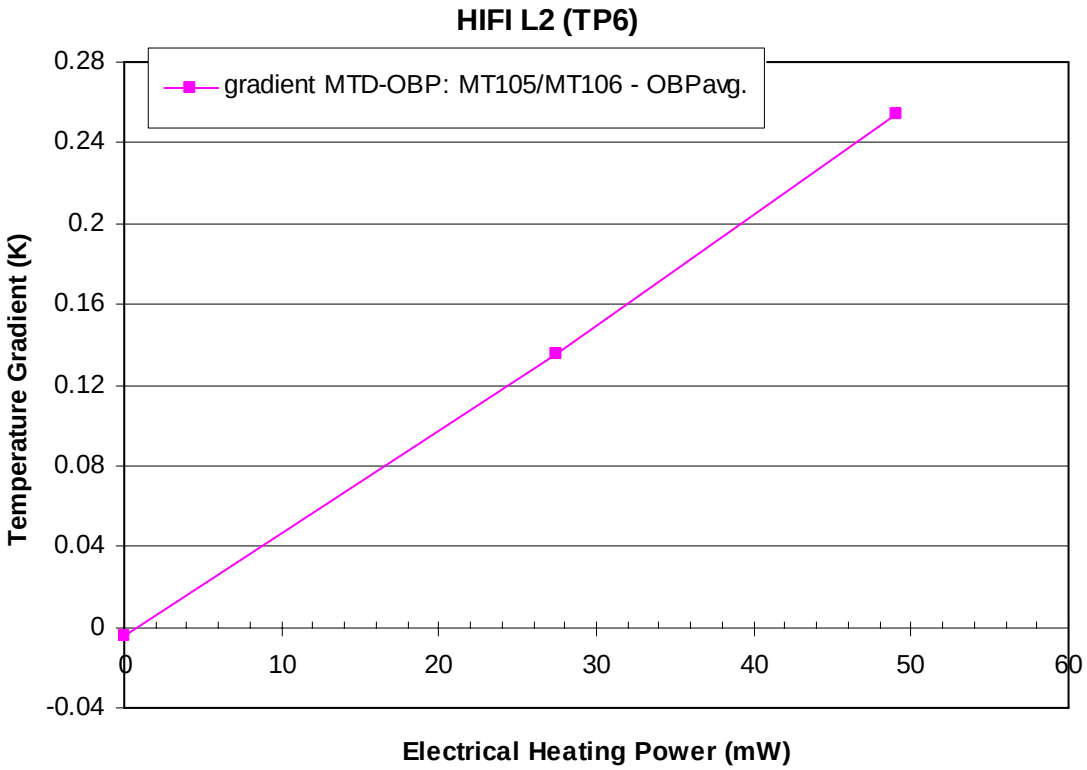

Figure 5.3-4: Gradient between HIFI L2 MTD and OBP versus Heating Power

5.4 SPIRE JFETs (TP4)

An overview of the temperature sensors used for the L3 I/F system is given in **Figure 5.4-1** and **Figure 5.4-2**. Photographs of relevant L3 temperature sensors are presented in **Figure 5.4-3**, **Figure 5.4-4** and **Figure 5.4-5**.

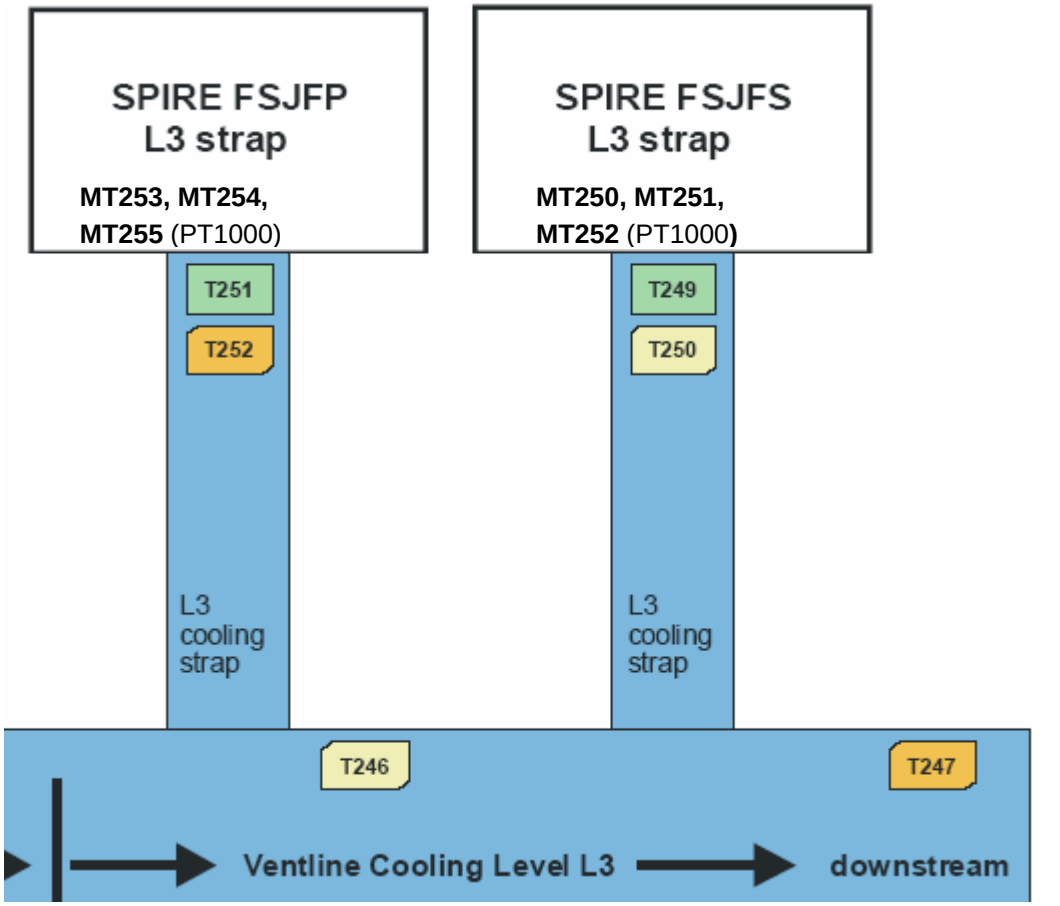

Figure 5.4-1: Overview on L3 FM and JFET MTD Temperature Sensors

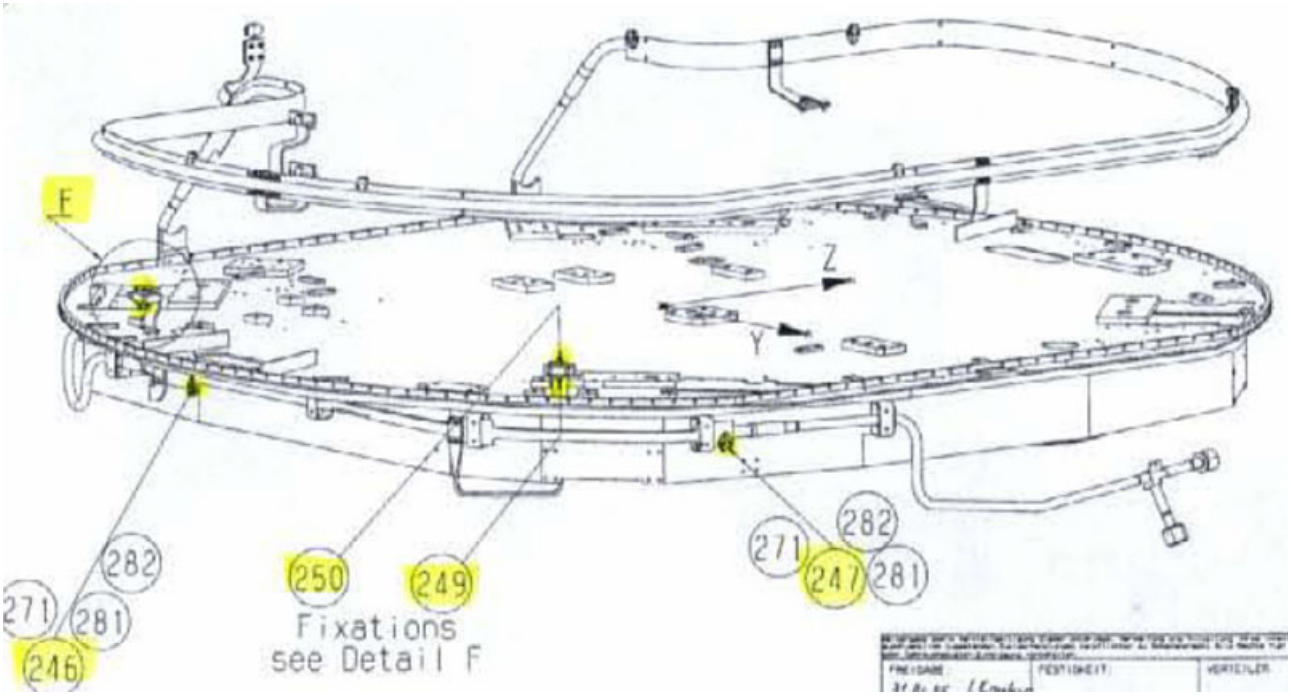

Figure 5.4-2: Distribution of Temperature Sensors on the L3 Ventline and L3 Interfaces

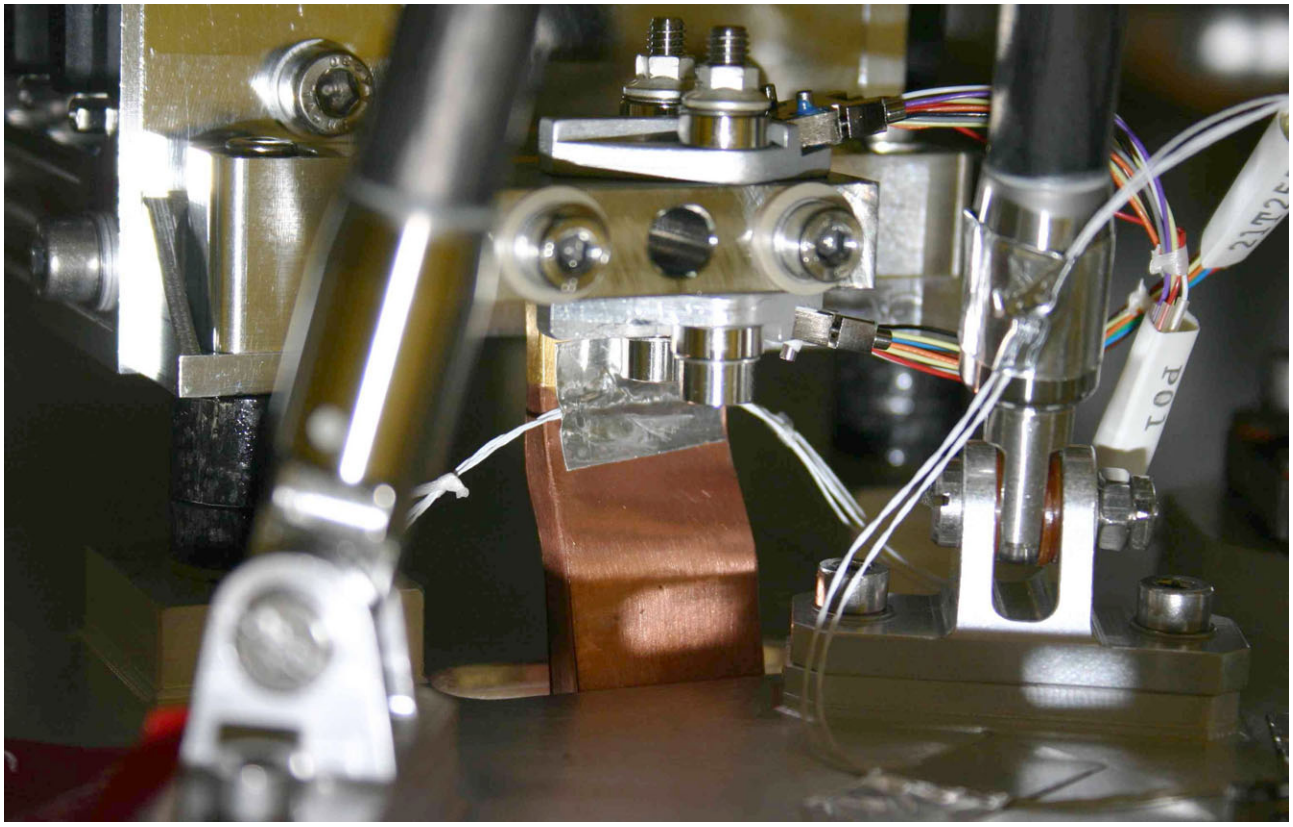

Figure 5.4-3: Temperature Sensors T251 and T252 – SPIRE L3 JFET-P

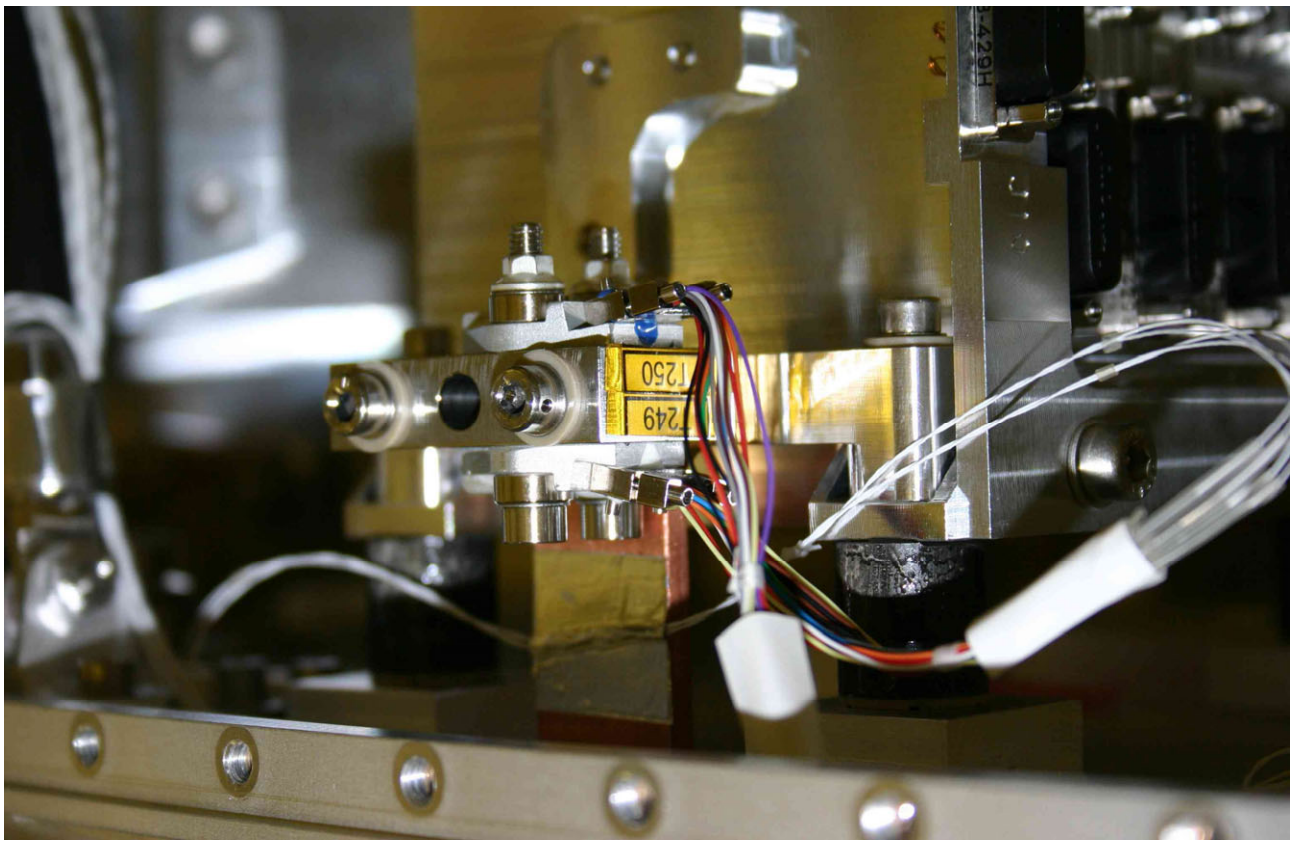

Figure 5.4-4: Temperature Sensors T249 and T250 – SPIRE L3 JFET-S

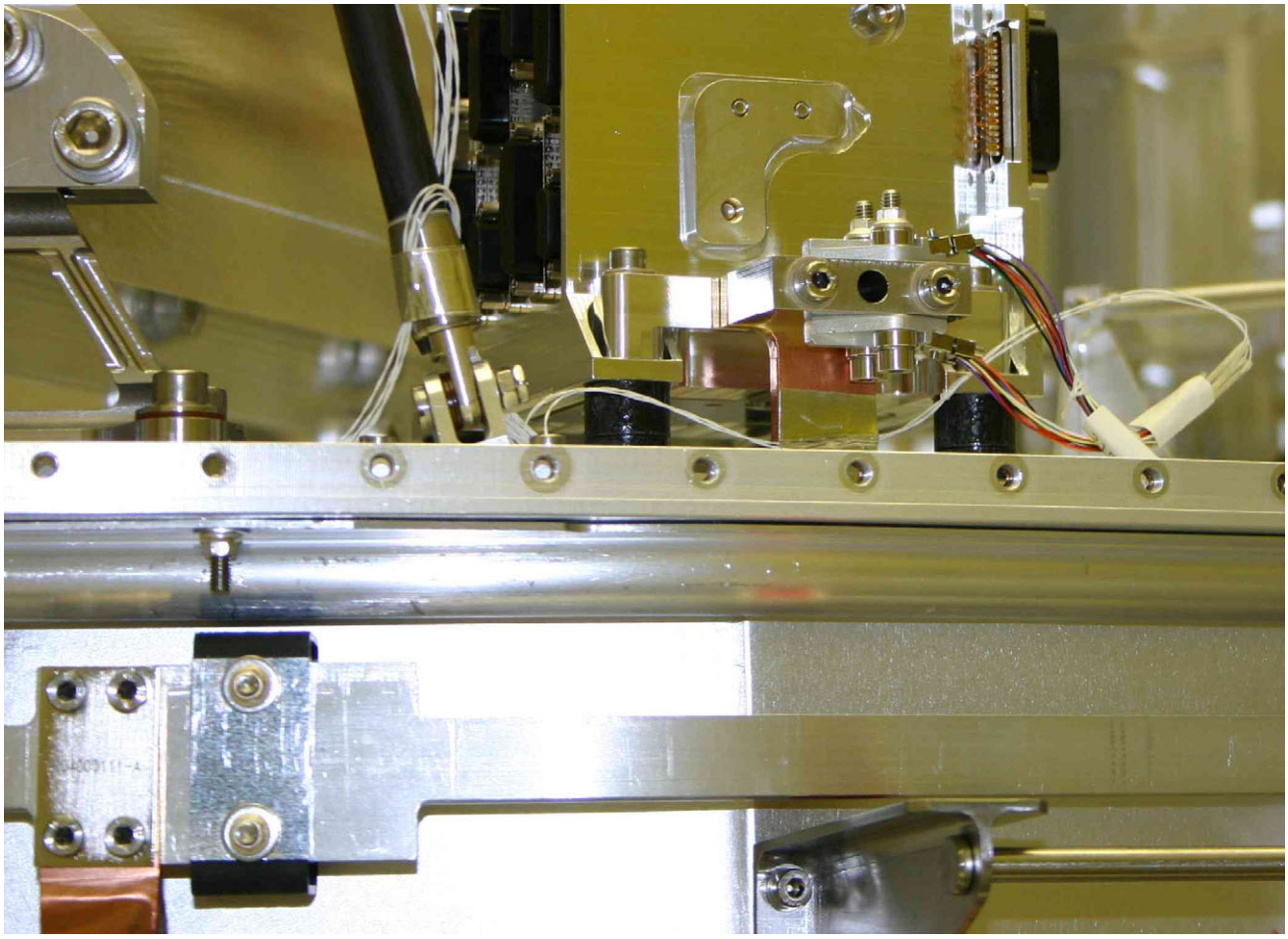

Figure 5.4-5: Temperature Sensors T249/T250 and L3 JFET-S Ventline I/F

The JFET temperature and electrical heating power evolution is shown in **Figure 5.4-6** as well as the heat absorbed by the helium of the L3 ventline system. In case of no electrical heating only about 2 mW are absorbed which is the conductive heat from the JFET harness that is directly routed to the JFET boxes without dedicated anchoring at the OBP. In addition ~54% of the JFET-P electrical power and ~67% of the JFET-S power is rejected by the L3 ventline system.

The temperature gradients versus electrical MTD heating power are shown in **Figure 5.4-7** for the JFET-P operation and in **Figure 5.4-8** for the JFET-S operation. The gradient along to the JFET-P strap to the ventline (T252-T246) is negative for all heating power which makes no sense and is in disagreement to the absorbed heat by the helium shown in **Figure 5.4-6**. Therefore, the accuracy of the sensors T246 and/or T252 are questionable. The temperature gradients along the whole L3 ventline show a straight behaviour. The absorbed heat for no applied electrical power is calculated using the mass flow and T247-T258 leading to 1.8 mW both for JFET-P and JFET-S which is in line with the 2 mW roughly taken from **Figure 5.4-6**.

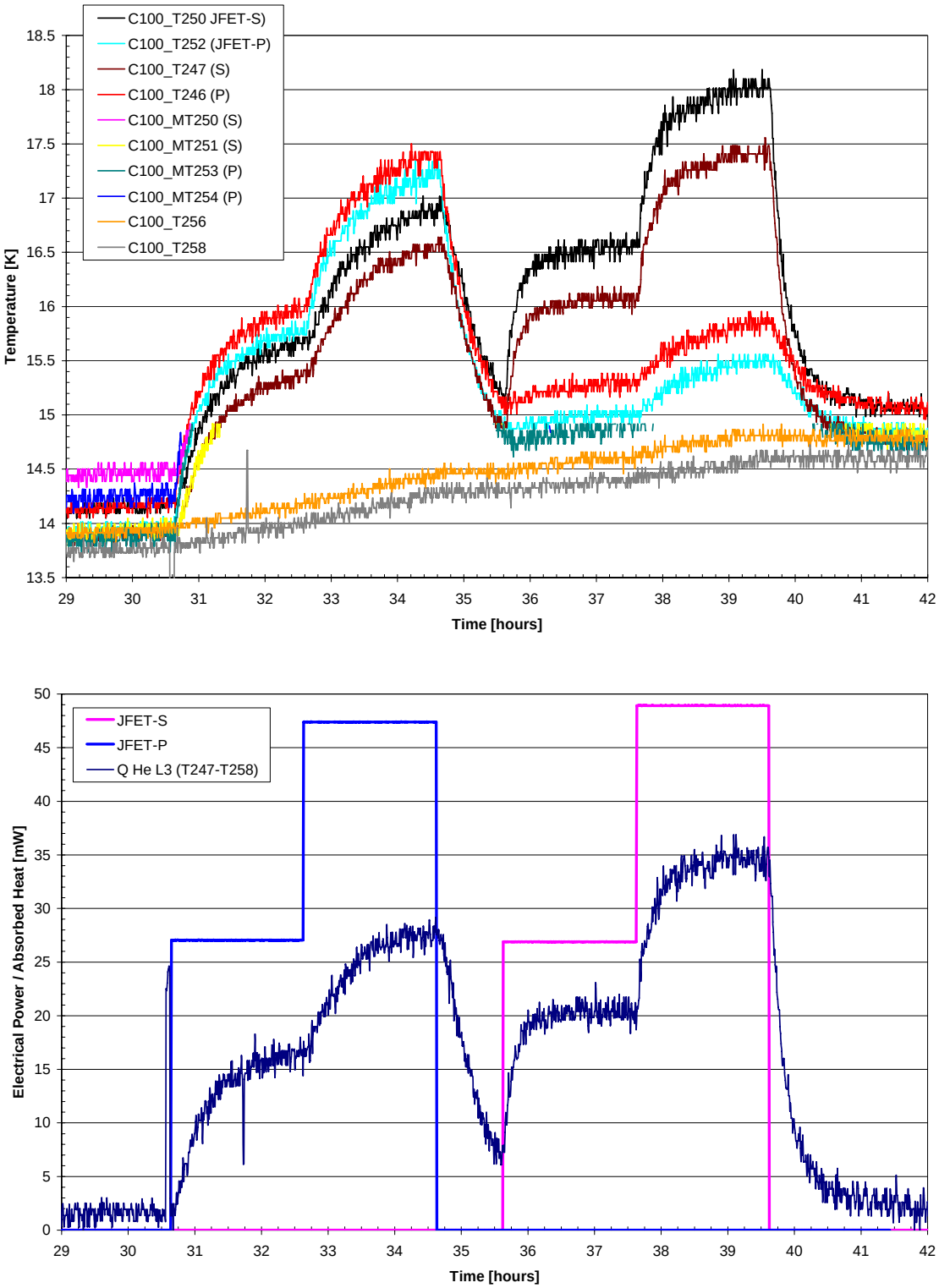

Figure 5.4-6: SPIRE JFET Power, Absorbed Heat and Temperature Evolution (TP4)

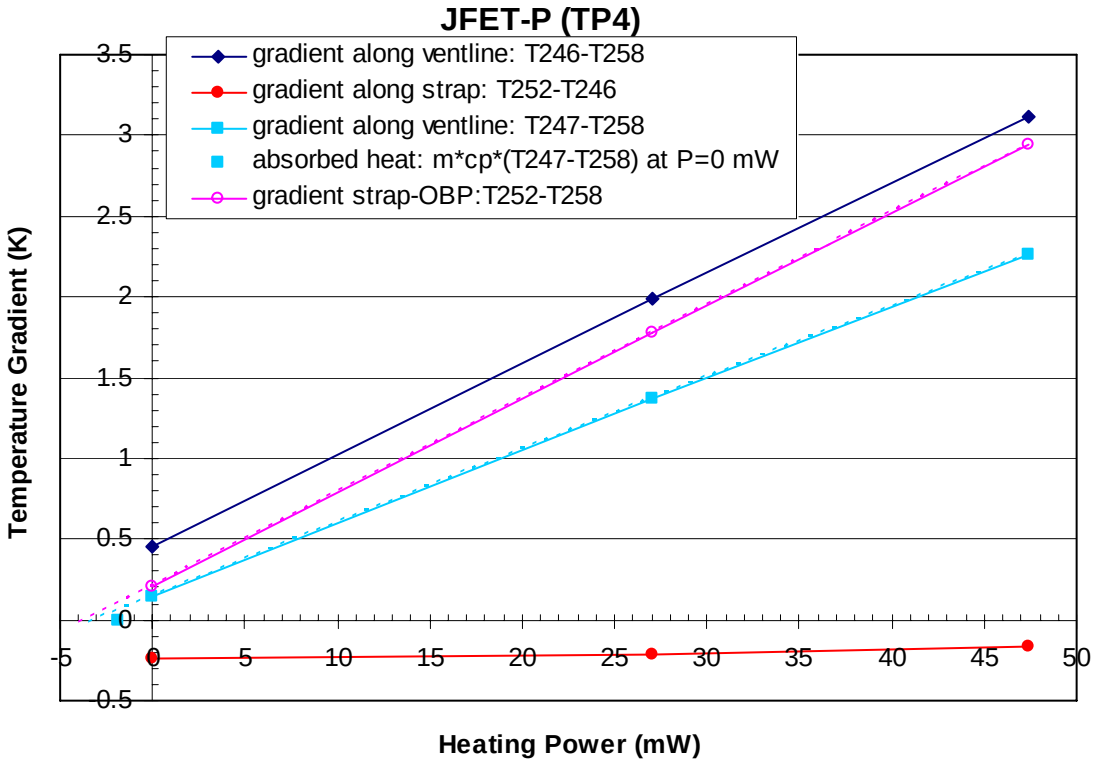

Figure 5.4-7: Temperature Gradients versus Electrical Heating Power at JFET-P I/F (TP4)

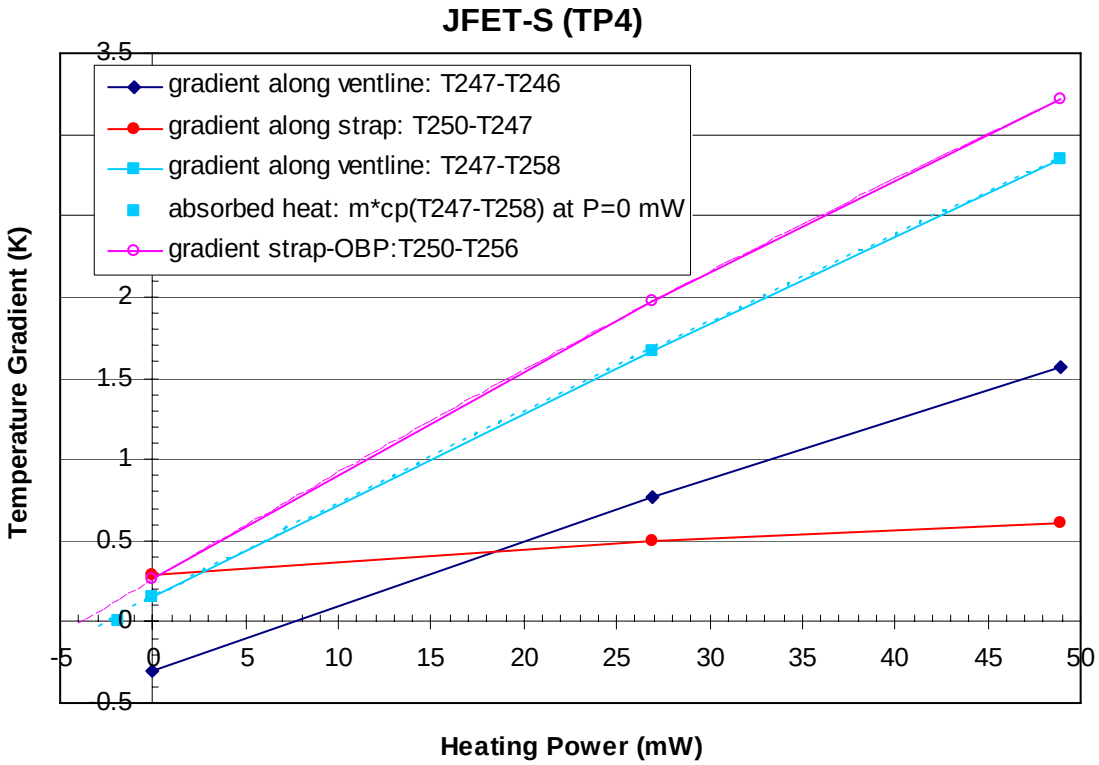

Figure 5.4-8: Temperature Gradients versus Electrical Heating Power at JFET-S I/F (TP4)

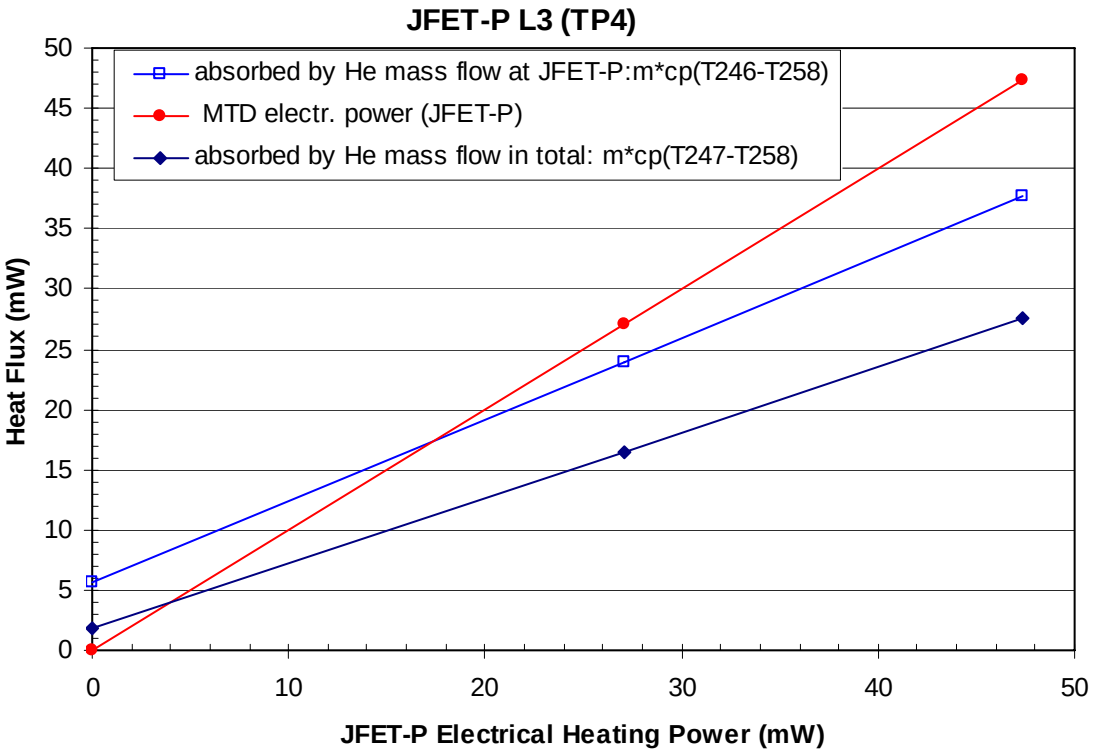

Figure 5.4-9: JFET-P L3 Heat Flow absorbed by Helium compared to Electrical Power (TP4)

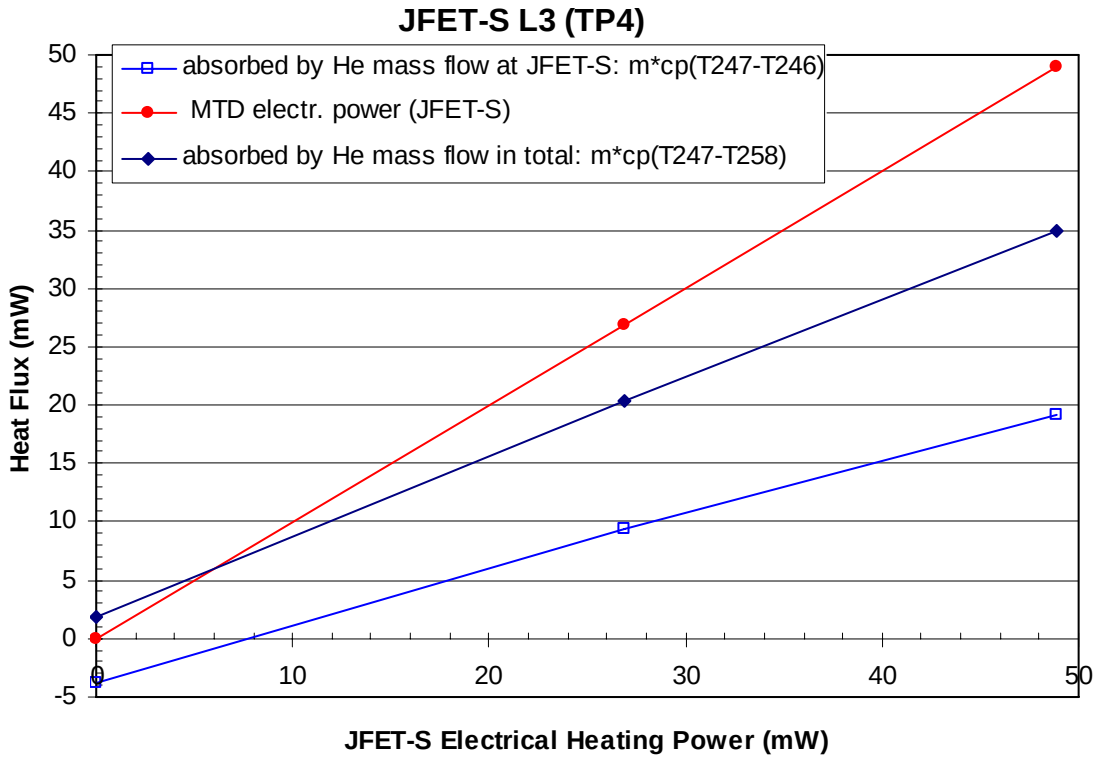

Figure 5.4-10: JFET-S L3 Heat Flow absorbed by Helium compared to Electrical Power (TP4)

5.5 SPIRE JFETs (TP6)

The JFET temperature and electrical heating power evolution is shown in **Figure 5.5-1** as well as the heat absorbed by the helium of the L3 ventline system. In case of no electrical heating only about 3 mW are absorbed which is the conductive heat from the JFET harness that is directly routed to the JFET boxes without dedicated anchoring at the OBP. In addition ~77% of the JFET-P electrical power and ~82% of the JFET-S power is rejected by the L3 ventline system. The heat rejected by the L3 ventline is higher compared to test phase TP4 (see previous section) because the heat transfer coefficient between ventline wall and helium is higher due to the higher mass flow in TP6.

The temperature gradients versus electrical MTD heating power are shown in **Figure 5.5-2** for the JFET-P operation and in **Figure 5.5-3** for the JFET-S operation. The temperature gradients along the whole L3 ventline show a straight behaviour. The absorbed heat for no applied electrical power is calculated using the mass flow and T247-T258 leading to 4.3 mW for JFET-P and 1.0 mW for JFET-S which is in the same order as the 3 mW roughly taken from **Figure 5.5-1**.

The heat absorbed by the helium along the L3 ventline is shown in **Figure 5.5-4** versus the JFET-P electrical heating power. For JFET-S it is shown in **Figure 5.5-5**. As mentioned in the previous section the reading of T246 is questionable; therefore the further evaluation is restricted to the total heat absorbed between L3 outlet (T247) and L3 inlet (T258). The L3 I/F conductance values are shown in **Figure 5.5-6** for both JFETs.

For the I/F heat flux the total absorbed heat by the helium m*cp(T247-T258) is taken as approximate value (knowing that any parasitic heat from the non heated JFET is neglected).

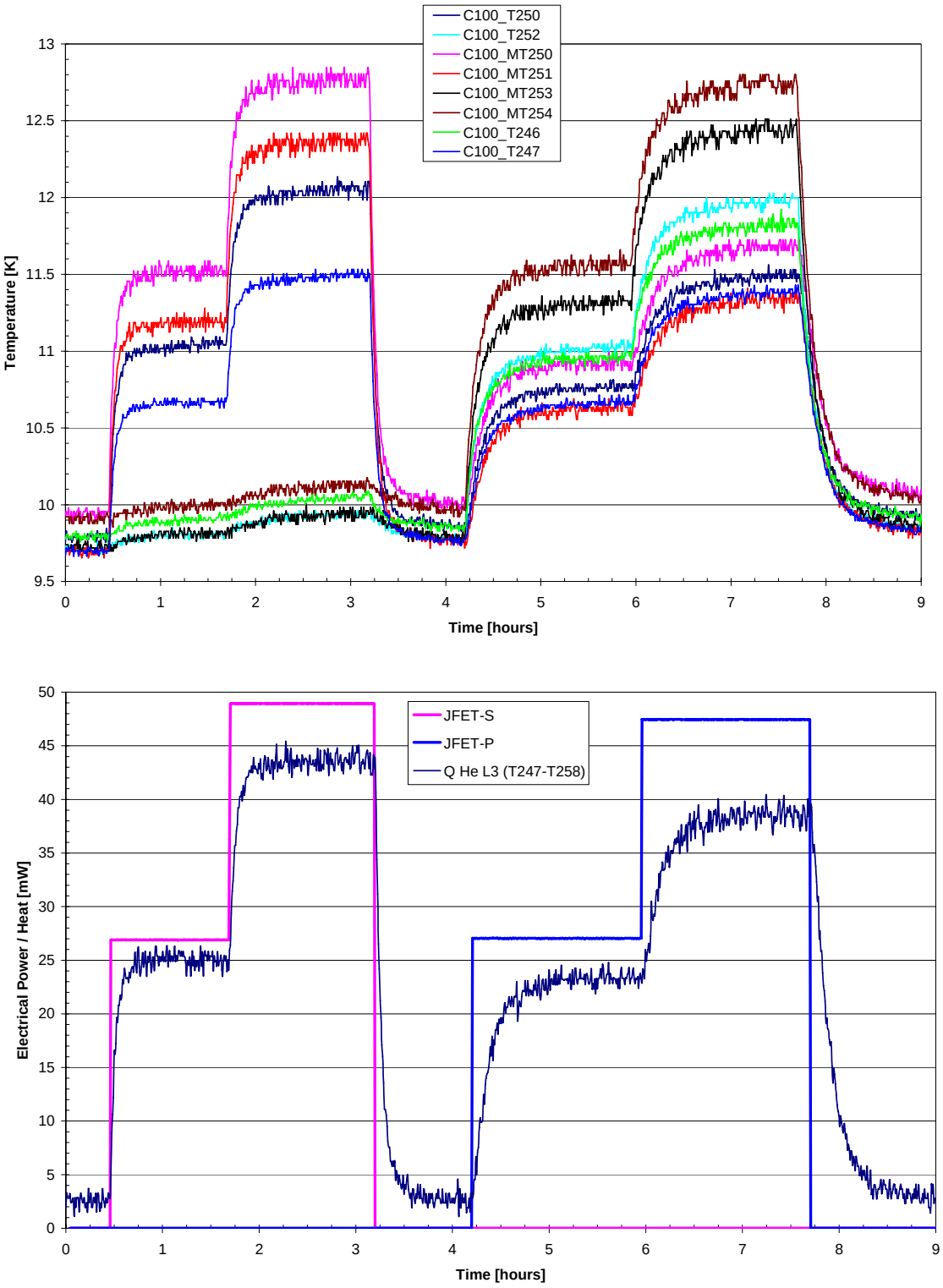

Figure 5.5-1: SPIRE JFET Power, Absorbed Heat and Temperature Evolution (TP6)

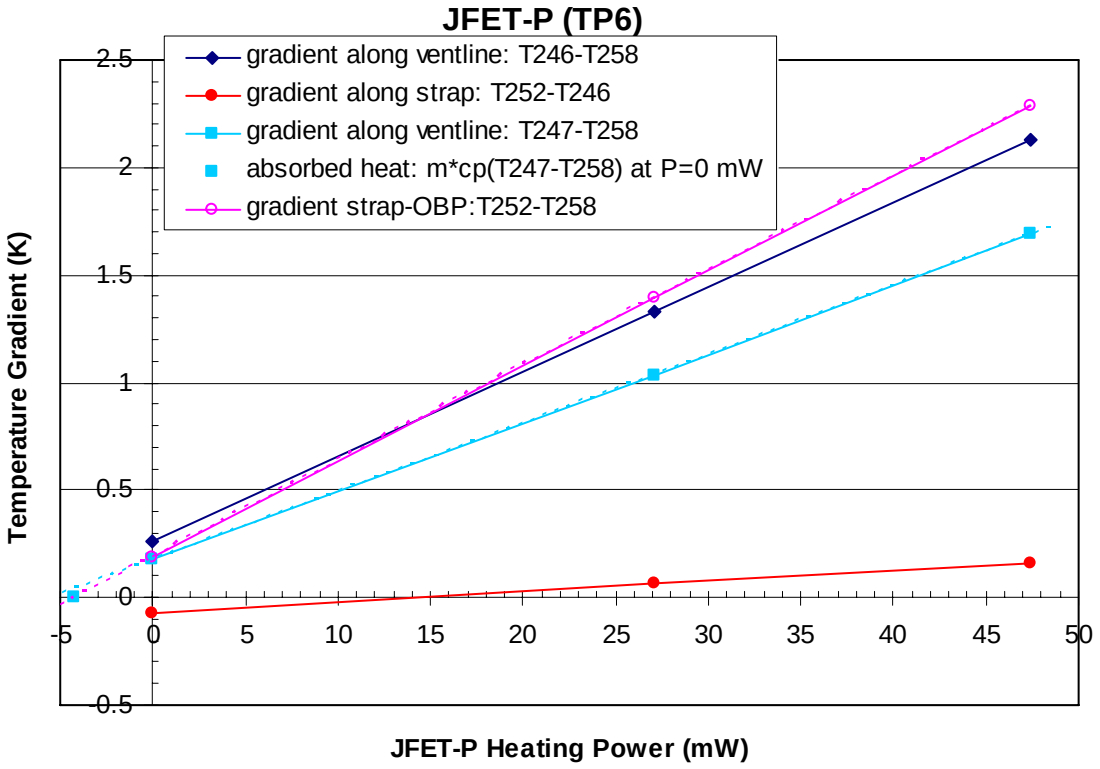

Figure 5.5-2: Temperature Gradients versus Electrical Heating Power at JFET-P I/F (TP6)

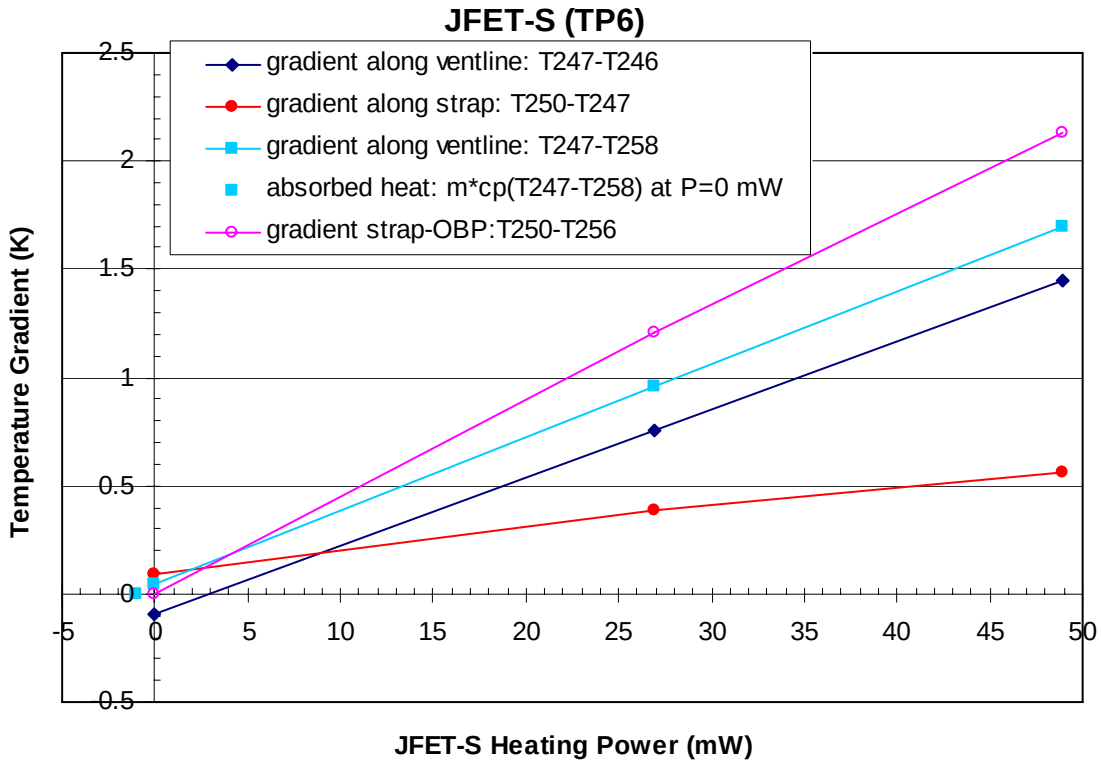

Figure 5.5-3: Temperature Gradients versus Electrical Heating Power at JFET-S I/F (TP6)

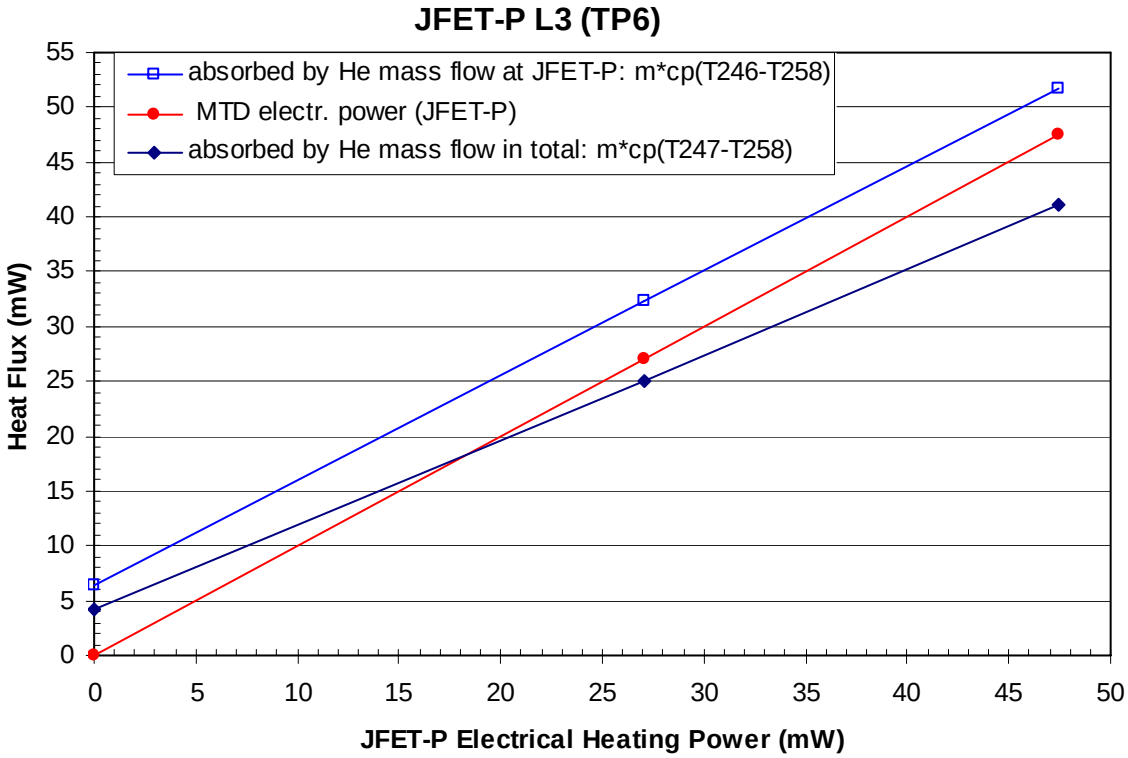

Figure 5.5-4: JFET-P L3 Heat Flow absorbed by Helium compared to Electrical Power (TP6)

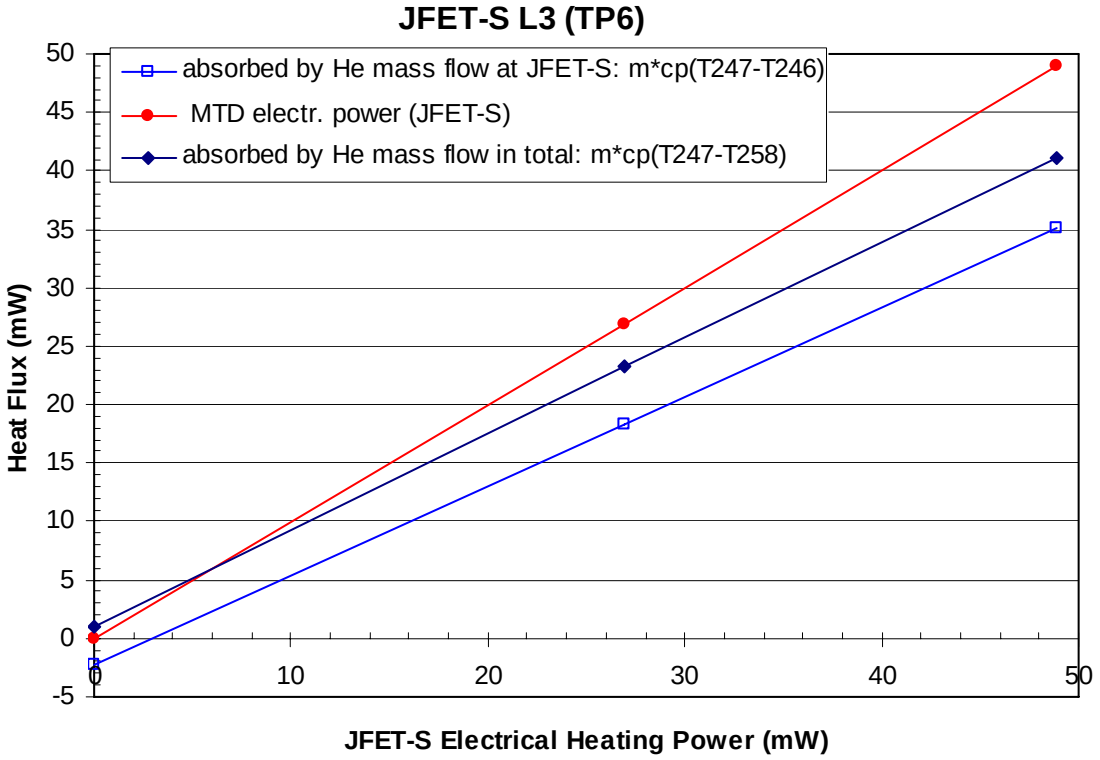

Figure 5.5-5: JFET-S L3 Heat Flow absorbed by Helium compared to Electrical Power (TP6)

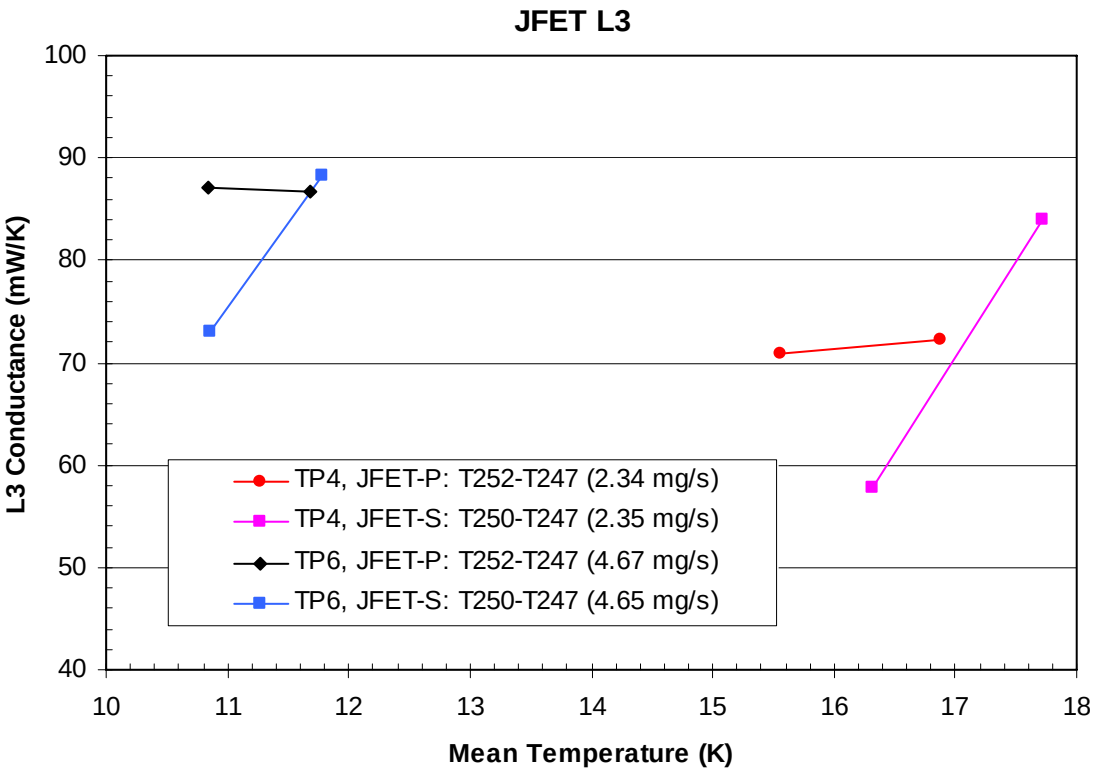

Figure 5.5-6: JFET-P and JFET-S L3 Interface Conductance (TP4 and TP6)

5.6 L2 & L3 Summary and Conclusion

Instrument Interface	Requirement	Measured during TP4			Measured during TP6		
	AD 01 to AD 03	Temperature	Mass flow	OBP	Temperature	Mass flow	OBP
PACS L2	12K @ 0mW	n.a.	2.36 mg/s	14-15 K	n.a.	4.7 mg/s	9-10 K
SPIRE L2	12K @ 0mW	n.a.	2.36 mg/s	14-15 K	n.a.	4.7 mg/s	9-10 K
HIFI L2 *(MT105/MT106)*	20K @ 22mW	14.8K @ 0mW	2.36 mg/s	14-15 K	10.1K @ 27mW 10.9K @ 49mW	4.80 mg/s 4.81 mg/s	10.5-11 K
SPIRE JFET-P L3 *(T252)*	15 K @ 50mW	15.8K @ 27mW 17.2K @ 47mW	2.30 mg/s 2.33 mg/s	14.3 K 14.0 K	11.0K @ 27mW 12.0K @ 48mW	4.67 mg/s 4.68 mg/s	9-10 K
SPIRE JFET-S L3 *(T250)*	15 K @ 25mW	16.6K @ 27mW 18.0K @ 49mW	2.34 mg/s 2.35 mg/s	14.6 K 14.8 K	11.1K @ 27mW 12.1K @ 49mW	4.64 mg/s 4.66 mg/s	9-10 K

Table 5.6-1: L2 and L3 Test Data versus Instrument I/F Requirements

6 Summary and Conclusions

All thermal performance tests carried out on the instrument MTD interfaces (L0, L1, L2, L3) during STM TB/TV test in the LSS at ESTEC are evaluated and reported. Furthermore, an extra test outside the LSS with a 90° tilted CVV was conducted in order to immerse the L0 open pods with liquid helium and thus to achieve quasi in-orbit conditions for those interfaces.

The thermal conductance of the L0 interfaces is determined by evaluating the gradient across each interface versus the applied MTD electrical heating power. The dependence of the temperature gradients from the applied power was almost linear. Comparison of the achieved conductance values with the instrument requirements demonstrates that except for HIFI all L0 requirements can be met. It should be noted that the HIFI L0 thermal link thickness was reduced by 28% due to new instrument I/F mechanical load requirements. To fulfil the requirement for the PACS Cooler Evaporator I/F the helium temperature must be lower than 1.668 K. All L0 results are compiled in **Table 3.6-1**.

The L1 thermal performance has been tested in two test phases (TP4 and TP6) with different helium mass flow rates: In TP4 the mass flow rate was about 2.3 mg/s which is the expected in-orbit flow rate; in TP6 the mass flow rate was about 4.7 mg/s. A further difference is that during TP4 the helium flow is routed via the PPS (valve V106 open) and during TP6 the PPS was by-passed (valve V104 open). The L1 conductance evaluation is also determined by evaluating the gradient across each interface versus the applied MTD electrical heating power, as well as the absorbed heat by the helium mass flow in the corresponding section of the ventline. Especially in TP4 a very good correlation between absorbed heat in the helium and electrical heating power can be observed. Unexpected behaviour of ventline temperatures occurred during TP6 and thus, especially the results for PACS are considered to be rather unreliable for this test phase. However the results obtained in TP4 show that all L1 instrument requirements are met with 2.3 mg/s helium mass flow rate. All L1 results are compiled in **Table 4.8-1**.

The L2 and L3 thermal performance has been also tested in the test phases TP4 and TP6. The temperature requirements for PACS and SPIRE L2 and the JFET L3 interfaces are not met with a mass flow rate of 2.3 mg/s. The L3 evaluation for the JFET-P revealed that the data of sensor T246 and/or T252 are suspect, because their data are in contradiction to the temperature increase of the L3 helium mass flow. The L2 and L3 performance data are compiled in **Table 5.6-1**.
A further outcome of the L3 evaluation is that the heat input of the JFET harness bundles to L3 is much smaller than expected. This means that most of the conductive heat from the JFET harness bundles is absorbed by the OBP (L2) and/or rejected by radiation of the bundles before reaching the JFET boxes. More detailed thermal analysis is necessary in this matter.

E N D O F D O C U M E N T

	Name	Dep./Comp.		Name	Dep./Comp.
	Alberti von Mathias Dr.	AOE22		Runge Axel	OTN/AOA54
	Barlage Bernhard	AED11	X	Schink Dietmar	AED44
	Bayer Thomas	AOA52		Schlosser Christian	OTN/AOA54
	Brune Holger	AOA55		Schmidt Rudolf	FAE22
	Edelhoff Dirk	AED2		Schweickert Gunn	AOE22
	Fehringer Alexander	AOE13		Steininger Eric	AED32
X	Fricke Wolfgang Dr.	AED 65	X	Stritter Rene	AED11
	Geiger Hermann	AOA52		Suess Rudi	AOA54
	Gerner Willi	AED11		Thörmer Klaus-Horst Dr.	OTN/AED65
	Grasl Andreas	OTN/AOA54	X	Wagner Klaus	AOE22
	Grasshoff Brigitte	AET12	X	Wietbrock Walter	AET12
X	Hauser Armin	AOE22		Wöhler Hans	AOE22
	Hendry David	Terma Resid.		Wössner Ulrich	ASE442
	Hengstler Reinhold	AOA 52	X	Alcatel	ASP
X	Hinger Jürgen	AOE22	X	ESA/ESTEC	ESA
	Hofmann Rolf	ASE442		**Instruments:**	
X	Hohn Rüdiger	AED65		MPE (PACS)	MPE
	Hölzle Edgar Dr.	AED32		RAL (SPIRE)	RAL
	Huber Johann	AOA52		SRON (HIFI)	SRON
	Hund Walter	ASE442		**Subcontractors:**	
X	Idler Siegmund	AED312		Air Liquide, Space Department	AIR
	Ilsen Stijn	Terma Resid.		Air Liquide, Space Department	AIRS
	Ivády von András	FAE22		Air Liquide, Orbital System	AIRT
X	Jahn Gerd Dr.	AOE22		Alcatel Bell Space	ABSP
	Kalde Clemens	APE3		Astrium Sub-Subsyst. & Equipment	ASSE
	Kameter Rudolf	OTN/AOA54		Austrian Aerospace	AAE
	Kettner Bernhard	AET42		Austrian Aerospace	AAEM
	Knoblauch August	AET32		APCO Technologies S. A.	APCO
	Koelle Markus	AOA53		Bieri Engineering B. V.	BIER
	Koppe Axel	AED312		BOC Edwards	BOCE
X	Kroeker Jürgen	AED65		Dutch Space Solar Arrays	DSSA
	Kunz Oliver Dr.	AOE22		EADS CASA Espacio	CASA
	Lamprecht Ernst	OTN/ASI21		EADS CASA Espacio	ECAS
	Lang Jürgen	ASE442		EADS Space Transportation	ASIP
	Langenstein Rolf	AED15		Eurocopter	ECD
X	Langfermann Michael	AOA51		European Test Services	ETS
	Mack Paul	OTN/AOA54		HTS AG Zürich	HTSZ
	Maute Thomas	AOA52		Linde	LIND
	Much Christoph	AOA53		Patria New Technologies Oy	PANT
	Müller Jörg	AOA52		Phoenix, Volkmarsen	PHOE
	Müller Martin	AOA53		Prototech AS	PROT
	Müller Ralf	FAE22		QMC Instruments Ltd.	QMC
	Peltz Heinz-Willi	AOE13		Rembe, Brilon	REMB
	Pietroboni Karin	AED65		Rosemount Aerospace GmbH	ROSE
	Platzer Wilhelm	AED2		RYMSA, Radiación y Microondas	RYM
	Reichle Konrad	AOA52		SENER Ingenieria SA	SEN
	Reuß Friedhelm	AED62		Stöhr, Königsbrunn	STOE
	Rühe Wolfgang	AED6		Terma A/S, Herlev	TER